May 2014

Design of a Protective Device for Head and Neck Injuries in Football

Evan Joseph Perry
Worcester Polytechnic Institute

Michele Lee Mensing
Worcester Polytechnic Institute

Ralle Adrian Rookey
Worcester Polytechnic Institute

Tyler Stephen Hanna
Worcester Polytechnic Institute

Zachary Kurt Hennings
Worcester Polytechnic Institute

Design of a Protective Device for Head and Neck Injuries in Football

A Major Qualifying Project Report

Submitted to the Faculty

of the

WORCESTER POLYTECHNIC INSTITUTE

In partial fulfillment of the requirements for the

Degree of Bachelor of Science

In Mechanical Engineering

Submitted by:

Tyler Hanna

Zachary Hennings

Michele Mensing

Evan Perry

Ralle Rookey

Submitted on May 1st, 2014

Key Words:

1. Football
2. Traumatic brain injury
3. Concussion

Approved:

_____

Professor B. J. Savilonis

_____

Professor E. Tüzel

Abstract

The goal of the MQP was to create a device to prevent concussions in football. Concussive football impacts were recreated with testing equipment including a guided freefalling 70lb helmeted head assembly, a 95lb suspended torso, and a recreated Hybrid III neck and head. Data was collected from accelerometers placed in the struck head. A rotational shock absorber was designed to transfer energy from the impacted head to the body of the player in order to reduce head velocities.

Executive Summary

Introduction

Every year there are nearly 48,000 reported cases of concussions in football ranging from pee-wee to professional level. An additional 35,000+ undiagnosed cases of concussions are expected to occur yearly, suggesting the need for a preventative device to reduce the likelihood of sustaining such a type of injury. Even with today's advanced helmet technology accompanied by protective rule regulations in football, there is still a high rate of TBI's (Traumatic Brain Injuries) in football. Advanced helmet technology protects players from high impact forces which may otherwise cause severe damage such as skull fractures. While the technology provides great protection against direct hits, the helmet, and other equipment for that matter, does not protect the player against the angular effects of a concussive-type impact. . In response to the gap in equipment technology to limit the rotational affects resulting from impacts during game play, **this project's goal was to limit the acceleration duration and to reduce the velocity of the head relative to the body during high impact forces through the design and manufacturing of a fluid shock absorber.**

Device Design

When considering the various design specifications that needed to be met in order to manufacture a meaningful product, the design team took into account the following criteria: comfort, ease of motion during normal game play, compatibility with existing equipment, minimal weight so as to not affect player's performance, affordability, manufacturability, and general ease to maintain and clean. Aside from the device's function with respect to preventing concussions, arguably one the most important design constraints was the need for the device to deliver minimal feedback forces under normal conditions but very high feedback forces, so as to simulate a stiff neck, during high impact collisions.

Through various design alternatives, the most promising design was a rotational shock absorber, shown in Figure 1 and Figure 2. The device supports the back of the helmet at all times and is attached to the back of the player somewhere between the shoulder blades. The rotational shock acts as additional stability for the head and neck during high impact collisions. The chamber at the base of the device is filled with fluid. The paddle, shown in magenta, moves according to head motion. The paddle will displace fluid through holes creating a resistive feedback force from the fluid in the chamber. This will dampen the collision on the head and transfer most of the impact energy to the torso. Different

Figure 1: Rendering of Shock Absorber Positioned with Helmet

Figure 2: Rendering of Fluid Shock Absorber

fluids, Newtonian and non-Newtonian, can be utilized in the chamber to gain different device response times and reactions.

Before the design was pursued further, initial fluid mechanics calculations and finite element analysis were performed to test the proof of concept. Below in Figure 3 are the results from the ANSYS Fluent finite element analysis. Various fluid speeds, representing varying impact severities, was processed through a paddle with an array of holes. The graph below shows the proof of concept is valid in that the device will give minimal resistance during low fluid speeds (small impacts) and high resistance during fast fluid speeds (large impacts) with a non-linear relationship between fluid speed and pressure in the chamber.

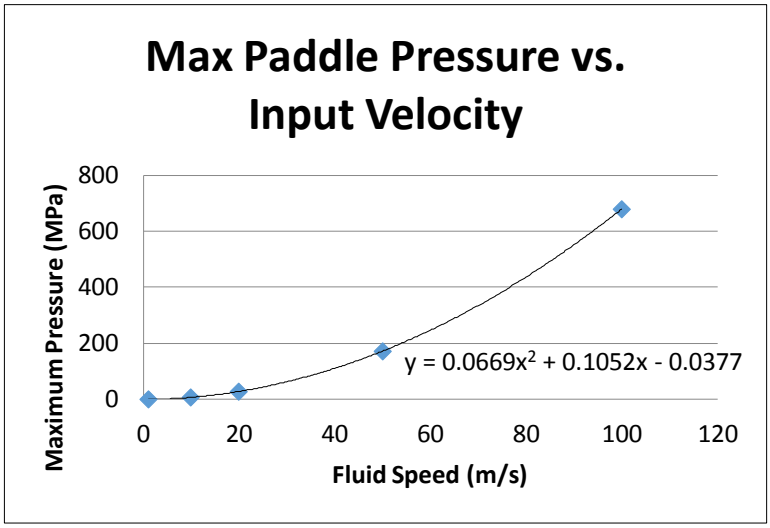

Figure 3: Graph of the fluid speed vs. reaction pressure from ANSYS Fluent

Once the concept was shown to be valid, the rotational shock absorber was machined. Governed by the requirement of very tight tolerances so as to maintain internal pressure, the group decided to machine the majority of the parts out of aluminum on the Haas Mini-mill CNC machines. Numerous components such as seal, O-rings, dowel pins, and bushings were incorporated into the design to provide robustness to the sealing nature of the part. The final product is shown below in Figure 4.

Figure 4: Manufactured rotational shock absorber. Left on torso supporting helmet. Middle casing half open to show paddle with holes. Right fully assembled device

Testing Methodology

The design team wanted to be able to replicate a concussive-type hit similar to other testing methods accepted by sports scientists in the field, and because of this, ultimately chose the creation of a vertical drop tester. The rig stood 16 feet tall and included two ¼" coated cables used as guides for the dropping of the *striking* into the *receiving* player. Overall, the player fell nearly twelve feet, attained a velocity of 7.5 m/s, and delivered a roughly 70g impact to the receiving player. To most accurately obtain data from the collision the *receiving* player was equipped with six single-axis accelerometers mounted on a unit sphere on the surface of the head and one tri-axial accelerometer mounted at the center. In addition to accelerometer obtained data, the team recorded high-speed footage of the collision to decipher impact velocity, head/neck deflection, and overall torso deflection. Figure 5 shows the final device attached to the player as well as the team's own *Hybrid III* neck model which was manufactured to accurately simulate the response of a human's neck during a collision.

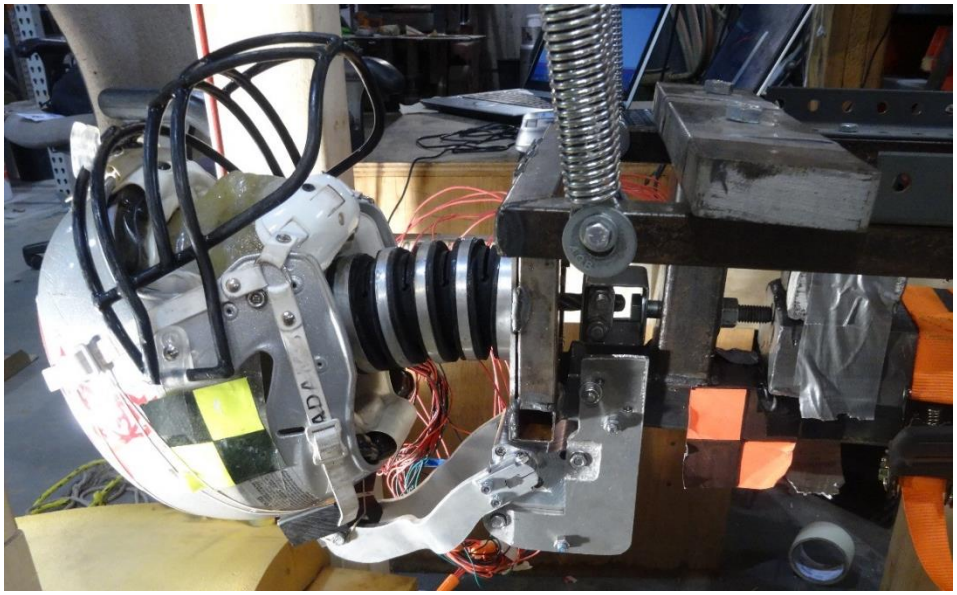

Figure 5: Struck Player - Accelerometers, Hybrid III Neck, and Device Mounted

Results

Through the use of high speed video footage (480fps) and recordings from tri-axial and single-axis accelerometers, various parameters of the head relating to concussions were obtained. The high speed footage allowed the team to determine the impact speed of the striking player, which was consistently 7.5 m/s. The video also allowed for analysis of the head rotation relative to the torso with and without the device. Accelerometer vs. time curves were obtained from both sets of accelerometers, with direction of acceleration obtained from the single-axis accelerometer array. From these accelerometer vs. time curve, the maximum speed of the head and peak acceleration were obtained.

The most important criteria for success of the rotational shock absorber was the calculation of the Head Injury Criterion (HIC). This is a scalar value that is a determinant for the severity of a collision and can be related to injury of risk of the struck player. The HIC is based on the acceleration curve, not just the peak acceleration.

$$HIC \equiv \left\{\left[\frac{1}{t_2 - t_1}\int_{t_1}^{t_2} a(t)dt\right]^{2.5}(t_2 - t_1)\right\}_{max}$$

Below in Figure 6 is a summary of the HIC values for the best hole combinations for each fluid tested. The orange line is the HIC value for no device usage. The 50W shock fluid with one 6mm hole in the paddle was the most effective at reducing the HIC value at 39% reduction.

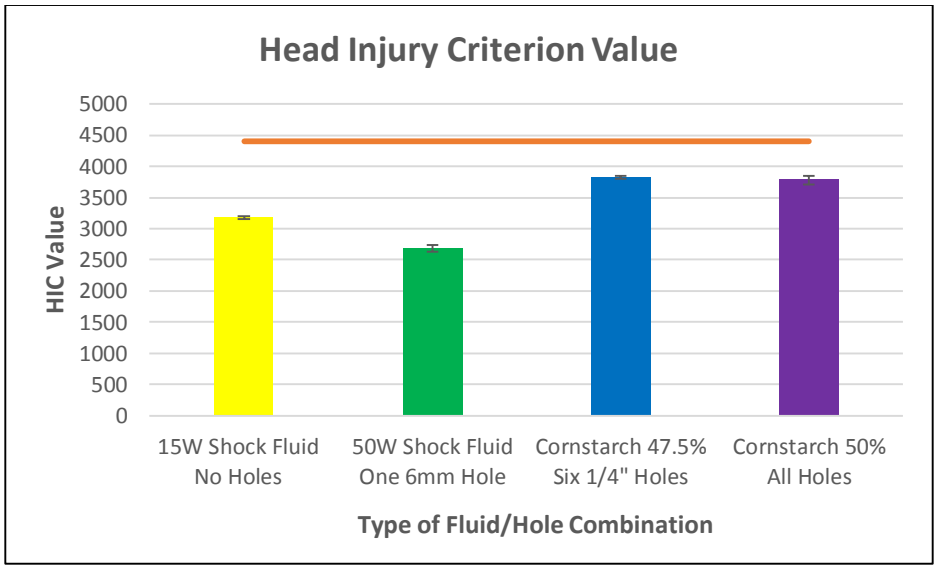

Figure 6: Bar chart of HIC values for the best hole combination of each fluid tested

Conclusion

Results from testing various fluid and hole combinations suggested that device reaction times were fast enough to change the acceleration experienced by the head of the struck player. Optimization of fluid densities, viscosities, and the correct hole patterns was one of the more difficult processes involved in the design and testing of the device. The team retrieved data which displayed reductions in the *Head Injury Criterion* values of the struck player's head acceleration when the device was in place. Of the ten fluid-hole combinations tested, the 50 weight shock fluid with one 6mm hole was the most successful in reducing key parameters associated with concussions. Compared to results of testing without the device, 50 weight shock fluid with one 6mm hole reduced the rotation of the head relative to the torso by 26%, the maximum velocity of the head by 8%, the velocity of the head at 30 milliseconds by 17%, the point of head deceleration by 35%, and HIC value by 39%.

While the results from this experiment are optimistic, a significant amount of future work could still be completed to further develop the device. There is still a wide variety of hole and additional fluid combinations which could be tested to optimize the results. Fluids, including a wider variety of shear-thickening fluids such as PEG and suspended silica nanoparticles, could be combined with a variety of paddle designs to allow for the modification of apparent shear rates, flow rates, etc. within the paddle compartment. Shear thickening fluids for example could benefit from changing the actual size and shape of the paddle so that fluid could be forced through a larger surface area encompassing both the holes in the paddle as well as the distance between the edge of the paddle and the case walls. Shear-thickening fluids such as cornstarch and water, which were originally thought to have performed well in the device, ended up performing poorly because the shear rates involved far exceeded the limits; after shear rates are exceeded the fluid begins to very rapidly shear-thin. Improvements to the design of the paddle and the area through which the fluid could flow could potentially lower shear rates so that shear thickening fluids such as cornstarch could be feasible options.

Acknowledgements

We would like to thank everyone who made this project possible. Professor Savilonis for always believing we could complete the project, no matter how ambitious, and guiding us along the way. Professor Tüzel for assisting with optimization techniques and offering guidance on equations of motion. The project would also not have been possible without the use of the Northeast Industrial Flooring, Inc. warehouse where we were able to execute testing. And a final thank you to WPI's Washburn and Higgins Machine shops where all of the machining of the device was conducted.

Table of Contents

List of Figures

List of Tables

1.0 Introduction

Each year roughly 450,000 sports-related head and neck injuries occur throughout the United States. This translates to roughly twenty percent of all traumatic brain injuries, according to the American Association of Neurological Surgeons [1]. A traumatic brain injury (TBI) can be defined as an impact, blow, or jolt to the head or neck region which causes a disturbance to the normal functionality of the brain, and therefore affects both the short and long-term health of the patient. Often times, a TBI may be caused by violent impacts, head and/or neck rotations, or dislodgement of brain tissue within the human skull. Subsequent effects may include unconsciousness, a loss of memory, or in severe cases, death. One of the leading sources of head and neck injuries in sports is football, which accounts for roughly 48,000 of the 450,000 total injuries ($\sim 10.67\%$) [1]. Because of the extreme relevance of concussions and TBI's in football, this project will focus on preventative measures and equipment of traumatic brain injuries in football.

Even with today's advanced helmet technology accompanied by protective rule regulations in football, there is still a high rate of TBI's. Helmets currently in use are only designed and manufactured to protect the skull from fracturing. While linear impacts, especially those that might lead to fracturing of the skull, play a large role in TBI's, researchers are finding that the duration of acceleration experienced and the velocity achieved by the head might be more at cause when a player sustains a concussion or other TBI [2]. The National Operating Committee on Standards for Athletic Equipment (NOCSAE), the organization which maintains the industry accepted testing standards for football equipment, does not require that any equipment address effects outside of initial impact [3]. The main qualification standard a NOCSAE approved helmet must meet is that it must structurally withstand 1200 Gadd Severity Indexes (GSI)[1], a measure of linear acceleration. In response to the gap in equipment technology to limit the duration of acceleration resulting from impacts during game play, this project's **goal was to limit the acceleration duration and reduce the velocity of the head relative to the body during high impact forces through design and manufacture of football equipment.**

The piece of equipment designed and manufactured for this project was a rotational shock absorber, meant to give extra support to the head by effectively strengthening the neck. The rotational shock absorber was designed to dissipate energy directed at the head to the shoulders, and therefore body, of the stuck player. As a proof of concept, the rotational shock absorber was tested only for functionality during impacts and was not designed for usability on human subjects. In order to properly demonstrate the shock absorber's effects on the rotations of a head during impacts and possible assistance with reduction of sustained concussions, two sets of experiments were performed. A testing procedure was identified and experiments were carried out to consistently achieve accelerations of the head of the stuck

[1] Gadd Severity Index is a measure of the integral of linear acceleration.

$$GSI = \int a^{2.5} dt$$

player that was in the range of concussive impacts. A second set of experiments were then performed, simulating the same conditions identified in the first tests, with the rotational shock absorber in place.

In the following content, the methodology of the design and testing of the rotational shock absorber, as well as the data evaluation, will be discussed in detail.

2.0 Problem Context

In order to effectively design protective football equipment, a thorough understanding of concussions and their role in football must be understood. This chapter explains the science behind traumatic brain injuries, their relevance to football in prompting rule changes and equipment research, and the various testing standards available for safety equipment.

2.1 Concussions

The following sections describe two of the key aspects of concussions: the physiology during and immediately after a concussion, and the types of impacts that might lead to a concussion. The physiology of a concussion speaks towards the functions of the brain on a cellular level immediately following a diagnosed or experimentally simulated concussion. The second section describes the types of physical impacts that can lead to concussions during head impacts.

2.1.1 Physiology

Unlike most injuries, such as broken bones or torn ligaments, concussions are undetectable by Magnetic Resonance Imaging (MRI). This inability to detect a concussion with traditional medical instruments makes rating the severity of a concussion difficult. Originally, it was believed that the duration of loss of consciousness was a reliable measure for determining the severity of a concussion. Recent research, however, has found duration of amnesia, or memory loss, to have a direct correlation with concussion severity [4].

Concussions usually occur when a rotational or angular acceleration force is applied to the brain, resulting in shear strain of the neural elements [5]. While immediate cell damage may occur, the disruption of neuronal membranes has the greatest effect on the inhibition of brain function. Upon experiencing a significant rotational acceleration, the nerve cells and axons become stretched and twisted, allowing potassium to be released into the extracellular space while also initiating depolarization of neurons. In an effort to restore the potential lost by this potassium efflux, sodium-potassium pumps within the brain must work overtime, requiring increased levels of energy in the form of ATP found in glucose. This increase in glucose breakdown by enzymes within the brain, known as glycolysis, leads to an increase in lactate production which has proven harmful to brain function. Excess amounts of lactate result in dysfunction of neurons by inducing membrane damage, increasing the possibility for cerebral edema, or swelling of the brain, as well as leaving neurons more vulnerable to a second injury [6]. Simultaneously, Excitation Amino Acids (EAA) are released which further stimulate the harmful potassium efflux [7].

During the release of potassium from stretched neurons, the neurons also intake calcium. Excess calcium accumulation within the neurons leads to impaired mitochondrial metabolism, in turn leading to energy failure within the brain and cell death. In experimental concussions, this calcium accumulation peaks after two days and resolves after around four days following the onset of a concussion. Furthermore, vital intracellular magnesium levels have shown to drop following a TBI and may remain low for up to 4 days.

Low levels of magnesium may lead to yet a greater influx of calcium into the neurons, and magnesium is vital in maintaining cellular membrane potential and in initiating protein synthesis [6].

Eventually, this continuous increase in potassium release leads to an increase in neuronal depolarization until the brain becomes too overwhelmed, resulting in complete neuronal suppression. When a neuron becomes suppressed it is unable to fire. Surrounding cells also begin to shut down as a protective measure to this neuronal suppression causing confusion, amnesia, and possibly even loss of consciousness.

Furthermore, it is expected that cerebral blood flow would increase in order to supply the increasing levels of glucose demanded by the sodium-potassium pumps trying to restore chemical stability within the brain. However, during the shutdown period this is not the case because a decrease in blood flow is actually experienced. Blood flow drops 50% to that of normal blood flow within two minutes and, on average, does not return to normal conditions for 10 days [7]. This gap in supply and demand of glucose results in a harmful energy crisis for the brain. While the immediate chemical reactions previously mentioned usually last no longer than 30 minutes, it takes days until the brain cells are fully able to restore homeostasis of the chemical balance. During this time, not only is brain function inhibited, but the brain is much more vulnerable to re-injury. In fact, a study by Guskiewicz found that 90% of second concussions suffered by athletes within the same season occurred within ten days of the first concussion [7]. In order to fully understand the reasons for this increase in repeated concussion rates, a number of stages must be examined.

It is understood that during the first 30 minutes of the incident of a concussion, cerebral metabolism is already at its peak as sodium-potassium pumps are overworking in an attempt to supply the demand of energy in the form of glucose. Any further demand in energy would push this energy demand beyond the limit. Cells injured during a first concussion may be able to recover, but a second concussion would almost definitely lead to cell death. In addition, if a second concussion or stimulation were to further increase calcium accumulation, the brain would lead to programmed cell death. Finally, concussions have shown to dramatically impair the function of neurotransmitters within the brain which have been shown to effect long-term potentiation, learning, and memory for up to 8 weeks in experimental brain studies. During this time, neurons are at increased susceptibility of depolarization, and a second blow would lead to an increase in energy demand and most likely cell death [6].

Brain trauma such as a concussion can cause long lasting effects in the brain. Repeated brain trauma can lead to a brain that is physically similar to that of a brain with Alzheimer's Disease (AD). Tau isoforms are found in the brain in plaques, exactly the same as found in a brain with AD, but are formed in different locations, namely the sulci and superficial cortical layers of the brain [8]. The physical size of sections the brain decreases and there is visible tissue damage. Symptoms are similar to those with AD such as memory impairment, but other symptoms include depression, behavioral change including increased aggression, and difficulty with motor functions. Many of the long term effects of the concussion are still being

discovered as a greater focus has been placed on understanding concussions due to the current attention on the subject matter.

There is still much to learn about the details of concussions and their short and long term effects. From the information known and experimental data collected, it is easy to understand why significant caution should be taken with concussions.

2.1.2 The Concussive Impact

Aside from the chemical changes of the brain during an injury, there is much unknown about the types of impacts that cause concussions. As stated earlier, concussions are undetectable by MRIs and therefore difficult to diagnose without significant symptoms. Determining an impact threshold which describes the likeliness of a brain injury based on impact data would allow concussions to become detectable with sensors in player equipment. For this project's purpose it is useful to understand the types of impacts that cause concussions so protective equipment can be designed appropriately. The following paragraphs describe other studies' approaches in finding the concussive-impact threshold as well as details about the types of impacts that typically cause concussions.

The most important measure of injury risk from an impact is the Head Injury Criterion (HIC) [9]. Based on the Gadd Severity Index, which the NOCSAE uses as a measure of helmet acceptability, the HIC is a value representative of injury severity based on magnitude and duration of acceleration experienced by the head. To calculate the HIC, only the magnitude of the head acceleration over time is needed, as shown below in Equation 1.

Equation 1: Head Injury Criterion definition based on the acceleration over time of a struck player's head

$$HIC \equiv \left(\frac{1}{t_2 - t_1} \cdot \int_{t_1}^{t_2} A(t) \cdot dt \right)^{2.5} \cdot (t_2 - t_1)$$

Multiple studies have attempted to relate the HIC value to injury risk of a player and severity of injury. Figure 7 below is a result of one of those studies, which displays Virginia Tech and National Football League (NFL) data taken during game scenarios. The relationship between HIC and injury risk is not linear. Since the relationship between HIC value and acceleration magnitude are not linear either, an increase in area under the acceleration curve could mean a significant increase in risk of injury for the player.

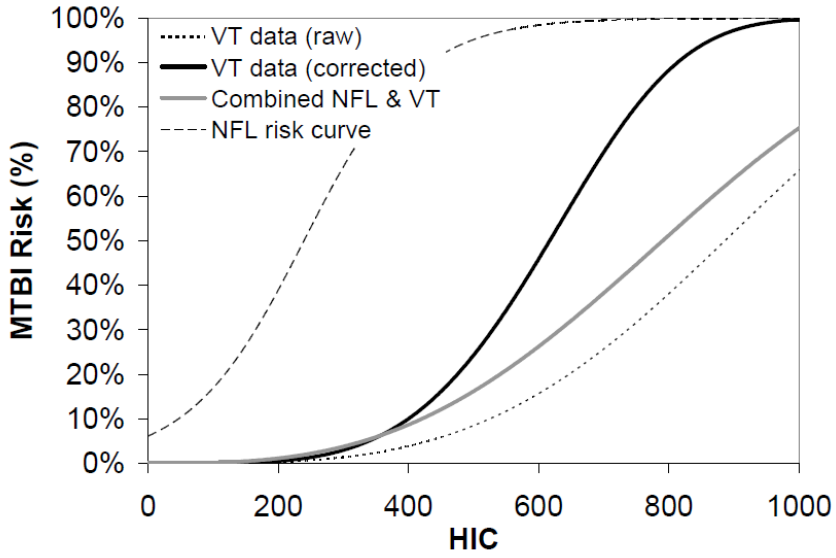

Figure 7: Relationship between the HIC value of an impact and its resultant risk of Mild Traumatic Brain Injury (MTBI)

The data in the graph shown above in Figure 7 is just one result from a long term study conducted by Virginia Tech. In an effort to define the relations between impacts, head kinematics, and concussion rates, Virginia Tech conducted research collecting real-time data from player's helmets [10]. Data was collected in a combination of trainer feedback on concussions symptoms and two methods of specially fit helmet accelerometers. Head accelerations were measured with the Head Impact Telemetry (HIT) system; a widely accepted method for measuring overall linear head acceleration. Rotational accelerations were measured directly with a Six degree of freedom (DOF) arrangement. Though, the HIT system had more success with reading concussions. Key information gathered during the Virginia Tech study included acceleration and velocity readings associated with concussive impacts and the location of impact on the head. It was determined for a concussive hit with sagittal plane rotation, the average linear acceleration was 102.7 g, rotational acceleration was 4986 rad/s^2, and rotational velocity was 22.1 rad/s. The study also found that rotational velocity sustained by a hit player had the strongest correlation with movement of the brain, and therefore potential concussion. The information found through the Virginia Tech research provides a deeper understanding of concussive impacts and serves as a model to develop better protective equipment.

Another study conducted by Pellman had the purpose of recreating game impacts in a laboratory setting to collect kinematic data and evaluate concussion biomechanics [11]. Pellman began by first evaluating videos of significant head impacts from NFL games occurring in a five year period. The video analysis revealed the majority (61%) of concussive hits were due to contact with another helmet, and that ground impacts made up an additional 16%. Analysis also revealed the average impact speed to be 9.3 m/s resulting in a change in head velocity of 7.2 m/s. To recreate these concussive hits, a freefall device was built which dropped one player onto another to simulate a typical hit. As in most human studies, the

Hybrid III male anthropomorphic test devices were used for impact testing. While Pellman recognized the significance of rotational acceleration contributing to concussive hits, he suggests that the official equipment standards which measure only linear impacts and accelerations are sufficient, and rotational affects should be left in research until more is understood.

In other studies, twenty-five helmet impacts were reconstructed using Hybrid III dummies. It was found that the greatest strains of the midbrain occurred after the initial impacts during testing, and the duration of the impact played a large role in the probability of a concussion. Higher durations of impact increased the rotational velocity the head achieved which raises the chance of concussion. By adjusting the neck stiffness in the dummy, it was found that head velocities were significantly lower [12]. This is due to the head and torso moving more as a singular unit instead of the head accelerating independently of the torso, creating a much greater moment of inertia. This suggests that neck strength has a significant contributing factor to concussion susceptibility [12].

2.2 The National Football League

Football, with an estimated 48,000 annual hospital-related head and neck injuries, ranks as the second most dangerous sport for traumatic brain injuries (TBI) [1]. With such a large number of injuries, and an estimated additional 20,000 undiagnosed injuries relating to the head and/or neck, one of the leading controversies in football is how to improve equipment to better protect the player from the dangers of the game. Starting in the 2013-2014 season, the NFL had allocated $10 million dollars to invest into the research and development of a more effective and safer helmet for players of all age and skill levels. The aforementioned investment, which seeks to prevent skull fractures as well as concussions, comes on the heels of one of the most controversial years in the NFL for rule changes, fines for player targeting, injuries, and long-term injury suits.

2.2.1 Safety Regulations and Rule Changes in the NFL

Since the turn of the century, numerous rule changes within the NFL have occurred in an effort to reduce the number of head and neck related injuries. Ranging from tackling and impact rules, to equipment regulations, the NFL has attempted to simplify and eliminate unnecessary variables which too frequently lead to exaggerated and violent impacts to the head and/or neck region. Rule changes, such as those that prohibit players from leading with the crown of their helmet, hitting a “defenseless” receiver above the chest area, leading helmet-to-helmet into an opponent outside the tackle box and more than five yards up field (ample time for the runner to build up speed), have accurately depicted the leagues intentions to decrease the number of injuries caused by direct impacts. Highlights of rule changes made by the NFL over the past ten years are described in the following paragraphs to show the attempt by the league, and by league officials, to decrease the number of risks for head and neck injuries.

Starting in 2011, the league initiated a “defenseless receiver” rule, which was the first true rule of its kind to seek protection against high-impact hits for struck players who were unprepared for such an encounter.

Defined in the 2011 NFL Rule Book, a defenseless receiver can be qualified as any player who "…has had no time to protect himself…."[13]. The intention of league officials through this rule, and other rules similar to it, is to protect players from concussive type hits that they are unaware and unprepared for.

Studies regarding the body's reaction to forcible contact to the head and/or neck region suggest that awareness is an important variable, playing a rather substantial role in determining the likelihood of sustaining an injury. Julian E. Bailes, a Neurosurgeon and Concussion Specialist from North Shore Medical in West Virginia, argues that "blindsiding" is one of the leading causes for concussions because of the inability of the individual to "brace" for the ensuing impact. In a recent article addressing various sources from which concussions can occur, Julian Bailes posted the following argument which deals directly with the *Defenseless Receiver* rule created by the NFL…

> "…the majority of concussion symptoms are cortical in origin, and headaches do not originate at the brainstem region but are vascular and supratentorial. Although the relative contribution of neck musculature is undoubtedly of vast importance, I don't think weak necks have been a major contributing cause of the majority of concussions in football, especially at the collegiate and professional levels. Rather than being caused by having a weak neck, I believe there is sufficient experiential and experimental evidence to conclude that being struck with high velocity forces and/or in an unprepared state (e.g. being "blindsided") is what leads to most traumatic brain injuries in sports [13]."

Other rules following the precedent set by the "defenseless receiver" rule include the more recent 2013 rules of "leading with the crown of the helmet" and "lowering of the head upfield with the intent to hit". The first penalty focuses on the definitive and malicious intent of a player to lead with the crown of the helmet into any portion of the opponent's body. The helmet is one of the hardest portions of athletic gear worn by the players, thus used as a weapon by players to deliver painful and devastating blows to opposing players. The second rule, created by the National Football League during the beginning of the 2013-2014 season, is very similar to the previously mentioned rule, with a more specific definition to penalize an upfield and projectile-like ball carrier. This rule targets runners who are outside of the tackle box (outside the hash marks) and more than five yards upfield from leading with their heads into any portion of the defender. Both rules address the issue of forcibly using the helmet as a dangerous weapon to transfer energy to an opponent.

2.2.2 Attitude of the NFL Regarding Traumatic Brain Injuries and Rule Changes

With all the rule changes in the NFL over the years, it is normal to expect opposing views from different groups of people in the league. Within the league, there are players, coaches, trainers, owners, and the office of the commissioner who all offer varying opinions when it comes to changing certain aspects about the game.

When a player receives multiple concussions throughout a football career, many people agree that some sort of long-term mental issues will have to be dealt with. Prior to the new "hard hit" rules, players were free to hit their heads as hard as they could and in any way they could to stop other players from advancing the ball. Most people were not entirely sure what long-term effects their bodies would experience when exposed to constant physical punishment sustained during NFL games, although some believed that the league itself was aware of these effects. In recent years, former players have been filing lawsuits against the NFL for withholding information regarding the long-term effects concussions can have on the human brain [14]. This issue adds the most controversy to the NFL concussion situation because it goes after the NFL for not taking action regarding the brain injury risk sooner.

As of June 2013, there have been 4,500 lawsuits filed against the NFL by former players involved in concussions for the long term injuries sustained by these players, most notably symptoms of dementia [14]. The main point that these players have been trying to prove is that the league promoted the physicality and durability of players, while also concealing the fact that players will most likely sustain long-term brain damage due to the brutality faced while in the league. In August of 2013, a settlement was agreed upon between player plaintiffs and the NFL to provide aid to former players through medical exams and compensation to 18,000 eligible retired players. The $765 million settlement is broken down as follows - $75 million will go towards medical exams for any of the retired players; $675 million will be going towards compensation to players and their families; and the rest will be put towards research into brain related football injuries [14].

Understanding the NFL conflict today is easier after looking into both sides of the issue. Current players are aware of the dangers concussions can cause in terms of brain damage, but many of them simply are not willing to "soften" the game and risk changing the way the sport is played. Many fans find the hard hits a very entertaining aspect of the game and do not wish to see them taken out. The commissioner understands the players' displeasure towards the rule changes but finds them necessary for the long-term protection of the players and as a way to prevent future lawsuits. Former players believe the NFL hid the evidence of long term damage from them while they were playing and feel that rules should be implemented to make the league safer. Though these statements from each party are obviously from person to person within the party, these are the general feelings regarding the concussion issue in the NFL today. While it can be difficult to please everyone, it would be beneficial to produce a piece of equipment that could prevent concussions before they happen, preventing long-term damage to these players even if the player is exposed to a hard hit.

Contrary to popular belief, concussions are not immediately caused by the impact, but rather from what follows. As previously mentioned, extreme rotation of a players head at incredibly high accelerations are major causes of concussions. While helmets are mandatory and do protect players from possible skull

fractures caused by a heavy impact, there is hardly protection out there that truly protects against the rotational aspect of players heads colliding.

2.3 Football Equipment

Even though American football started gaining recognition in the mid-eighteen hundreds, it was not until 1893 that the first use of a leather helmet was recorded during a college game [15]. A teardrop shape was incorporated into the manufacturing of the "crown" of the helmet and, in 1955, the first face mask was added to prevent face impact. This marked the beginning of the football helmet known today. Since then, changes have been made to incorporate air-pumped vessels to cushion the head, more secure chin straps to keep the helmet in place, and most recently, a new material choice and shape redesign [16]. While strides have been made in player protection over the last century, as previously discussed, there remains a lack of sufficient information for helmet manufacturers to effectively protect players from traumatic brain injuries during game play. The following sections describe the requirements for approved football equipment along with new and old products that are designed with additional concussion protection.

2.3.1 Equipment Testing

The National Operating Committee on Standards for Athletic Equipment (NOCSAE) regulates the standards which helmets, and other athletic gear, are tested. While NOCSAE standards are the only official standards used in approving football helmets for regular game play, the American Society for Testing and Materials (ASTM) has also published their own set of helmet tests. Since most products aim to satisfy ASTM or the American National Standards Institute (ANSI) standards, but NOCSAE had its own distinct standards for football helmets, the existence of multiple standards created confusion amongst helmet manufacturers and purchasers [17]. Both standards advocate for player safety, but neither claim to be a completely comprehensive testing standard. Due to the lack in clarity of safety for football helmet testing, many helmet manufacturers apply their own standards. While further concussion research is necessary to alter the official testing standards to incorporate rotational affects, there are companies designing products with this attribute in mind as detailed in the following section.

2.3.2 Current Concussive Reducing Products

The NFL Players Association and the board of the Commissioner have allocated 10 million dollars to the research and development of new helmet technology. This funding surrounds the centralized goal of developing, testing, and implementing possible new technology to gather information and/or to provide alternative equipment to aid in the minimization of injuries from high impact collisions.

To better understand the approach of each product in better protecting players, a variety of products currently on the market are introduced and explained. These products are separated into three categories: exterior protection, interior protection, and neck rolls. Exterior protection and interior protection both have a heavy focus on head protection, whereby exterior includes products that are add-ons to existing, mandated equipment, while interior protection involves design and manufacture of new

equipment that incorporates concussion reducing techniques. Neck rolls include equipment whose purpose is head injury reduction but do not directly target head protection.

Exterior Protection Products

In hopes of reducing concussions, Guardian Caps has developed a product which claims to absorb roughly 33% more energy than a traditional Riddell football helmet. By utilizing a soft, multi-cell shell on the surface of the existing helmet, the company argues that the amount of energy absorbed by the head, and therefore the amount of head and neck injuries caused by impacts, is decreased significantly. The *Guardian Cap* is made of 37 soft cells strung together to form one lightweight (less than 7 ounces), waterproof, and detachable surface structure for the conventional football helmet. In addition to the improved impact resistance, the design also incorporates fixture points which enable the majority of the device to move independently of the helmet, enabling angular and rotational forces to be reduced. Figure 8 shows the application of the *Guardian Cap* on an existing helmet.

Figure 8: The Guardian Cap fitted to a typical football helmet

The present design of the *Guardian*, although gaining popularity and approved for official use in many high schools, has multiple drawbacks. Adding more weight to the helmet is not desirable for players as it adds strain to the neck and is unattractive to most. By using the *Guardian Cap* the player is "modifying" the helmet and therefore ending all certifications and warrantees guaranteed by the helmet manufacturer. While effective in transferring energy to reduce likelihood of a concussion, the *Guardian Cap* is lacking in critical areas that would encourage more players to use it.

A different approach from outer helmet cushioning to concussion reduction is the Riddell 360 facemask. The *Flex Face Guard*, below in Figure 9, is coupled with hinge clips that hold the facemask to the side of the helmet, and has been shown to absorb more energy from an impact than traditional facemasks. The hybrid carbon steel and polymer material is able to absorb the impact energy through deflection, rather than translating all of the energy into rotational motion through the helmet. The hinges incorporated into the design are efficient at absorbing energy from a frontal blow, where roughly 70% of concussions originate [18].

Figure 9: The Riddell Flex Facemask mounted on the 360 helmet

Riddell has shown that although the helmet weighs slightly more than the traditional *Riddell Revolution Helmet* (4lbs 8oz versus 4lbs 2oz), the Flex Facemask offers enhanced player protection. Currently, Riddell is promoting the helmet to the NFL level to take place of the aging Riddell *Revo* technology, while also trying to reduce the overall cost of the nearly $400 helmet [19].

Interior Protection Products

In an alternate approach to helmet add-ons with extra concussion protection, multiple companies are redesigning entire helmets to include extensive concussion prevention features. 6D-ATR1 helmets, developed largely for motocross and off-road recreational vehicle use, provide new technology which specifically aims to reduce rotational forces on the head and neck during an accident [20]. The helmet, shown in Figure 10 below, is designed with two separate layers: one internal padding layer and one hard external shell join together by means of several Omni-Directional Suspension (ODS) components.

Figure 10: ODS Suspension Components- 6D-ATR1 Helmet

The ODS components provide this 6D helmet with translational energy absorption. The design uses multiple “layers”, enabling the inner portion of the helmet to remain still with respect to the outer helmet upon an impact. When a translational impact is applied, the outer shell can “slide” or “shear” past the inner layer while the shocks effectively work to absorb and diminish the energy that otherwise would cause an angular acceleration of the head and brain. The technology has not been applied to contact sports such as football yet, and the $700-900 helmets are an expensive alternative.

Massachusetts based company, Xenith, has recently created a new helmet that incorporates several of the previously mentioned design alterations. The production of the Xenith-X2 helmet in 2011 began with the company's goal to provide better fit, comfort, and protection for players. An image showing the internal shock resistor and elastomeric chin strap components can be seen below in Figure 11.

Figure 11: Xenith X2 shock and chin strap components

The fit of the X2 helmet to each player is unique in that, conversely to competitors' designs, there is no inflatable liner. Instead, the X2 utilizes a *Fit Seeker* silicone technology which enables proper fitment to the head at the top and sides [21]. In addition, the chin strap was redesigned to ensure proper placement of the helmet about the head and to take full advantage of the shock absorber technology while also tightening upon impact. An important design criteria for the X2 is the claim that the helmet provides better protection. Similar to the 6D-ATR1 helmet, it incorporates the use of fluid dynamic shocks to absorb energy and shear if necessary to reduce overall translational energy. The company's *Shock Bonnet* also utilizes suspension components to aid the external helmet shell to rotate without directly affecting the innermost shell [21]. This actively decreases energy transition to the head, therefore reducing the angular acceleration of the brain within the head.

Neck Rolls

The neck roll is the name applied to a variety of devices designed to fit into the top of players' shoulder pads and protect against hits that cause hyperextension. The problem with this is that it sits behind the player's head a few inches without being in constant contact with the helmet. Though this design may help decrease neck injuries among players, it doesn't counteract the initial acceleration of the head and therefore doesn't aid against concussions. In the NFL, it is rare to see a player with any sort of equipment protruding from the back portion of the pads designed to protect the neck. Neck rolls came to be popular because of the intimidation factor rather than their practical use. A 2011 New York Times article titled "Glory Has Faded for the Neck Roll; Memories Have Not" questioned former NFL players about what they thought of neck rolls when playing in the league. "Growing up, man, everyone wanted a neck roll, I mean everyone. It was the thing. Neck rolls were hot." said former New York Giants player Deon Grant [22]. This quote alludes to the visual appearance making the neck roll an attractive piece of equipment; not its functionality.

2.4 Dynamic Hardening Materials

With the intent of reducing motion of the head relative to the body it is implied that a device will be designed that resists motion of the head upon an impact. Because the time in which a concussion occurs is in the order of milliseconds it is necessary for this device to be in contact with the head at the moment of impact. A design constraint however is to not restrict the natural motion of the player. The main difference between head motion during normal movement versus after impact is the velocity and acceleration of the head; during normal motion, head velocity is around 0.1m/s where upon impact head velocity is around 4m/s, an order of magnitude 40 times greater [23].

In order to reduce the relative motion of the head to the body at high velocities but maintain full range of motion at low speeds, it is apparent that a material that is compliant at normal head speeds yet hardens upon a high energy input could be very useful.

Materials with this ability are generally liquids. Dilatant liquids increase viscosity with increasing shear strain rate. There are dilatant liquids with the ability to achieve near solid states at high shear strain rates due to tremendous increases in viscosity.

Dilatant liquids are used most commonly in body armor, where when impacted by a projectile the liquid increases viscosity to the point where it is able to arrest the projectile's motion. Some sports gear uses dilatant fluids, namely the material D3O, in protective gear and padding. D3O is a commercially available material.

Poly Ethylene Glycol (PEG) is a common material, and is the dilatant liquid used in body armor. It is often mixed with particles to adjust its shear thickening abilities; the PEG in body armor utilizes a silica nanoparticle suspension. It has the ability to increase viscosity by over 1000% [6].

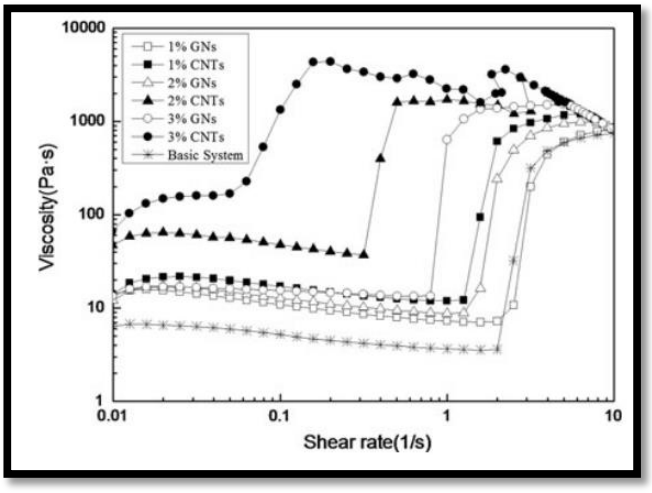

Figure 12: Viscosity vs. Shear Rate

Cornstarch mixed with water also creates a dilatant fluid that acts in a similar way to PEG. Though much cheaper than PEG, it can be used to represent all dilatant fluids due to its shear thickening property. Shown below in Figure 13 is the viscocity vs. shear rate graph of this fluid at different cornstarch concentrations [24].

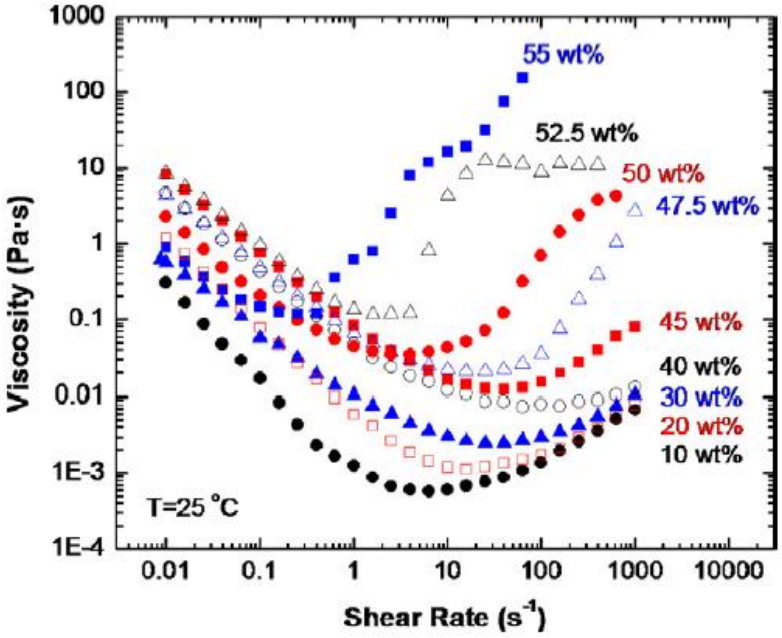

Figure 13: Graph of shear rate vs. viscosity of various corn starch and water mixtures.

The graph shows how each concentration's viscosity acts at different shear rates. It can be seen how high some of the viscosities become at higher shear rates. Though none of the viscosity changes act as sharply as PEG's do, the 47.5-55% cornstarch weight mixtures change viscosity enough to represent a dilatant fluid. These mixtures can be useful for concussion prevention on the football field because low shear rates would allow movement during regular player movement while high shear rates would increase viscosity and make things harder to move during a concussion inducing hit. If the high viscosities could be harnessed to make a players head harder to move, a concussion could potentially be prevented.

3.0 Methodology

With a significant amount of research completed, the team had an in-depth understanding into the mechanisms causing concussions and current trends in football and football equipment. The following section describes, in detail, the initial design process leading up to the final device design. First, a number of design specifications were formulated and weighted, which then helped conceptualize various initial design alternatives. These various designs were then compared in depth with respect to the design specifications, and a final alternative was chosen. Preliminary, proof-of-concept calculations were completed on this design both by hand and with the use of ANSYS software.

3.1 Design Specifications

Based on current research surrounding head and neck injuries, and the accepted equipment for use in football, this project's **goal is to limit the acceleration duration and reduce the velocity of the head relative to the body during high impact forces through design and manufacture of football equipment.** All designs and testing will be made to fit the dimensions and critical physical properties of the Hybrid III 50th percentile male head and neck model. The Hybrid III male dummy is the standard crash test dummy for use in the automotive industry, and is widely used in recent football helmet related research. Additionally, due to player attitudes around equipment, this study aims to design equipment that would be generally accepted by the football community as an alternative product.

The final design will be tested for the following parameters:

- Sustained head velocity
- Sustained head acceleration
- Rotational displacement of the head with respect to the torso

While the above parameters will be recorded, it is the Head Injury Criterion value that is the true measure of success of the device. The final design aims to reduce the HIC value by 25%.

3.1.1 Constraints

To ensure the design meets expectations of players as well as safety requirements, the following design constraints were generated (in no particular order):

1. Must be compatible with existing equipment.
2. Must be able to be removed separately from the helmet and other equipment.
3. Must not pose a danger to user or other players (no sharp edges).
4. Must sustain highest impact per NOCSAE football helmet standard tests – 5.5 m/s (17.94 ft/s) impact to all six impact locations.
5. Must sustain operating temperatures ranging from -28.8°C to 48.8°C (-20°F to 120°F).
6. Must not restrict player head and neck movement by more than 20%.
7. Will not cause pain to the user.

8. Moisture retention should be limited.
9. Must weigh less than five pounds.
10. Must be marketable for less than $200.
11. Must be able to be cleaned free of sweat, dirt, and other foreign objects.
12. Material and parts must be available and reasonably workable.
13. Design should be kept simple, while still accomplishing the goal.

Most of these design constraints focus on functionality of the equipment outside of the goal of reducing the velocity of the head. Safety issues during play, player comfort, and playing conditions were all taken into consideration. The first three design constraints address the safety and compatibility of the designed equipment. While the new equipment must fit comfortably on the player and securely attach to other equipment, it is also important that the equipment be able to be removed as a separate entity. This is to accommodate the player in a situation of immediate medical attention due to neck injury where all of the equipment, except the helmet, needs to be removed.

Items four and five address the ensured integrity of the designed equipment during normal play. While the tests run in this study are to determine mainly rotational experiments, it is necessary to also ensure the equipment can withstand the roughness that is football. The only equipment standards NOCSAE upkeeps for football are helmets, faceguards, and gloves. The team decided it would be sufficient to perform the highest impact NOCSAE helmet test while the designed equipment is secured. If this impact at speeds of 17.94 ft/s is sufficient to structurally test helmets, then it should be sufficient to structurally test the designed equipment. Temperature conditions also play a role in the integrity of the protective equipment, especially if new materials are to be used. The operating temperature range specified is representative of the coldest and hottest NFL games on record.

The sixth through eleventh design constraints address what a player wants and expects from protective equipment. While the goal of the design is to reduce head movement during impacts, the designed equipment cannot restrict a player's movement otherwise. Players that need to be able to turn their heads quickly or have full range of motion of their neck during play will not use equipment that would impede that. Other aspects that might affect a player's decision to use a certain piece of equipment include a secure and comfortable fit. The equipment's ability to not retain sweat is a must, as it the user's responsibility to properly clean the equipment after each use. The weight of five pounds was determined as a middle ground for upper body equipment: most helmets range between three and four and a half pounds, while most shoulder pads average around ten pounds. Finally, the production price was constrained at $200. This was also determined by common helmet prices, ranging upwards of $300, and other upper body equipment prices.

The above design constraints were then rank-ordered, a process that involved comparing each design constraint to one another, and deciding if one was of greater importance to completing the goal or if they held the same weight (see Table 1). A score of 1 was given to constraints that were more important, 1/2 to constraints that were of equal importance, and 0 to those that were less important. The totals were calculated across the rows. The results of this rank-order system were used in the alternative analysis to better populate the decision making matrix.

It should be noted that these design constraints are intended for a final, wearable product. While our project focused solely on a proof-of-concept device due to time and cost restrictions, these constraints were still vital in the design of the device with future prototypes in mind. Therefore, many of these constraints are irrelevant for the device tested throughout this project, but were vital in the design process as well as in future work.

Table 1: Decision making matrix of major design constraints

Constraints	Easily Removable	Impact	Oper. Temp.	Not restrictive	Comfort	Moisture Retention	Weight	Danger	Price	Ease of Cleaning	Part Availability	Simplicity	Total
Easily Removable	-	0	1	0	0	1	0	0	0	0	0	0	2
Impact	1	-	1	1/2	1/2	1	1	0	1	1	0	1	8
Operating Temp.	0	0	-	0	0	1/2	0	0	0	0	0	0	1/2
Not restrictive	1	1/2	1	-	1/2	1	1/2	0	1	1	1/2	1	8
Comfort	1	1/2	1	1/2	-	1	1/2	0	0	1	1/2	1	7
Moisture Retention	0	0	1/2	0	0	-	0	0	0	1/2	0	0	1
Weight	1	0	1	1/2	1/2	1	-	0	1/2	1	1/2	1/2	6.5
Danger	1	1	1	1	1	1	1	-	1	1	1	1	11
Price	1	0	1	0	1	1	1/2	0	-	1	1/2	1/2	6.5
Ease of Cleaning	1	0	1	0	0	1/2	0	0	0	-	0	0	2.5
Part Availability	1	1	1	1/2	1/2	1	1/2	0	1/2	1	-	1	8
Simplicity	1	0	1	0	0	1	1/2	0	1/2	1	0	-	5

3.2 Description of Design Alternatives

Through team brainstorming, discussion, and research, we developed multiple design concepts. They were all presented and discussed as a group, pointing out some preliminary concerns in designs and noticing certain promising aspects. The five most promising designs were chosen and further developed. They are each described below with concept sketches, and a Decision Making Matrix (Table 2) was used to help systematically choose the best design.

3.2.1 Design 1: Fluid Neck Roll

The Fluid Neck Roll incorporates partially collapsed vinyl or other flexible yet un-stretchable polymer sacks filled with a dilatant fluid. The sacks are connected to each other by tubes and valves, and the sacks are mounted to a structural surface mounted to the shoulders, as shown below in Figure 14. As the head moves around, fluid is pushed into other sacks as it is displaced out of the compressed sack. The other sacks inflate and remain touching the head regardless of head position. The valves allow control of the speed at which the fluid can move from sack to sack, and will in theory resist fluid movement at high velocities. This will prevent the sack from collapsing when the head moves from a high impact force.

Benefits:

- Always in contact with helmet without needing to be attached to helmet
- No moving parts
- Should not inhibit movement
- Would be very similar in appearance to conventional neck rolls

Drawbacks:

- Worries about popping the vinyl
- Difficulties with leak-proof attachment to base of neck roll
- Heavy due to large amount of fluid
- Cost of large amount of dilatant fluid

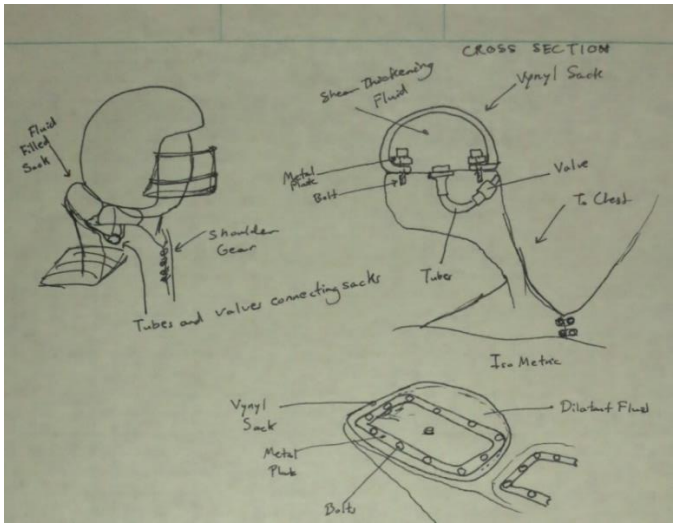

Figure 14: Concept design of the fluid filled neck roll

3.2.2 Design 2: Rotational Shock

The idea behind this design is that the back, vertical portion is allowed to rotate forward and backwards, as well as rotate side-to-side, with the use of two pivot points. The back portion is intended to follow the motion of the player's helmet with the incorporation of tethers or any other means necessary. The key feature of this design deals with the rotating mechanism. The back portion is attached to a "paddle" that rotates within a cylindrical space, as shown in the bottom diagram of Figure 15, and this whole space is filled with a dilatant, or shear-thickening, fluid. Under normal motion, the fluid will be very thin, allowing this paddle to move relatively easily, thus allowing unrestricted motion by the player. However, when the helmet experiences a sudden impact, the energy will be transferred through the paddle and the dilatant fluid will experience shear-thickening, absorbing the kinetic energy. As the fluid thickens, the rotation of the back portion will slow down greatly, as well as the player's head.

Benefits:

- Mechanical – parts can be machined
- Allows full motion under normal conditions yet limits these motions under hard impacts
- Fluid can be easily adjusted to modify properties
- Paddle mechanism can be easily modified to change mechanical characteristics
- Shear-thickening fluid is commercially available and can easily be made

Drawbacks:

- Does not provide the best protection against sideways rotations
- May be heavier than other designs (depending on material)
- Parts are exposed – may be damaged when hit by other players
- Tethers are not ideal – would be best if no attachment to helmet was needed
- More moving parts than purely material solution

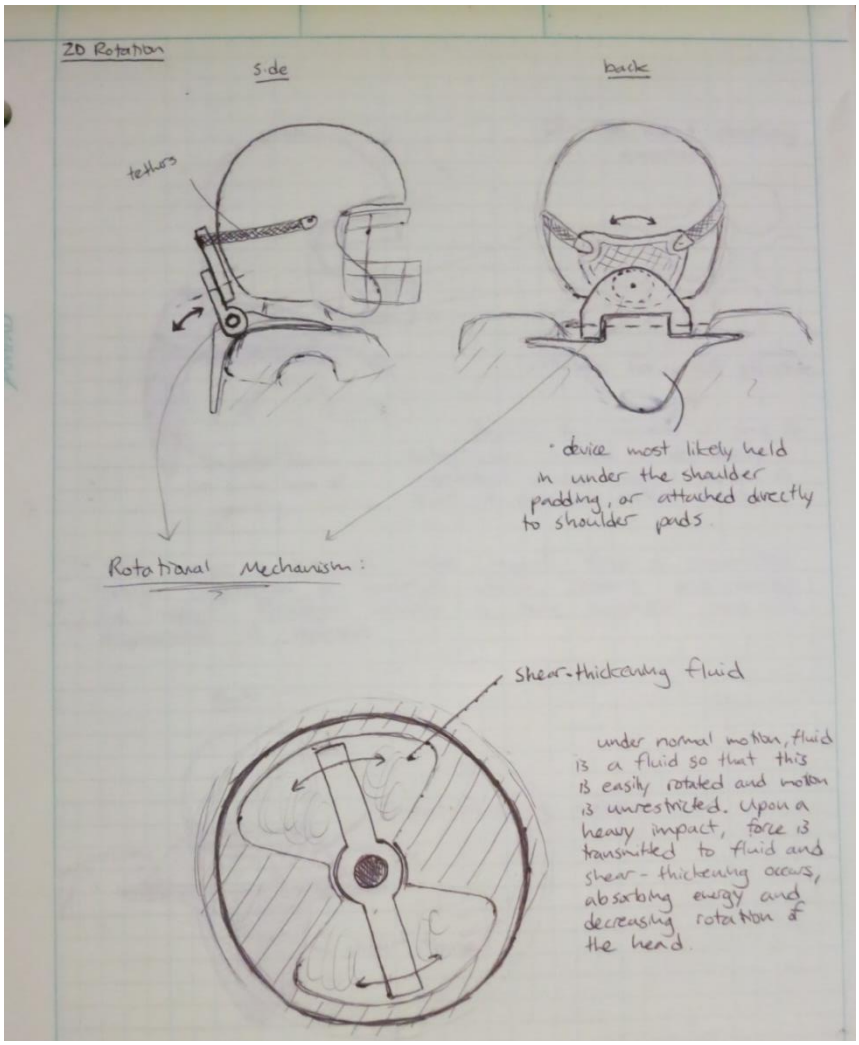

Figure 15: Concept drawing of the 2D rotational shock design

3.2.3 Design 3: D3O Neck Roll

D3O is a special impact absorbing material which is capable of being soft and flexible when unloaded, yet hardens under a heavy impact. It is currently used by a significant number of companies for a variety of applications, including shoulder/knee pads, BMX helmets, ski gear, and more.

This design is very similar to a traditional neck roll in shape and location, with the exception being the portion in contact with the helmet, made out of a special type of impact absorbing material. The lower portion can be made out of some type of foam or plastic. Under normal playing conditions, the goal with this design is to provide a material that is as soft and flexible as possible so that motion is unrestricted for the player. However, when hit with a hard impact that causes the helmet to come in contact with the material at a high velocity, the material will harden and absorb the impact energy while also limiting the rotational displacement and velocity of the head. When the effect of the impact is dissipated, the material would then go back to its soft, flexible state. A visual of this is provided below in Figure 16.

Benefits:

- Has potential to be very lightweight
- No moving parts – simple
- Benefits of traditional neck roll without the motion restrictions
- Material proven to absorb energy (D3O)

Drawbacks:

- Material may be hard to obtain/expensive
- Manufacturability – do we have the ability to form this material into the shape we want?
- Material may not be as flexible as we want it to be – will still limit motion to certain degree
- We do not have the freedom to change material properties

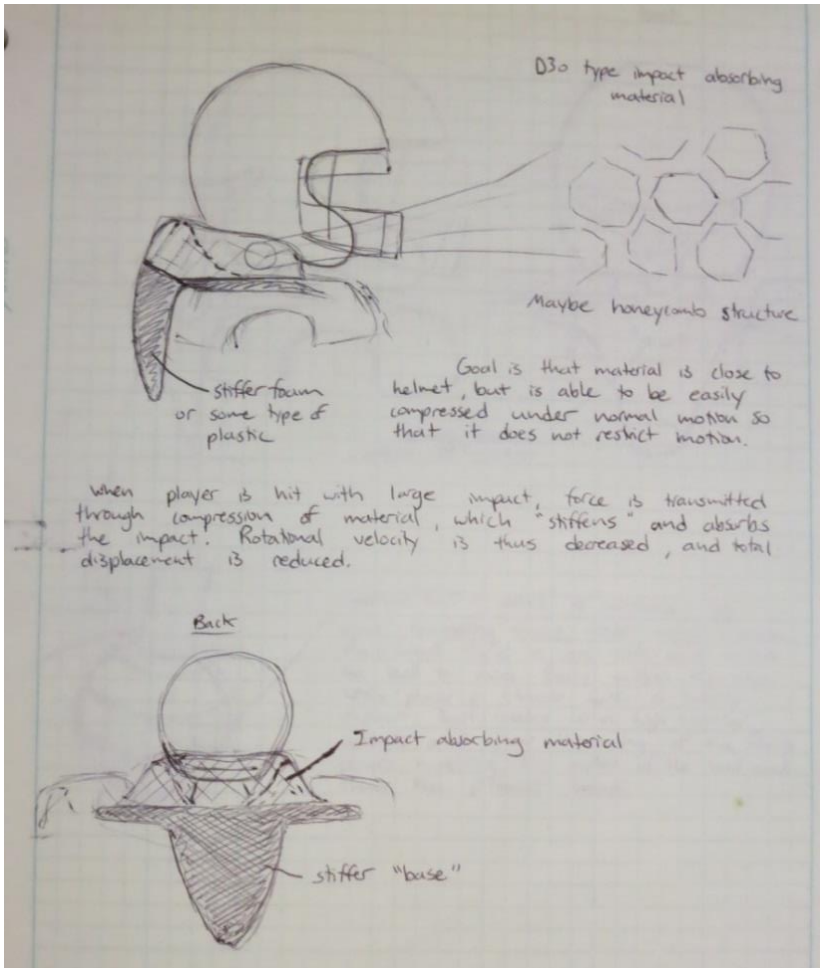

Figure 16: Conceptual design of the D3O neck roll

3.2.4 Design 4: 3D Spherical Rotating Shock

While trying to improve on the 2D rotational shock idea which is limited by the fact that each shock can only move in one plane, we came up with the idea of a three-dimensional shock. Rather than trying to account for the multiple degrees of freedom of the head by adding multiple traditional rotating shocks to the back piece, as shown in the 2D rotation drawing in Figure 15, it was decided to try to take care of every degree of freedom with one, confined, spherical ball rotating shock.

The spherical ball-in-cup idea is able to limit rotations front-to-back, side-to-side, around the centerline axis from the base of the neck up through the top of the head, as well as any combination of these. This design also incorporates a shear-thickening fluid within the "cup" that the spherical ball sits in. As shown in the diagram below in Figure 17, the ball and socket would not be smooth – they must include some type of shape that would actually transmit forces to the fluid. Therefore, under normal motion, the ball is able to move almost completely freely with little resistance from the fluid, yet when a heavy impact transmits a high force to the fluid, it thickens and thus absorbs the shock. This can accomplish the same as the 2D rotational shock except in every direction.

Benefits:

- Is able to restrict rotation about every axis
- Limited number of moving parts
- Only one fluid-filled section – less potential for leaks
- Only contacts the helmet in the back – does not get in the way of the player like traditional neck roll
- Can be machined
- Allows for experimentation with different fluids

Drawbacks:

- Effective seal between ball and socket will be vital to success of product
- May be difficult to machine certain parts (ball, socket)
- Location of the pivot point not ideal for sideways rotations – may cause critical moments around the neck
- Must be attached to the helmet for maximum potential

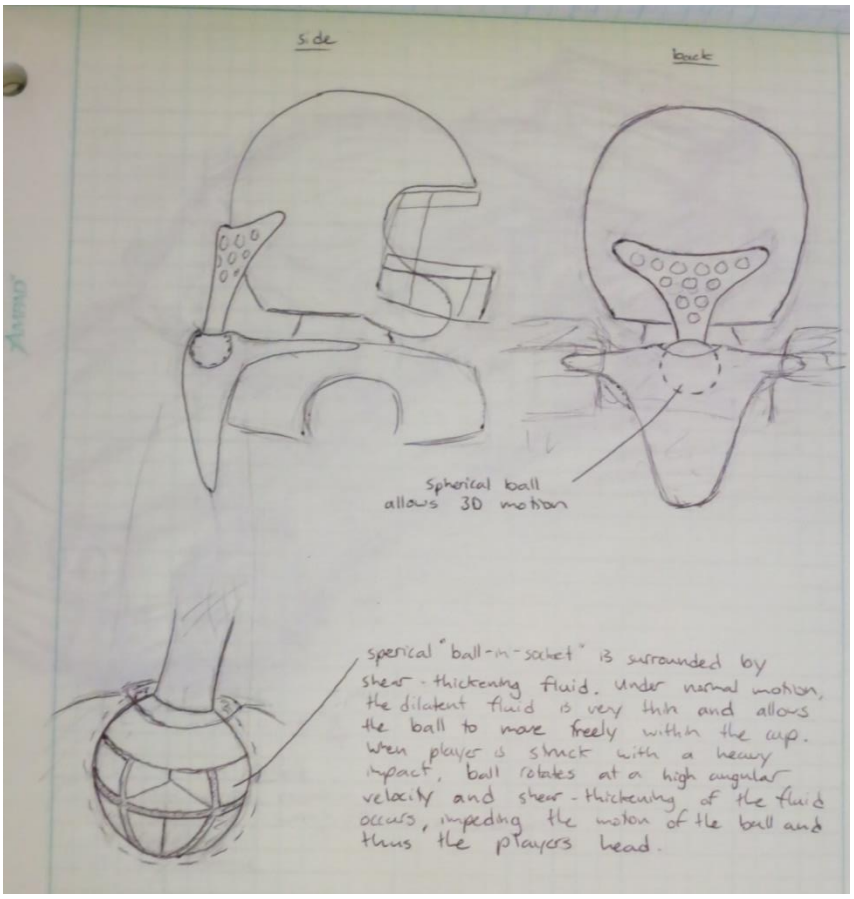

Figure 17: Conceptual design of the 3D rotational shock

3.2.5 Design 5: Rotational Shock Neck Roll

The rotational shock neck roll allows a more traditional neck roll that does not incorporate a displacement of a smart material directly as its stiffening media. Instead, lightweight pads are extended up to the center of gravity of the head and helmet that are lightly spring loaded towards the helmet, as shown below in Figure 18. They remain in contact with the helmet at all times without being attached and apply force perpendicularly to the helmet. The pads are attached to rotational shocks that resist movement if the helmet pushes quickly on the pads from an impact. It is essentially a neck roll that is always there and can move easily until impact occurs. The outside of the pads and the shocks will be covered in a soft foam or other material - it will appear as though there is no mechanism.

Benefits:

- Lightweight
- Easy to machine
- No complex parts
- Strong
- Simple
- Would not restrict motion

Drawbacks:

- Shocks may need to be rather large to resist the motion
- Still requires possibly expensive dilatant fluid, though most likely not a significant amount
- Would not stop the head if hit in chest from front

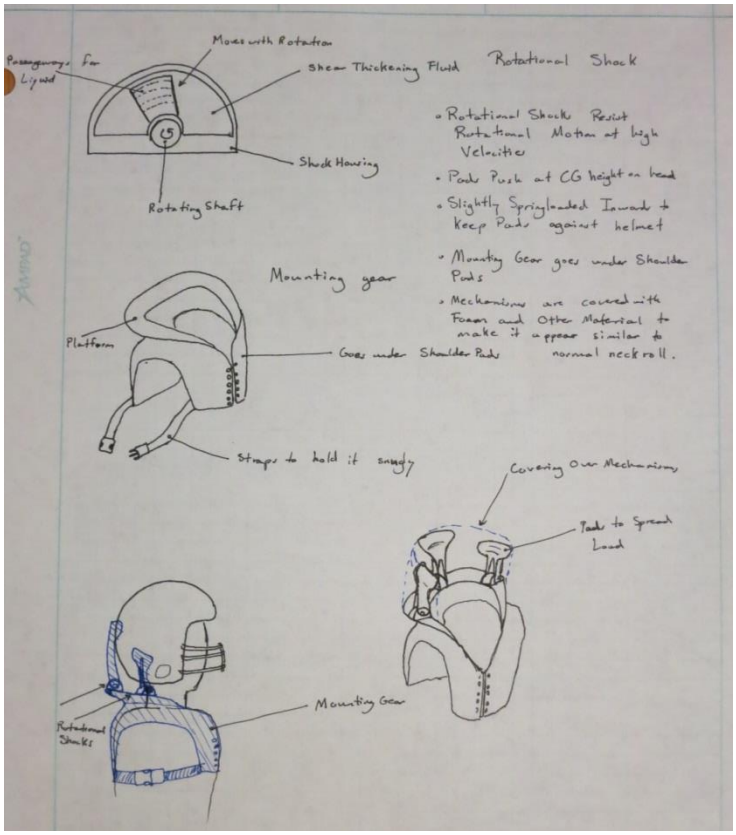

Figure 18: Conceptual design of the rotational shock neck roll

3.3 Analysis of Design Alternatives

As mentioned previously, a decision making matrix, shown in Table 2, was created to help choose the best design. Similar to the rank-ordering done in Table 1, each design constraint was given a relative weight. In order to normalize the weights, we ensured each constraint accounted for a percentage of the overall design. With the total of the weights being 100, this means we felt that the ease of removing the apparatus was 6% of the design. Each design was then rated at each design constraint on a scale of 1 through 3; 1 representing a design that fulfilled the constraint poorly, and 3 representing a design that warranted an excellent fulfillment of design constraint. The score of each design was multiplied by the weight and added to create the total score for each design. The maximum score a design could receive is 300.

Table 2: Decision making matrix of the preliminary design options

Constraint	Weight	Fluid Neck Roll	2D Rotational Shock	D3O Neck Roll	3D Rotational Shock	Rotational Shock Neckroll
Easily Removable	6	3	2	3	2	3
Impact	12	2	2	3	2	2
Operating Temp.	2	3	3	3	3	3
Not restrictive	12	1	2	1	2	2
Comfort	10	2	2	3	2	3
Moisture Retention	2	2	3	2	3	3
Weight	7	1	2	1	3	3
Risks Posed	20	3	2	3	2	3
Price	7	1	3	1	2	2
Ease of Cleaning	2	2	2	2	2	2
Part Availability/ Manufacturability	12	1	3	2	2	3
Simplicity	8	2	3	3	2	3
Total		**190**	**231**	**232**	**211**	**267**

3.4 Proof of Concept

The chosen design is the Rotational Shock Neck Roll which proved to be superior in most of the design constraints (see Table 2). Two important constraints that this design was clearly excellent in were risks posed and part availability/manufacturability. We believe this design poses very little danger to the wearer and other players because while it is not directly attached to the helmet, it will be pressing against the helmet at all times leaving no space for a pinch point like in some of the other designs. We also felt that with this design the materials were all readily available to us-common metals, fluids, plastics-and that the machining was within our capabilities as a team.

3.4.1 Preliminary Calculations

In order to prove the feasibility of the rotational shock concept, it was necessary to examine the fluid flow through the device. While we all felt that such a design would react as expected, it is important to determine that such a response is possible with the design size constraints we have. For example, if it was proven that our design would work, but with a diameter of 12 inches for the shock compartment, this design would clearly not be feasible based on size constraints.

The rotational shock idea is very similar to that of common shock absorbers, except involving rotational rather than translational motion. The governing mechanism for this design is the displacement of a fluid, within a confined compartment. The “lever” extending from the base of the device to the outer shell of the helmet will be directly connected to a “paddle” located within a semi-circular cross-sectional compartment, as shown in Design Alternative 5 above. As the paddle is rotated through the compartment, fluid within the compartment is forced through a hole(s) in the paddle. At normal operating speeds, the goal is that the shear rate and subsequently the viscosity of the fluid will remain relatively low, ensuring that the fluid will travel through the hole with ease and the lever will not restrict any head motion by the player. Upon a heavy impact, with both high accelerations and velocities acting on the lever by the helmet, a much greater fluid flow will be required to pass through the hole(s) in the paddle, significantly increasing the shear rate of the fluid. This increase in shear rate will cause the fluid to shear-thicken, increasing the viscosity greatly. This increase in viscosity will increase the pressure difference across the hole, providing the paddle with much more pressure than experienced under normal condition, which will in turn provide a counteracting force on the helmet. This force will act against the motion of the head, thus reducing both the accelerations and velocities experienced by the head.

To prove the possibility of this, the general Hagen-Poiseuille equation was used which can be rearranged to produce:

$$\frac{dP}{dx} = \frac{8\mu Q}{\pi r^4}$$

Here Q is the volumetric flow rate through the hole, μ is the dynamic viscosity of the fluid, and dP/dx is the pressure difference between the inlet and outlet of the hole. In order to calculate the volumetric flow rate through the hole in terms of the angular velocity of the paddle, one can write:

$$Q = \frac{dV}{dt}$$

$$V = (\pi R^2)\left(\frac{\theta}{2\pi}\right)L$$

where R is the radius of the cylindrical chamber, θ/2π is the percent of a full circle the chamber actually is (i.e. if the change is half a circle, this ratio would equal 0.5), V is the volume of the chamber, and L is the length of the chamber. Differentiating the volume with respect to time, one gets:

$$\frac{dV}{dt} = \frac{\pi R^2 L}{2\pi}\frac{d\theta}{dt}$$

$$\frac{dV}{dt} = 0.5R^2 L\frac{d\theta}{dt}$$

where

$$\frac{d\theta}{dt} = \omega = \frac{v_h}{d}$$

Here v_h is the translational velocity of the head at the point of contact between the helmet and the lever, and d is the distance from that point of contact to the axis of rotation. Substituting this expression into the previous equation, one gets:

$$\frac{dV}{dt} = \frac{R^2 L v_h}{2d}$$

Finally, using the original Haben-Poiseuille relationship and combining with the above equation, one gets:

$$\frac{dP}{dx} = \frac{8\mu}{\pi r^4}\frac{R^2 L v_h}{2d} = \frac{4\mu R^2 L v_h}{\pi d r^4}$$

$$dP = \frac{4\mu R^2 L v_h}{\pi d r^4}dx$$

Understanding that dx is the total length of the hole, we arrive at the following equation for the change in pressure:

$$\Delta P = \frac{4\mu R^2 L v_h x}{\pi d r^4}$$

In this equation, it is assumed that there is negligible pressure at the outlet of the hole, so ΔP is fully equal to the inlet pressure, which is equal to the pressure within the compartment that is being compressed. This pressure can then be converted into a force given that:

$$\Delta P = \frac{F_{avg}}{A}$$

$$F_{avg} = \Delta P \cdot A$$

Here A is the total area on the paddle that the pressure is acting on. Assuming a minimum of 0 force acting at the rotational axis and a maximum force acting at the outermost section of the paddle, furthest away from the rotational axis, it was therefore assumed that the average force is acting at a distance of 2/3R, or 2/3 the radius of the paddle.

In order to calculate the force acting back on the head at the point of contact between the helmet and the lever, a simple moment analysis was performed:

$$\left(F_{avg}\right)\left(\frac{2}{3}R\right) = (F_H)(d)$$

where F_H is the force acting back on the helmet. Rearranging:

$$F_H = \frac{\left(F_{avg}\right)\left(\frac{2}{3}R\right)}{d} = \frac{(\Delta P \cdot A)\left(\frac{2}{3}R\right)}{d} = \frac{4\mu R^2 L v_h x}{\pi d r^4}\frac{A\left(\frac{2}{3}R\right)}{d}$$

$$F_H = \frac{8\mu R^3 L v_H x A}{3\pi d^2 r^4}$$

where:

$$A = RL - \pi r^2$$

Looking at the equation above for the force acting on the head, a number of important relationships can be observed. For one, the greater the viscosity, length of the compartment, and thickness of the hole, the greater the force acting back on the head will be. The force increases quadratically with an increase in the paddle radius, as well as with a decrease in the radius of the hole. Furthermore, decreasing the moment arm, d, will also increase the force exponentially by a factor of 2.

A Microsoft Excel program was created to quickly calculate the force acting back on the head based on these parameters. As a reference, a few different values were input to understand the difference in forces experienced. The following estimates were used in our calculation: moment arm was assumed to be 15 cm, the radius of the paddle was assumed to be 7 cm, the length of the compartment was assumed to be 4 cm, the radius of the hole was assumed to be 1 cm, the depth of the hole was assumed to be 1.5 cm, the viscosity of the fluid assumed to be 1 Pa.s, the velocity of the head assumed to be 0.1 m/s, and the

force acting on the helmet was assumed to be 0.2 N. This is a representation of the model under normal operating conditions. Assuming a hit increases the velocity of the head to 7 m/s and the increase in shearing of the fluid causes it to rise to 100 Pa.s, the force acting back on the head, with all other values held constant, would be 1350 N. Clearly, a significant increase in force acting back on the head is achievable.

In order for the fluid to undergo shear-thickening, a change in shear rate must be evident. Shear rate through the hole can be calculated using:

$$\dot{\gamma} = \frac{8v_f}{2r}$$

Here v_f is the average velocity of the fluid through the hole, and $\dot{\gamma}$ is the shear rate. In order to calculate the velocity of the fluid through the hole, one can use:

$$Q = v_f A$$

$$v_f = \frac{Q}{A}$$

Based on the calculations above, one gets:

$$Q = \frac{dV}{dt} = \frac{R^2 L v_H}{2d}$$

Therefore,

$$v_f = \frac{R^2 L v_H}{2d\pi r^2}$$

$$\dot{\gamma} = \frac{2R^2 L v_H}{d\pi r^3}$$

Based on this equation, we can see that as the velocity of the head increases, so does the shearing rate. This is vital because in order for the fluid to thicken, it must experience a greater shearing rate which is proven with this equation.

While these equations appear to provide significant evidence for our design, in reality, there are a significant number of additional factors which must be taken in to consideration. A number of assumptions go along with these equations, including steady-state flow which clearly is not the case for this device. Therefore, more advanced calculations, most likely involving computer modeling, will be necessary to gain a more in-depth and accurate representation of the device.

3.4.2 Finite Element Analysis

To test the theory of the Newtonian fluids acting inside the device, ANSYS Fluent finite element analysis software was used to simulate pressures acting on the paddle. A rectangular duct with a wall in the middle was modelled to represent the casing and paddle. The wall inside the duct was fitted with holes to represent the holes in the paddle. A fluid was then programmed to flow at a specified velocity from one side of the duct to the other, through the holes in the wall, to simulate the paddle moving in the casing. A graphic showing the flow model is displayed below in Figure 19.

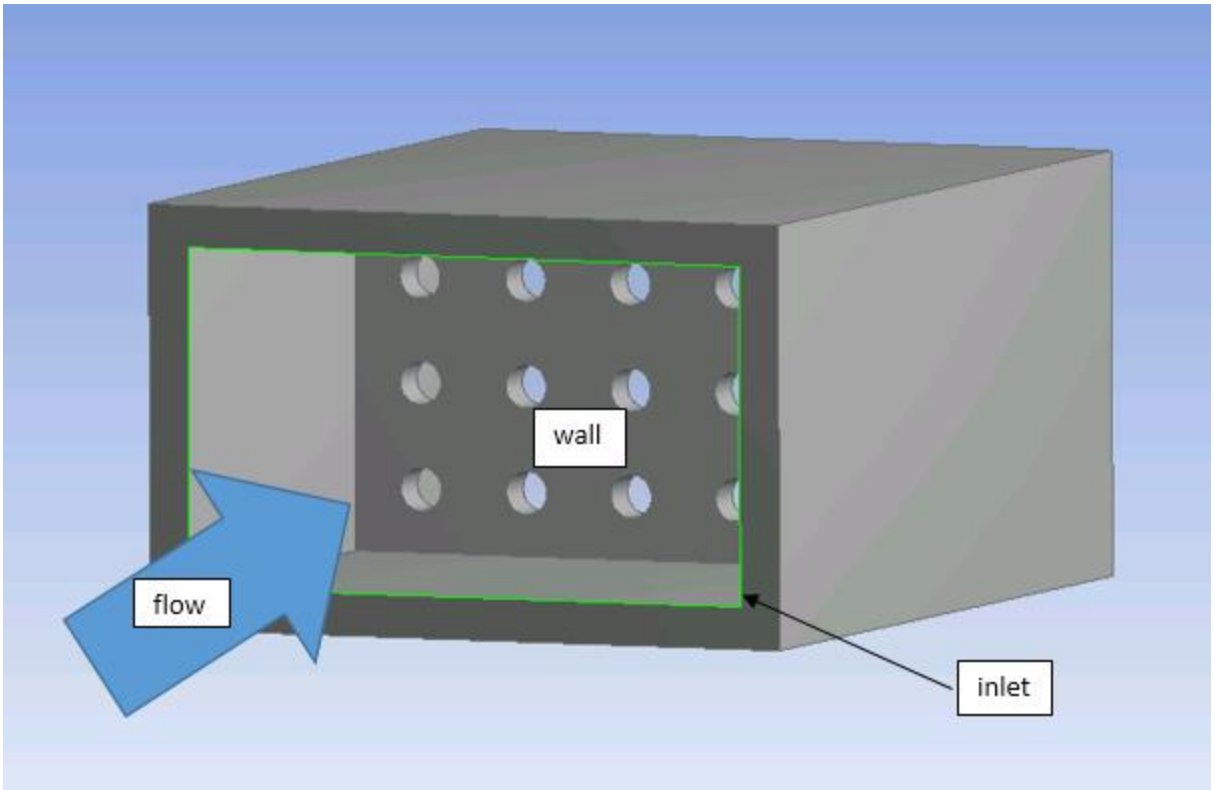

Figure 19: ANSYS Fluent analysis of fluid flowing through paddle

The fluid velocity was initially set at low speeds and increased incrementally to high speeds representing a full range of player head movement from nominal conditions to concussive-type impacts. Various fluids were tested within the ANSYS program in order to understand the relationship between different viscosities and densities as well as the relationship that hole patterns had with these fluids.

Engine oil tests were run at 1, 10, 20, 50 and 100 m/s inlet velocities and the maximum pressures on the paddles were recorded. These fluid speeds relate to head speeds between .18 m/s and 18 m/s. The range for typical head speeds from typical football impacts is between 3 m/s and 9 m/s. The graphic below shows a pressure contour graph of one of the engine oil flow trials. This trial's velocity was set to a speed of 1 m/s and the maximum pressure on the wall can be observed as the darkest red color.

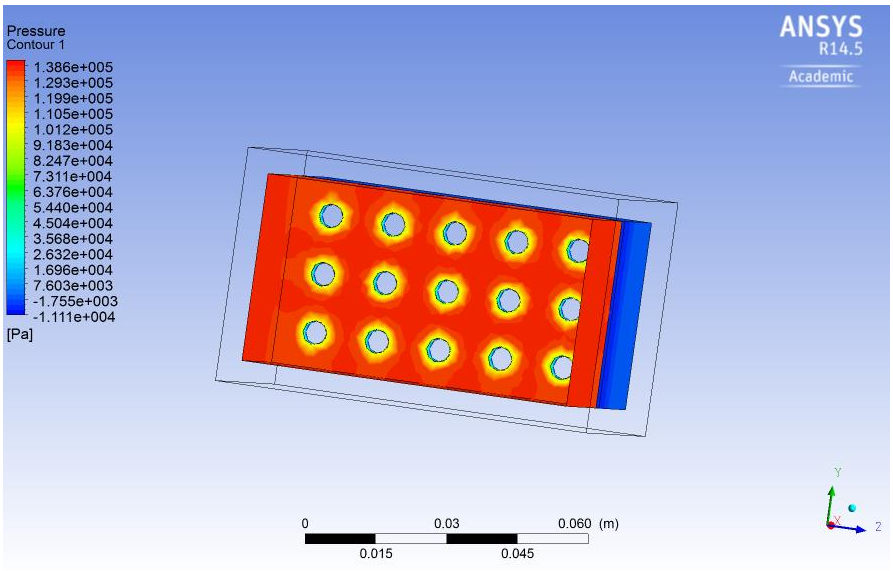

Figure 20: Example pressure distribution on paddle within ANSYS

Figure 20 above shows that most of the pressure on the wall is uniform with sudden pressure drops close to each hole. Data from all five trials were recorded and the maximum pressures are displayed on the graph below.

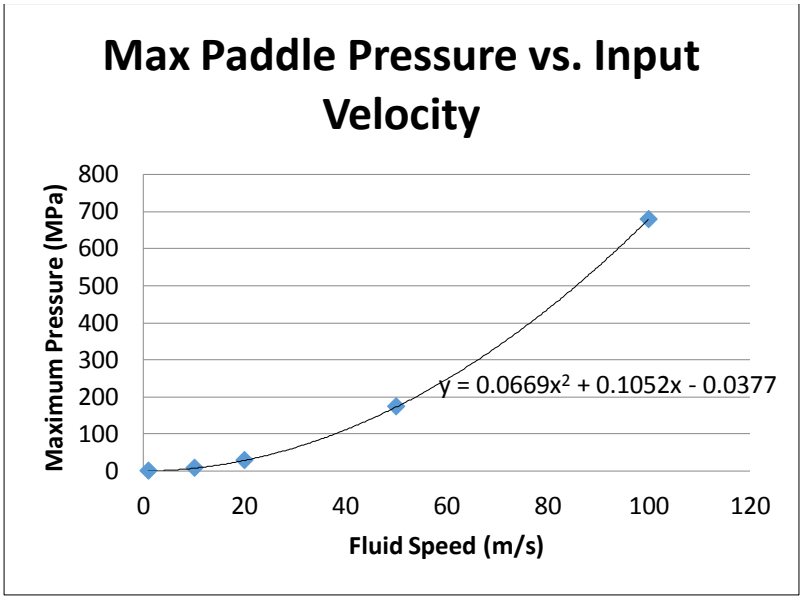

Figure 21: Paddle pressure versus input velocity of paddle

Figure 21 above shows that at low fluid speeds the pressure will be very low and at higher speeds the pressure will rise steeply. This suggests that when a football player is moving his head during a game normally, there will be limited resistive forces from the device due to the low pressure in the device. During a large impact force however, the fluid speed is much greater, causing the device to resist the motion of head through exponentially higher internal pressure.

4.0 Final Design

With the proof of concept calculations complete, the rotational shock absorber design was expanded upon to manufacture. The design went through multiple iterations before the final product. The following sections outline the design process and manufacture of the rotational shock.

4.1 Design Iterations

With the rotational shock neck roll design chosen, the final design was modeled in SolidWorks 2013. A variety of iterations were made before a final design was produced. Since the most important and complex component of the device was the two case halves, the section containing the rotating paddle and fluid, the initial design iterations consisted solely of changes to this component. Once a final iteration and design for the case half was agreed upon, the team moved onto designing the remaining components.

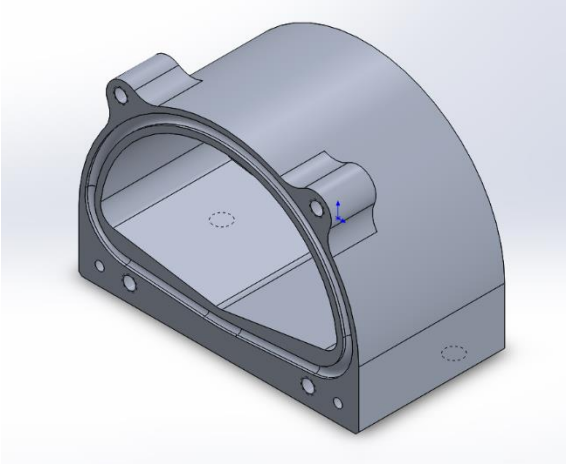

Figure 22: Isometric view of the first design iteration for a case half of the rotational shock absorber.

Figure 22 above displays the very first iteration of one of the case halves. While the final design is fairly different in appearance, most of the vital features of this design remain throughout each iteration, involving mainly slight modifications to their size and placement. In order to hold the two case halves tightly together, four #10-24 bolts were used. To align the two case halves nearly perfectly, one case half needed dowel pins press-fit into two holes, while the other case half would have holes just large enough for the dowel pins to fit. The combination of these dowel pins and the four bolts would ensure a tight, restrictive fit between the case halves. A rubber O-ring was chosen to ensure that the surfaces in contact between the two halves are sealed effectively to avoid pressure leaks. As a result, it was necessary to include an O-ring groove into one of the halves.

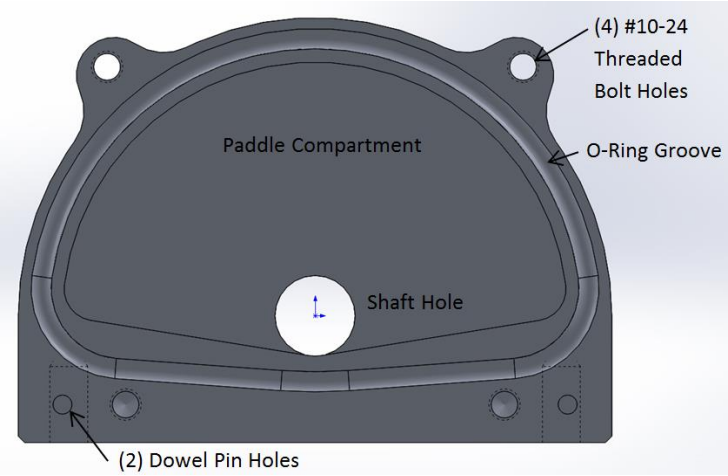

Figure 23: View of the inside of one of the case halves with call-outs to main design features.

With these defining features determined, the iteration process began. It should be noted that the two case halves are nearly identical with only slight logistical differences, and the case half in focus throughout the design iterations contains the O-ring groove, the threaded #10-24 holes, as well as the press-fit dowel pin holes.

The major area for improvement on design iteration two deals with the large sections of material in the bottom right and left corners of Figure 24 below. While it was initially thought that this section could be utilized as an attachment point for the device by drilling and tapping holes in the bottom surface, it was determined that this was not the most resourceful method of doing so as this section adds a significant amount of unnecessary weight.

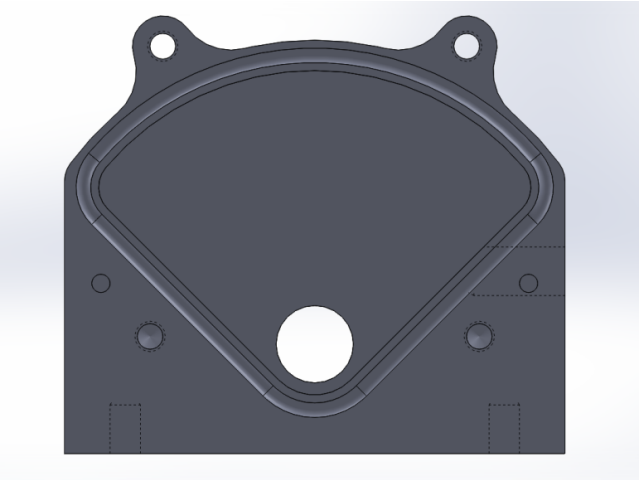

Figure 24: Iteration Two

Design iteration three was created while attempting to reduce unneeded material, as shown in Figure 25 below. All of the major features can be seen – the four #10-24 threaded holes, the two dowel pin holes,

the 90 degree paddle compartment, the O-ring groove, as well as the shaft hole – in addition to two additional ¼" holes. Rather than use threaded holes as attachment points, it would be both stronger and help minimize the size of the device by using ¼" diameter holes as the attachment point. While the amount of unnecessary material was reduced, the design lacked the desired symmetry and hence iteration four was completed.

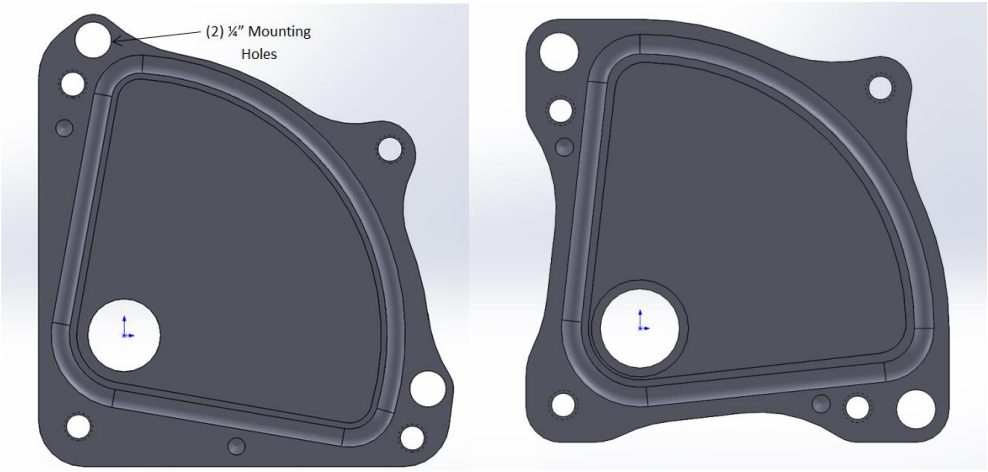

Figure 25: Iteration Three (left) and Iteration Four (right)

As shown in Figure 25 above, design iteration four incorporates all of the vital features while also involving symmetry and removing even more unnecessary material. In order to arrive at this design, it should first be noted that the angle of the paddle compartment was slightly decreased as it was realized that in order to achieve a full 90 degrees of paddle rotation, the compartment could be slightly smaller due to the fact that the thickness of the paddle is much less than the diameter of the paddle section through which the shaft is positioned. This decrease in size allowed all vital features to fit nicely within the paddle while also allowing removal of all unnecessary material. The final design will be discussed in much greater detail in the following section.

4.2 Design Description

In order to effectively explain the final design of the device, it is most beneficial to understand the key features of the device and how these led to major design features. The key requirements vital in ensuring proper performance of the device included:

- Tight-tolerances and Maintenance of Internal Pressure
- Player Interferences and Pad Placement
- Instant Response Reaction of Device
- Performance Tuning
- Manufacturability/Machinability

Some of these requirements are further broken into sub-sections describing specific design features included to support the major requirements of the device.

4.2.1 Tight-Tolerances and Maintenance of Internal Pressure

To maintain internal pressure within the paddle compartment, tight-tolerances were essential in many of the device components. In addition to these tight tolerances, a variety of components were included to provide a tight seal between the internal compartment and ambient air, including an O-ring and seals. The reasoning behind the use of certain specific components is explained in the following sections.

O-Ring Groove

To ensure a perfect seal between the two case halves to prevent pressure from escaping from the internal paddle chamber, the team decided that an O-ring would be the best method of providing this seal. As a result, one of the case halves incorporated an O-ring groove to hold the O-ring in place, while the surface on the other case halve remained flat to compress the O-ring within its groove.

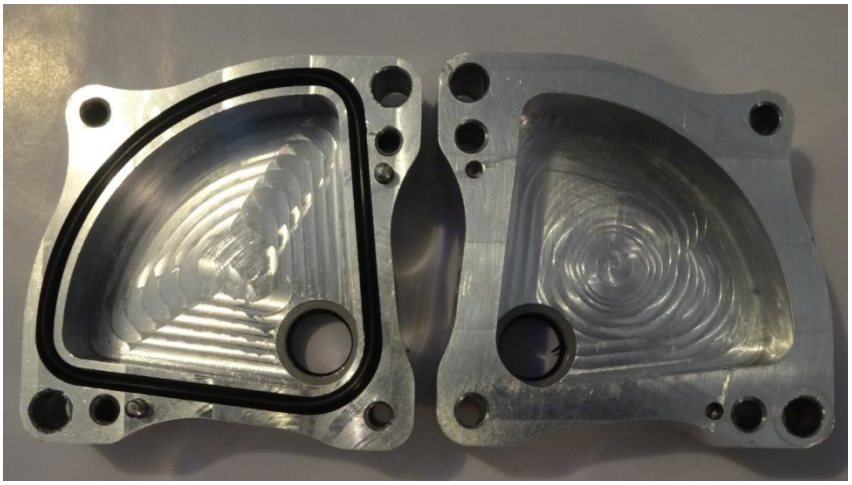

Figure 26: O-ring in groove on left, flat surface on right

As shown in Figure 26 above, the case half on the left contains the groove for the O-ring with the O-ring currently in it, while the case half on the right simply has a flat surface to compress the O-ring. In order to design the groove, a number of important parameters were considered including the total length of the groove, the cross sectional area of the groove, tooling readily available to machine the groove, as well as the percent diameter of O-ring to be compressed, all vital in ensuring a proper seal. Because there are limited O-ring sizes available from the manufacturer, an iterative process was required to finalize the size of the groove as well as the size of the inner paddle chamber.

Firstly, a 3/32” soft buna-N O-ring with a durometer hardness of A50 was selected, providing better sealing properties when compared to the normal buna-N O-rings with a durometer hardness of A70. The softer O-rings were also preferred as they require less force to compress, beneficial in minimizing the forces on the aluminum threads holding the halves together. As illustrated in Figure 27 below, one can see that the

final design included an O-ring groove length of 7.51 inches. The O-ring chosen had actual inner and outer diameters of 2.237 inches and 2.443 inches, respectively, resulting in a central cross-sectional circumference of 7.35 inches using:

$$circumference = \frac{(D_{in} + D_{out})}{2} \cdot \pi$$

where D_{in} is the actual inner diameter and D_{out} is the actual outer diameter. Based on these lengths, the O-ring is stretched approximately 2.20 %, very close to the recommended 2% stretch [26].

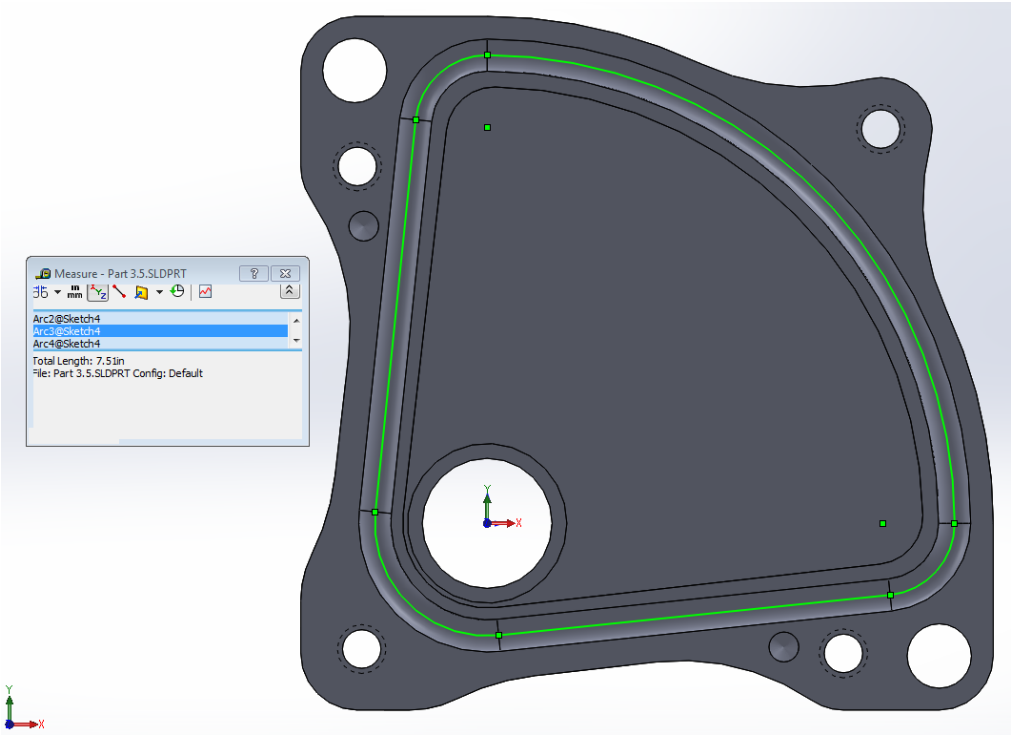

Figure 27: CAD model highlighting O-ring groove length

Furthermore, it was necessary to ensure that the O-ring groove was designed properly to allow enough area for the O-ring to fully compress within. In order to machine this groove, a standard 1/8 inch ball end mill was utilized. The 3.32" O-rings have an actual diameter of 0.103 inches, ensuring that they would fit nicely within the 0.125 inch wide groove. Based on this diameter, the cross sectional area of the O-ring was calculated to equal 0.0083 in^2. As shown in Figure 28 below, the cross-sectional area of the groove is dependent on the size and shape of the end mill, as well its depth. Based on simple geometry, this area was calculated with the equation

$$A_{cs,groove} = 0.5\pi {r_{em}}^2 + ((D - r_{em}) \cdot 2r_{em})$$

where r_{em} is the radius of the end mill bit and D is the total depth of the groove. Using values found in the figure below, the result is a cross-sectional area of 0.009 in^2. Based on these cross-sectional areas, there

is 0.001 in^2 of cross-sectional area open with the O-ring fully compressed, therefore the O-ring would be compressed the maximum possible while leaving the smallest possible gap in the groove. The figure below demonstrates the size of the uncompressed O-ring compared to the size of the groove. The 17% diameter compression of the O-ring was acceptable provided that static O-ring should not be compressed more than 30% [25].

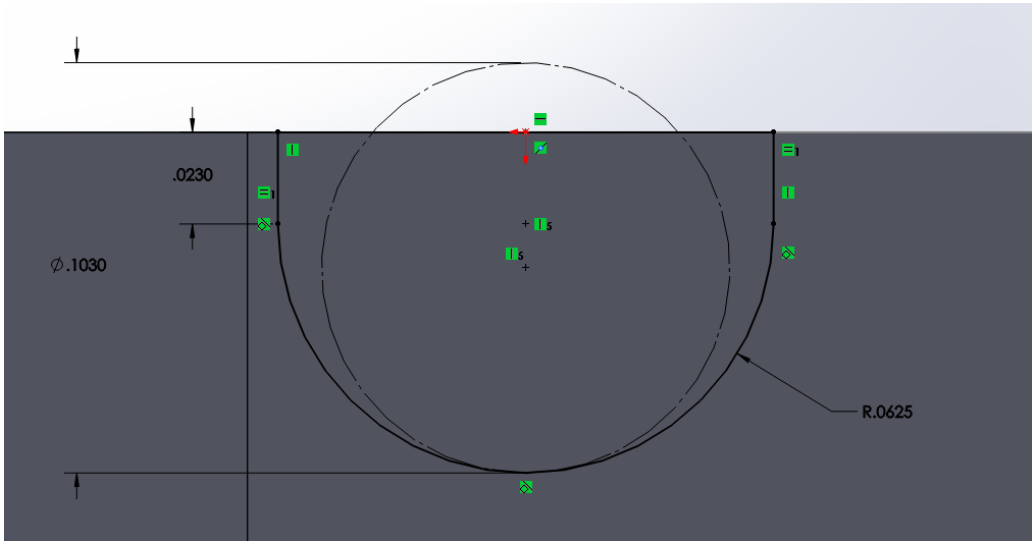

Figure 28: CAD cross-sectional view of O-ring groove and O-ring with dimensions

The O-ring fit into the groove exactly as expected. The case-halves were dismantled and reassembled countless times throughout testing, all through which the O-ring never showed any signs of damage or tears as would occur if the O-ring was pinched in any way. Furthermore, no leaks between the two case halves were observed throughout any testing of the device, proving the design effectiveness of the O-ring groove.

Delrin Acetal Resin Bushings

With such tight tolerances between the paddle and the internal case walls, even tighter tolerances were necessary between the case halves and the steel shaft in order to avoid any unwanted contact between the case walls and paddle. Additionally, it was beneficial to reduce friction around the shaft to allow easy, un-inhibited movement of the device under fluid-free conditions. Therefore, a number of options were considered including needle bearings, some type of bushing, or even direct contact between the case halves and the shaft. The third option was quickly discarded as aluminum to steel contact would not only involve rather significant frictional forces when in contact, but also would most likely result in the aluminum wearing rather quickly throughout our testing. Needle bearings would provide a tight tolerance, friction-free fit, but both size limitations and the desire to keep total weight of the device to a minimum prevented use of needle bearings. It was agreed that some form of bushing would be ideal.

It was immediately chosen that a plastic bushing would be preferred over any other material. With a wide range of plastics to choose from, Delrin acetal resin stood out due to its moisture resistance, smooth/lubricated surface, wear-resistance, and ability to hold tight tolerances. Furthermore, Delrin acetal resin is known for its use in parts requiring both strength and rigidity, specifically including bushings.

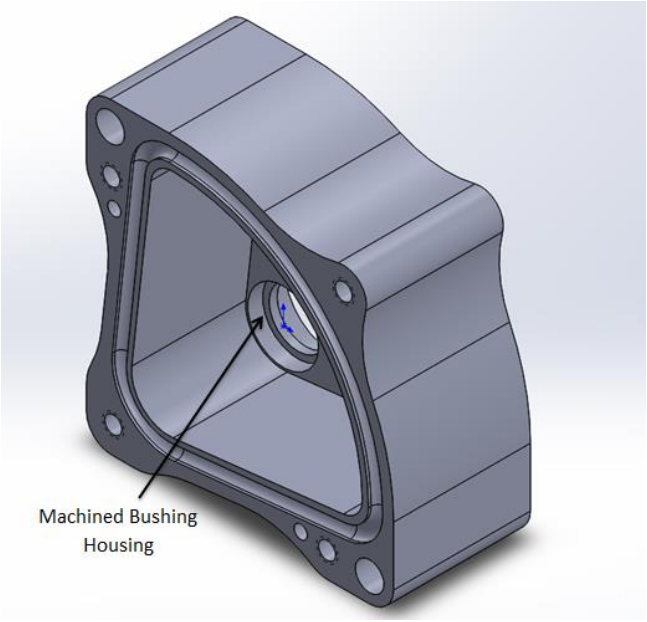

Figure 29: CAD image depicting interior bushing housing

The cases were designed to include a small housing, only 0.62 inches in diameter and 0.13 inches in depth, within the side walls to accommodate a small, thin bushing. This housing can be seen in Figure 29 above. We chose to go with a rather thin bushing with a thickness of only 0.06 inches to both fit well within the device as well as to minimize total shaft displacement if the bushing were to compress when under a high force. The bushings were turned out of a solid rod on a manual lathe, involving reaming the inside diameter with a 0.5000 inch diameter reamer to provide a tight-tolerance fit with the shaft. A clear image of the bushing within a case half can be seen in Figure 30 below.

Figure 30: Delrin acetal resin bushing firmly in place within case half housing

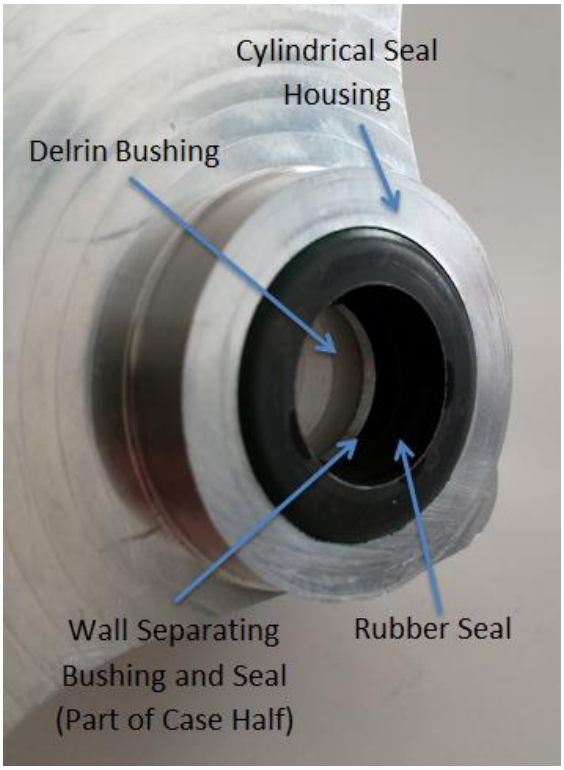

Figure 31: Seal, case, and bushing interface

Shaft Seals

In addition to the O-ring used between the two case halves, a tight seal was necessary between the steel shaft and the case halves to prevent any pressure leaks at this component interface. With such tight tolerances between the steel shaft and the Delrin acetal bushings, it was predicted that a significant amount of the pressure would remain within the compartment with such little space for it to escape. However, to ensure a proper seal, high pressure metal-rubber shaft seals were chosen. In order to hold this seal in place, it was necessary to incorporate a seal housing on the outside of both case halves which the seals could be pressed into. A clear figure defining the shaft housing, seal within the housing, as well as the location of the Delrin acetal bushing can be found in Figure 31.

Pressing the seals into their housing was accomplished as expected – a fairly tight fit but not to the point where any damage was done to the seal or the pocket it was pressed into – which was a good sign that proper dimensions were chosen. As shown in Figure 32, the steel shaft also fit very tightly in the seal, and no leaking problems were encountered throughout the testing of the device.

Figure 32: Steel shaft through rubber seal on assembled device

Dowel Pins

The tight tolerances between the moving paddle and case walls required everything to be aligned very precisely, more precisely than the bolts holding the case halves together could enable. Therefore, dowel pins were chosen to be added to the device on one of the case halves, and alignment holes in the other case half. This allows a near perfect alignment of the two case halves.

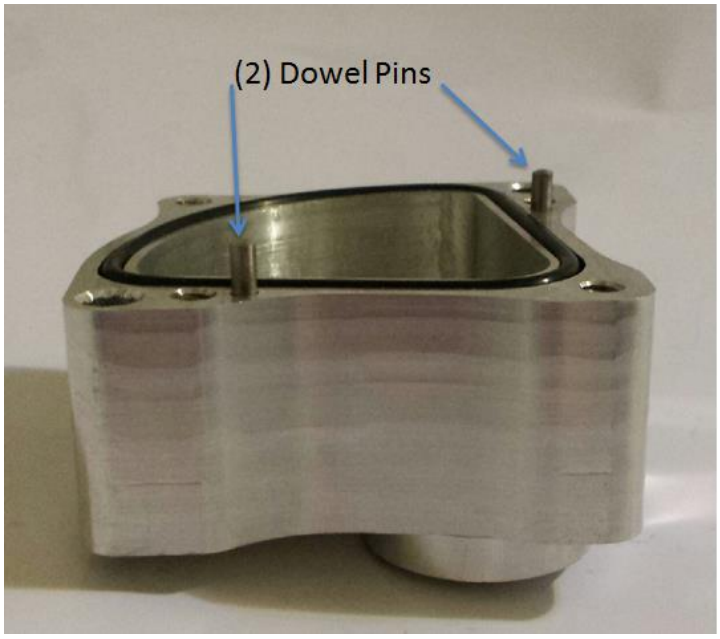

Figure 33: Dowel pins pressed into O-ring case

4.2.2 Player Interference and Pad Placement

Determining the size of the case halves, in turn directly influencing the size of the internal paddle compartment, was somewhat of a tradeoff between three factors: total size, weight, and design effectiveness. While increasing the size of the compartment increases the effectiveness of the device as a shock absorber, it also negatively increases the room required to mount the device on the player, along with increasing the total weight. A major concern was that a player would be unwilling to wear a device that weighs a significant amount and also takes up a significant portion of space around their head, hindering both their comfort and range of motion. On the other hand, too small of a device may provide greater comfort to the player, but it would also decrease the ability of the rotational shock to absorb impacts as effectively. Therefore, it was agreed that a practical device would fit nicely within the empty space evident between the back of the neck and the surrounding shoulder pads without extending significantly beyond the shoulder pads. This empty space can be seen in Figure 34 below. Based on rough estimates, the team concluded that the side profile of the device should be able to fit within a 3 inch x 3 inch square area, and the total length should not exceed 4 inches, approximately the diameter of a human neck.

Figure 34: Empty space in shoulder pads

The location of the device relative to the body is important as it determines a number of vital factors including the length of the arms as well as their shape, the placement of the pad relative to the helmet and arms, and most importantly, the total range of motion of the pad and arms and consequently the paddle within the cases. Ideally, the goal was to achieve as much rotational motion out of the paddle a possible throughout the player's normal head movement. Greater rotation of the paddle correlates to greater fluid flow and in-turn greater mass transfer as the paddle forces fluid from one side of the paddle to the other, along with greater rotational velocities of the paddle, all of which benefit the effectiveness of the device. In order to achieve this, the device was positioned with the shaft being as close to the base of the neck as possible without causing any potentially harmful interference with the player, as shown in Figure 35. Not only was this beneficial to the effectiveness of the device, but it was also an accurate representation of where the device could possibly be mounted in a wearable final product. This location allows for easy mounting to the shoulder pads if needed, while also minimizing size of the device as a whole.

Based on this device location, it was important to design the arms and the pad to ensure that throughout the range of head motion, the only device component in contact with the helmet was the pad. As a result, the arms were designed with a slight curve in order to ensure that the bottom edge of the helmet would never come in contact with these arms. This curve can be seen in the aluminum arms shown in Figure 35 connecting the black, plastic pad in contact with the helmet to the device mounted to the torso. Prior to actual testing of the device, it was unknown by the team exactly how the helmet would move throughout the impact motion. In order to allow easy adjustability of the pad on the arms if needed, the team chose to make three positions available for pad mounting. Furthermore, the mounting between the pad and the arms strategically consisted solely of one bolt, allowing for easy

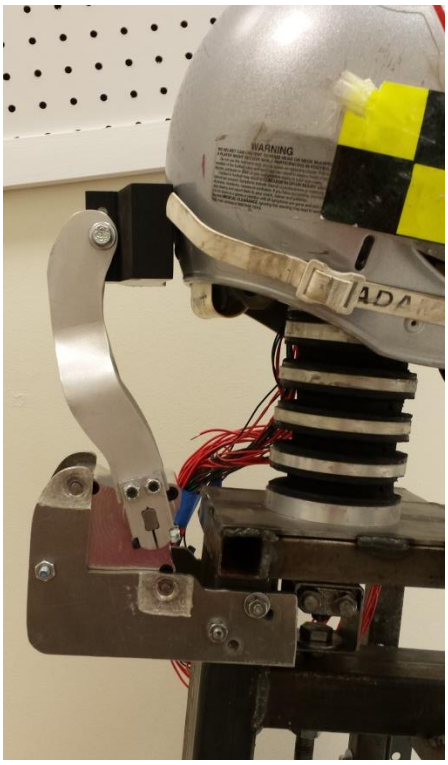

Figure 35: Interface between device and helmet/torso used in testing

angle adjustments between the pad and the arms to maintain the desirable contact between the pad and the helmet throughout testing.

As Figure 35 shows, it may appear that the plastic pad is located too close to the bottom edge of the helmet. This is not the case, however, for slow motion footage obtained through testing showed that the initial impact caused the helmet to compress toward the player along their vertical axis, or the axis from the top of the head to the bottom of their feet. After this compression had occurred, the pad became very close to the middle of the helmet, at which point the head began to rotate. The pad subsequently remained in contact near the middle of the helmet throughout the impact, which is ideally what would provide the most significant protection for a player.

While initial iterations of the device included a paddle compartment allowing for a full 180 degrees of rotational paddle motion, it was quickly realized that this was unnecessary. Simple kinematic analysis of forward to rearward head motion of various team members while wearing a helmet indicated that 90 degrees of motion would be more than sufficient in order to prove the concept of the device using our testing methods. Additionally it was decided that the project would solely test crown-to-crown impacts as they are the most common concussion-causing hits. Given the size limitations of the device, the reduced rotational motion allowed for a larger paddle within the same volume which was beneficial for the overall effectiveness of the device. This was especially important as the team wanted to maximize the potential size of this device for initial proof-of-concept testing.

With all of these factors determined, the final step involved positioning the paddle correctly on the shaft. This was one of the last steps involved in the manufacturing of the device as it was determined with everything in place – the device mounted on the torso, the arms and pad resting against the head, etc. – so that the paddle was mounted on the shaft in a position that allowed a full range of motion of the head following the impact. The most important consideration was that the paddle would not bottom out on any internal case surfaces throughout the range of motion of the neck. In order to ensure that this did not happen, stops were also placed on the mounts attaching the device to the torso solely as a precaution to pretend possible paddle damage.

4.2.3 Instant Response Reaction of Device

In order for the device to effectively help prevent concussions, the device had to react within around 6 milliseconds of an impact. Clearly, this very small time window pointed towards the need for the device to remain in constant contact with the helmet, allowing immediate transfer of impact energy and motion into the device without delay. This important design consideration was not only taken into account during the initial design concept phase of the project, but also throughout the design and manufacture of the final device. Although the chosen design ensured such contact between the plastic pad and the helmet, it was important to ensure that the pad motion could also directly be transferred into paddle motion. With

a handful of parts ultimately between the pad and the paddle, this meant that there could be nearly zero slack within all connections.

Figure 36: Clamp tightly fastened to steel shaft

Clamp-Shaft Interface

One important design consideration with regards to effectiveness in translating energy quickly from the point of impact to the paddle was the connection between the arms and the steel shaft. It was ultimately decided that a type of clamp which could be tightened to the shaft would be ideal, with the arms bolting to the ends of this clamp. Having a separate clamp component from the arms was also beneficial as it allowed for an easier process of creating new arms if necessary and negating the need for any special machining processes. While it may have been possible to tighten this clamp to the unmodified shaft relying solely on frictional forces between the two components, it would be beneficial to incorporate a more secure method given the high forces that would be experienced during the impact. As a result two, parallel flat sections were machined in the shaft to provide sufficiently large clamping surfaces to attach to securely without the risk of rotational displacement. To fit properly, the clamp design involved the removal of a rectangular cross-sectional area, allowing a tight fit with the profile of the shaft. A slit would also be cut into the clamp, allowing the clamp to tighten to the shaft with the use of a nut and bolt. On the opposite end, the arms would be securely attached to the clamp with two nuts and bolts. Clearly, this clamp design ensured no play between the arms and the paddle, and can be seen in Figure 36 above.

Shaft-Paddle Interface

With the arms securely attached to the shaft, the next important design consideration involved securely attaching the paddle to the shaft. In order to potentially test different paddles, the paddle needed to be easily removed from the shaft, requiring some method of securely attaching the two components. A simple and effective strategy to accomplish this was to incorporate two bolts passing through two holes in the shaft and threading into the paddle. Course thread #10-24 bolts were chosen as these would provide stronger aluminum threads having increased distance and material between threads. A hole large enough to house the head of these bolts would go in the very end of the paddle, allowing the head of the bolts to sit directly against the steel shaft. This was necessary in order to avoid contact between the bolt heads and the internal compartment walls, while also allowing a tight clamp force between the shaft and the paddle, thus increasing any chance for movement between the two. The design is shown in Figure 37.

Figure 37: Two recessed bolts holding shaft and paddle together

Purge Hole

The final measure taken to ensure an instant response time dealt with the inclusion of a purge hole in addition to the fill hole for the device. A purge hole helps prevent air bubbles from forming within the chamber during filling as any air bubbles are able to easily escape through this additional hole. The absence of air bubbles within the chamber is important because unlike the various fluids used throughout testing, air is a compressible fluid. If there were any air bubbles within the chamber, this could potentially allow the paddle motion to compress the air pocket, in turn decreasing the mass flow effects evident from forcing the fluid through the holes in the paddle. Figure 38 shows both plugged and unplugged fill and purge holes in the device.

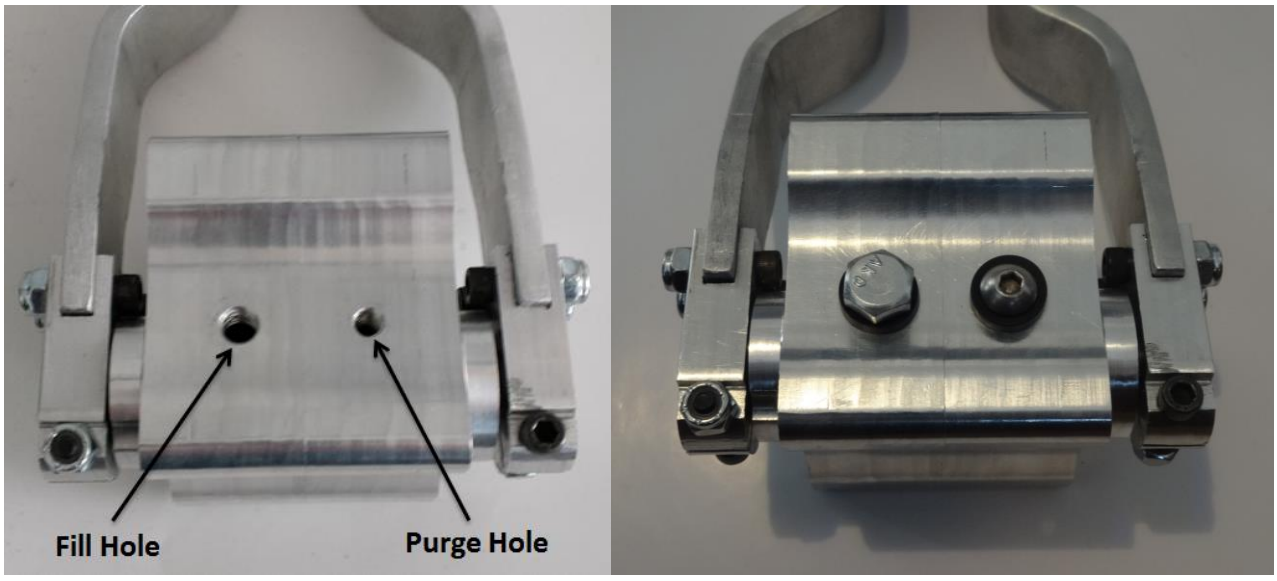

Figure 38: Fill and purge holes with (right) and without (left) drain plugs

4.2.4 Performance Tuning

In order to test with multiple kinds of fluids, including non-Newtonian fluids, the device was designed with a paddle-to-shaft connection that was easy to remove; this was necessary as the numerous viscosities and densities of the fluids being tested required paddle hole tuning to allow similar low loading behavior to reflect the desired feedback to the head at normal head velocities. This feedback should be relatively low to allow players a full range of motion. Therefore when each fluid was tuned, it was verified that during normal head motion that feedback was reasonable. To tune the non-Newtonian fluids, it was considered to make paddles that intentionally had large paddle-to-case-half clearances to best utilize the non-Newtonian fluids by keeping shear rates very low. Paddles with different hole size combinations, as well as paddles with mechanical valves were considered for alternative paddles to be tested. Because only one shaft was necessary, holes were drilled through the shaft to attach to threaded holes in the paddle itself. The shaft could then be bolted to the paddle, and the bolt heads were recessed into the shaft to prevent interference.

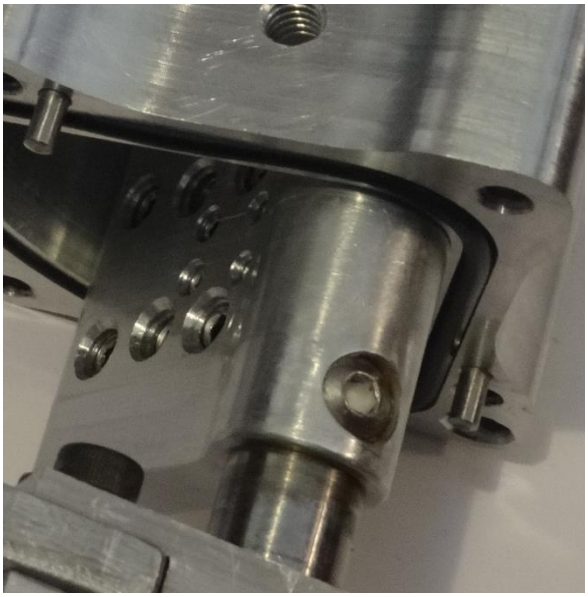

Figure 39: Bolted connection between paddle and shaft

Holes were drilled in the paddle to allow for easy tuning of the device with different fluids. These holes were tapped, and then could be plugged with set screws. Six quarter inch holes, two #8 holes, and two #6 holes were made in the paddle which allowed for fine tuning of the paddle with the smaller holes while allowing its properties to be adjusted greatly by opening or plugging the quarter inch holes. The hole area directly relates to the pressure developed in the case half, as the velocity of the fluid through the hole greatly increases at the same flow rate when hole area is decreased. The inlet pressure increases as hole size decreases, and this pressure directly relates to the pressure in the case, and therefore the feedback force on the head.

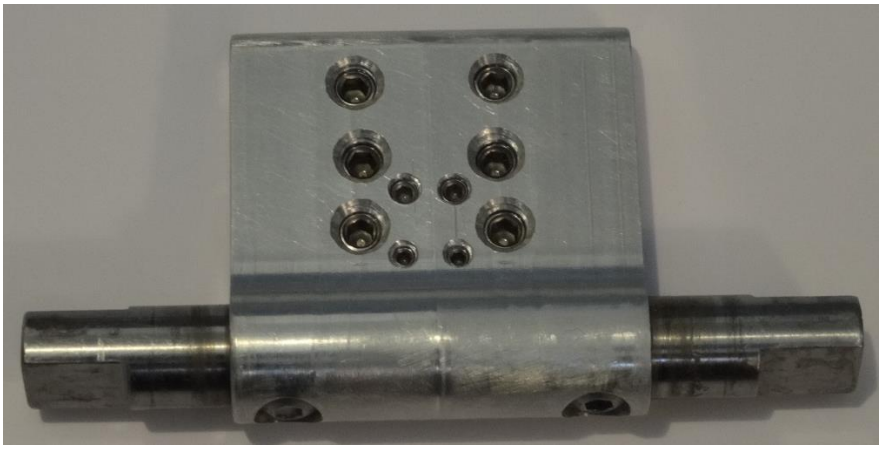

Figure 40: Six 1/4" holes (large) two #8 holes (medium) two #6 holes (smallest) all plugged with set screws

4.2.5 Machining

The majority of the manufacturing of the device was done using CNC milling operations. The main reason for choosing this manufacturing process was the tight tolerances of the device, namely the 0.005" clearances between the paddle and case walls. The tight clearances within this part of the device prevent fluid from passing around the paddle and thereby reducing its effectiveness as a fluid shock absorber. The tight tolerances allow high pressures to build in the casing which is necessary for the device to resist motion of the impacted head, as pressure in the case pushing on the paddle is responsible for pushing directly on the head. Achieving the precision necessary would have been nearly impossible without some form of automated process. Available for use were HAAS mini mill CNC machines which were chosen due to their high precision and low cost of operation. Other possible options may have included any form of automated precision molding or 3D printing of parts, but these processes would either result in weak parts or a high cost of manufacture that would exceed the budget. Because the device needed to withstand impact forces, the material chosen for construction had to be able to withstand high stresses. Also, the device needed to be easy to machine while also being as inexpensive as possible, therefore aluminum was chosen as the material for construction of almost the entire device as it is a relatively inexpensive, strong, and an easy to machine material.

Effect on Design

The design of the device was influenced by the nuances of the CNC machining processes. With CNC machining, stock material must be clamped tightly in a vice to prevent the milling operations from disturbing the positioning of the stock. The vise only clamps parallel surfaces properly, therefore if multiple operations were necessary to completely machine a single part, the first operation done on the part needed to result in a pair of parallel surfaces. The parts would also have to have enough area being clamped in the vice for the vice to effectively grip the parts, a term known as "stickout." The case halves involved multiple machining operations and therefore had to be designed with parallel faces, as shown in Figure 41.

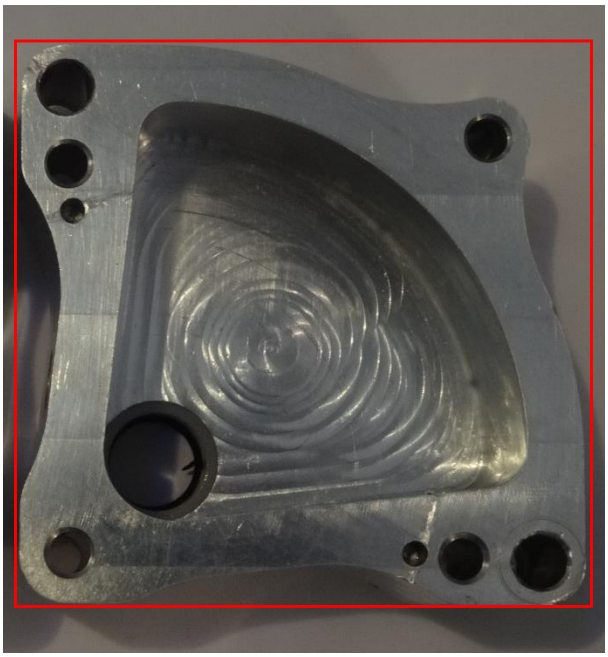

Figure 41: Parallel faces of the case half

Other parts requiring multiple machining operations included the shaft, the clamps, and the paddle. An example of a final, machined clamp is shown in Figure 42 below.

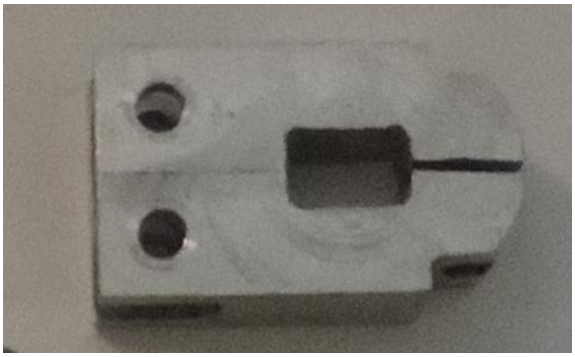

Figure 42: Flat parallel faces are apparent on clamp

The paddle, however, gave no option of creating parallel faces in any location that could have been clamped securely. Therefore, vice jaws were machined that the paddle could be squarely clamped in the vice with.

Machining Considerations

To machine the device, the CNC mills had to be programmed with the correct tool paths, tools, and tool speeds for each of the operations. The correct feed rates and spindle speeds were chosen from tables available from the manufacturers of milling tools. Depending on the depth of cut and diameter of the cutting tool, considerations had to be made for the amount of material to be removed in each pass to

minimize deflection of the tool, and therefore, maximize precision for the part. For example, when machining the case halves and paddle, a 3/8” endmill was used to cut over an inch in depth. The step down was decreased to prevent the endmill from deflecting near the bottom of the cut. All holes drilled were first spot drilled by a center mill to accurately locate the entry of each hole. When drilling the 0.5” hole for the shaft in the paddle it was unknown if the drill bit would deflect when drilling 2” into the material. This hole needed to be very precise so that the paddle was oriented perfectly in the case to prevent binding with the tight clearances. The hole was therefore drilled before the outer paddle shape was cut in a separate operation. This allowed for the aluminum stock to be completely in the vise which prevents defection of the stock and of the bit. Because the shaft was nearly exactly a half inch, to prevent any play between the shaft and paddle, it was decided to drill the hole with a 31/64” drill bit and then ream it to a half inch. This worked very well as the resulting hole was very straight and located correctly, and the paddle had no detectable play when slid onto the shaft. In Figure 43 each component of the device is shown.

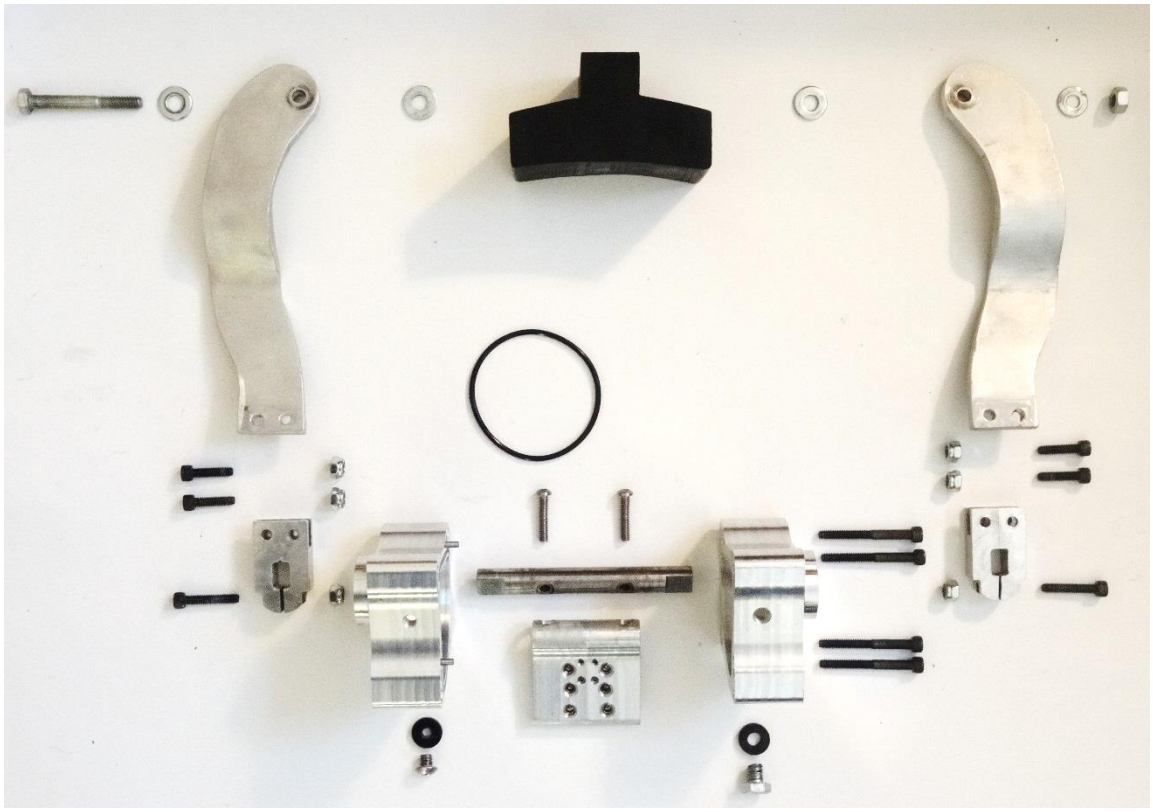

Figure 43: Exploded view of final manufactured device

5.0 Testing

Design and construction of the head device and testing assembly was a rather sophisticated procedure. In order to obtain the most accurate results it was necessary to design a test assembly that would enable comparable and repeatable results. It was also important to ensure that data obtained throughout our testing was comparable to previously published data involving similar testing techniques, requiring the use of similar testing equipment and procedures. Therefore, the team replicated the popular *Hybrid-III* model and recreated a collision between two players via a vertical drop mechanism, a commonly used method. One head, which represented the hitting player, was accelerated to roughly 9.0 m/s by means of gravity. The second head, representative of the targeted player, was fixed in-line with the hitting player so that a collision between helmets would ensue – thereby causing a concussive type hit under nominal conditions. To best prevent excessive rotational acceleration in a short period of time, often responsible for causing a player to become concussed, the design team designed a fluid shock absorber which would simultaneously absorb and divert energy from the impact away from the head and neck. The resulting device was attached to the targeted player. In order to obtain numerical data, six accelerometers were attached to the head of the targeted player to compare head acceleration data throughout testing. The design and construction of both the device and the test rig were essential in order to obtain useful data for determining the effectiveness and efficacy of the concept.

5.1 Test Rig Construction

The design of the test rig for comparing impact results against baseline testing was a major undertaking which was necessary in order to accurate qualify the conceptual design. To most accurately replicate a concussive-type football impact it was decided to fabricate a head, neck, and torso comparable in function to the Hybrid III model.

Using previous experimental procedures for reference, the design team started by designing a model which could accurately replicate a human neck. Scientists and engineers working on the *Articulated Total Body* (ATB) model have attempted to replicate kinetic responses of a human neck by means of a *Hybrid III* simulated neck assembly. Shown in

Figure 44, the device is constructed from 75 durometer Butyl rubber, aluminum vertebrae disks, and a steel neck tensioner cable. Significantly high costs for the Hybrid III products prevented the team from using these, so the team was forced to reverse-engineer these products. To best replicate the *Hybrid III* neck model, the team utilized ¼" aluminum vertebrae disks, a combination of 70 durometer Neoprene rubber disks, and a ½" diameter 6 ply steel cable for tensioning. The aluminum disks were turned on a manual lathe by the team, and the rubber was modified with various tools including a Dremel to obtain the desirable shape. Each layer of aluminum/rubber was glued in place using a cyanoacrylate adhesive – Loctite 496, and bolts were recessed into the end aluminum disks to allow mounting of the neck. Upon initial testing, it was quickly determined that the 70 durometer rubber was simply too stiff to allow

accurate displacement of the head. Therefore, the neck was recreated using ¾" 50 durometer Neoprene rubber sections, and each section of Neoprene rubber was modified with an anterior cut as shown in both images below in order to simulate the ability of the neck to bend rearwards. Testing a variety of neck tensions, the team agreed that a neck tension of roughly 5.6 ft-lbs produced the most replicable results compared with previous tests.

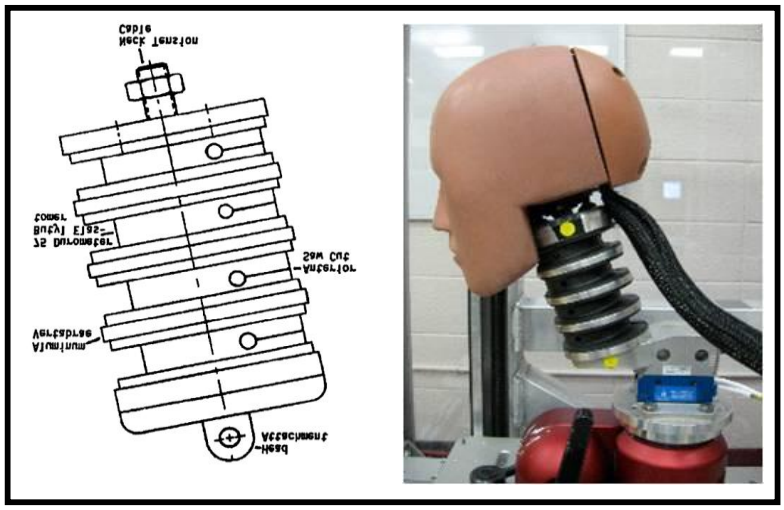

Figure 44: Hybrid III Neck Model

With the neck assembly completed, the team had to devise a way to create a head that connects to the neck. The necessity to create a head to wear a football helmet was important in order to make the impact as realistic as possible. To begin the process, the design team resourced a dummy male hairdresser head with reasonable dimensional accuracy. The manikin was then wrapped in a layer of adhesive tape in order to protect it from the mold material and prepped for casting. A five gallon bucket, together with a section of cardboard used to separate the two hemispheres of the head for the completion of the mold, was used to hold the dummy head and cement mixture for the creation of the mold. Figure 45 shows the final product of the cement head mold.

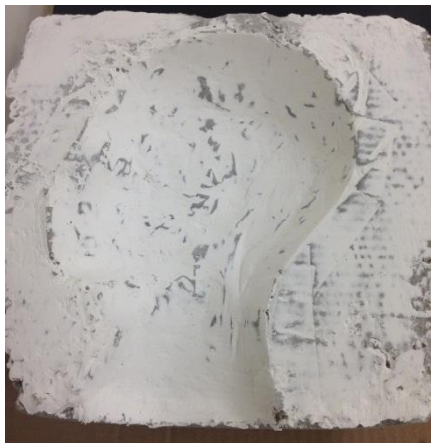

Figure 45: Cement Mold for Creation of Epoxy Head

Having created the two cement mold halves, it became necessary to select a material to cast the head with. Desiring a material that was relatively shock resistant, durable, and strong in both compression and tension, the design team opted for a two-part epoxy. This thermosetting material was ideal not only for its superior strength and resilience, but also due to its uniform curing, essential for such a large cavity. The two halves of the mold were coupled together and any voids/imperfections were corrected with a sanded layer of joint compound. Prior to pouring the epoxy into the mold, three threaded rods were attached to the mold so that the neck could be easily attached to the head with the rods securely positioned within the cured epoxy. The resulting head produced in the mold with the epoxy can be seen prior to pouring and in its final state in Figure 46 and Figure 47, respectively.

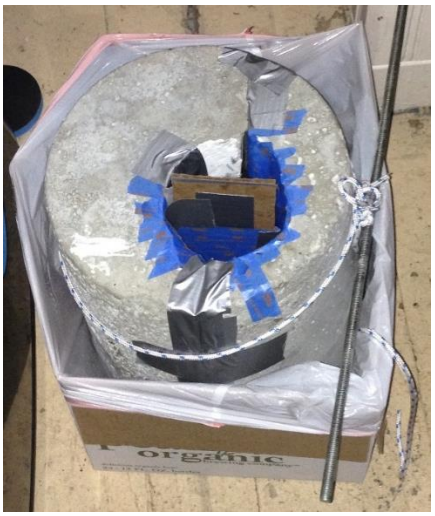

Figure 46: Cement Mold Prior to Epoxy Casting

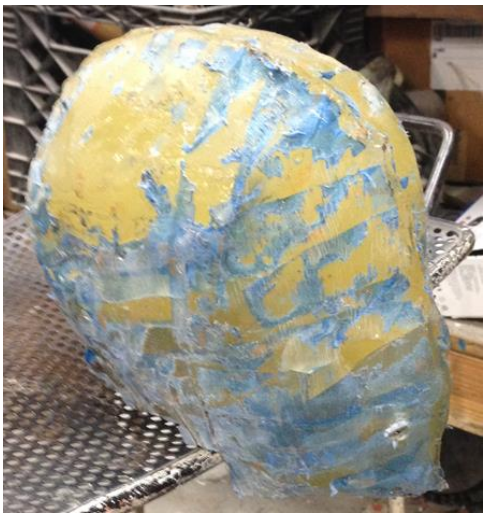

Figure 47: Epoxy head prior to final cleaning

With the threaded rod secured in the head during the epoxy curing process, a simple plate was fabricated to effectively connect the epoxy head to the neck. The top section of the steel plate attaches to the threaded rods in the epoxy head, the bottom section attaches to the three bolts in the top section of the neck, and the void between the two sections houses a U-clamp to hold the steel cable in place. The final assembly of the head and neck can be seen in Figure 48 below; notice how the neck is rigidly attached to the steel plate, and therefore the head, but is not restricted from flexing.

Figure 48: Attachment of the neck to the torso

Having already created a head for the neck assembly, the team decided to produce another head for the striking player. Another head was created in order to retain a realistic impact simulation and to prevent needing to make alterations to the helmet for mounting. The second head was molded with epoxy and also included threaded rod for mounting. The two heads, created with a realistic weight and center of mass to a human head, were subjected to impact and vibration tests and validated as robust parts for testing.

Dissipating energy and diverting it away from solely the head and neck was accomplished largely through the rotation of the torso. Rather than angularly accelerating the lightweight head (roughly 8 lbs.), the design team desired that a large portion of the energy from the impact would be disposed by accelerating the much heavier torso. A large overall torso weight means more energy can be dissipated through dynamic motion, reducing the likelihood of sustaining a concussion. The importance of the torso as a source for the energy to exit the assembly was extremely important to the testing of the device, and therefore, it was paramount for the team to design a torso that accurately reflected a human subject.

When considering the design of the torso, several key features became apparent: the torso must be strong enough to endure dynamic motion about the test rig, the torso had to weigh an accurate amount relative to a human subject with the weight distributed realistically, and finally, the torso had to be free to rotate and/or pivot while also serving as the fixture point for the neck and head assembly of the hit player. These design constraints dictated the torso's final form: a roughly 14"x30"x10" steel structure fixed to a testing

rig via a set of springs. The torso incorporated a flat surface to securely attach the neck to, as well as a lower bar to easily attach the device to the unit. The torso also involved a simple method of tensioning the neck involving the steel cable being attached to a bolt in tension so that this single bolt could be used to accurately tension the neck. This tensioning mechanism can clearly be seen in Figure 49 below.

To replicate a human torso, it was necessary to add weight until the whole torso section weighed around 90 pounds, along with distributing this weight amongst the upper and lower sections correctly while also enabling the assembly to rotate within the rig. The lower portion of the torso was weighted to approximately 35 pounds, while the upper portion was weighted to 55 pounds. The suspension method for the torso enabled the body to rotate and translate after the impact was sustained, imitating how an actual human body would react on the football field. As previously mentioned, it was extremely important to make sure that the torso was able to move to ensure that the energy could be dissipated outside of the head and neck. A picture showing the torso, as well as the mounted neck and head, can be seen below in Figure 50 and Figure 51.

Figure 50: Neck/Torso Assembly with Cable Tensioner

Figure 51: Torso, Neck, and Head Assembly (Iso)

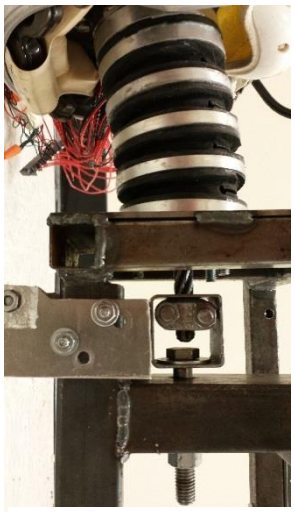

Figure 49: Torso, Neck, and Head Assembly (Side)

Having completed the construction of the *struck* player, the design team manufactured a device to simulate a *striking* player whom would deliver the concussive-type blow. The team designed and built a steel structure to attach the head of the striking player to. One of the main design considerations for this device involved trying to keep any moments created about the steel cables (the attachment point for the device) minimized. To accomplish this, the location of the impact, or the crown of the helmet on the striking player, was kept as close to the cables as possible. Furthermore, the device must be strong enough to withstand weight being added and be able to withstand the high impact levels. When deciding how to mount the head of the striking player to the rig, it became apparent that a dynamic assembly was only necessary for simulating the reactionary effect of a head-head impact. To most efficiently accomplish this

goal, the epoxy head was mounted to the steel structure via an adjustable shock. The shock provided the necessary recoil in the neck during impact to simulate a human impact while providing enough rigidity to stand up to the nearly 80g expected resultant impact acceleration. To attach this structure to the test rig, which was to be designed as a vertical drop test with in-line tensioned guide cables, a total of eight metal pulleys for ¼" wire rope were purchased and mounted to the device near the crown of the striking player's helmet. With the head mounted, the device was loaded with weight until a total of 65 lbs. was achieved. The resulting assembly showing the shock, roller bearings, and mounted head can be seen below in Figure 52.

Figure 52: Striking Player

The final portion was the test rig itself. Standing some 16' tall and weighing in excess of 100 lbs., the rig was created in order to simulate a concussive-type hit by means of a vertical drop test. The majority of the structure was constructed from wood for ease of use, manipulation, and overall affordability. Two coated 7-braided steel cables were connected from the bottom of the rig to the top where they were attached with a single bi-directional threaded coupling which enabled the team to simultaneously tension both cables. The base of the rig was roughly 3 feet wide, 6 feet long, and 4 feet tall in order to facilitate the mounting of the torso for the struck player. To help facilitate the lifting of the striking player to its correct position at the top of the rig for testing, the team incorporated a very rudimentary pulley system with a quick disconnect to disengage the rope and pulley system prior to dropping. To fix the player atop the rig, and to repetitively drop it with as little horizontal motion as possible, a safety release system designed from steel was manufactured and enabled to "lock" into place until the time of the drop. Figure 53 below shows the cable tensioner and release mechanism while Figure 54 shows how the torso is attached to the rig with the springs to simulate the reaction of a human body during a large impact.

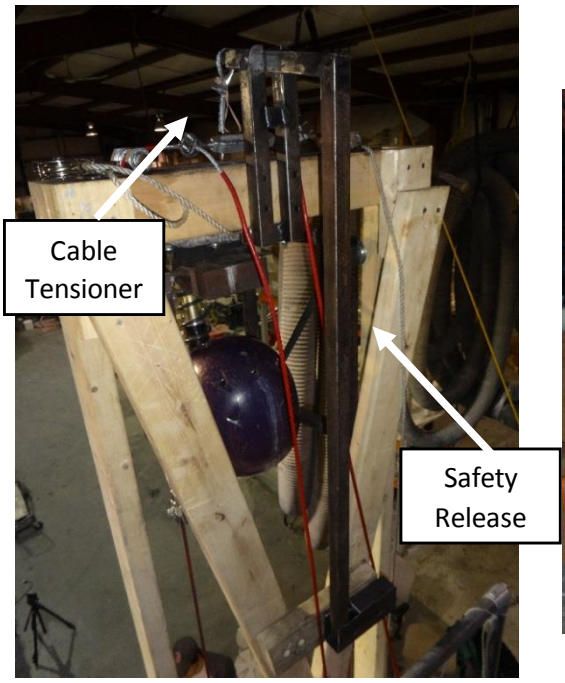

Figure 53: Test Rig- Cable tensioner and safety release meachanism

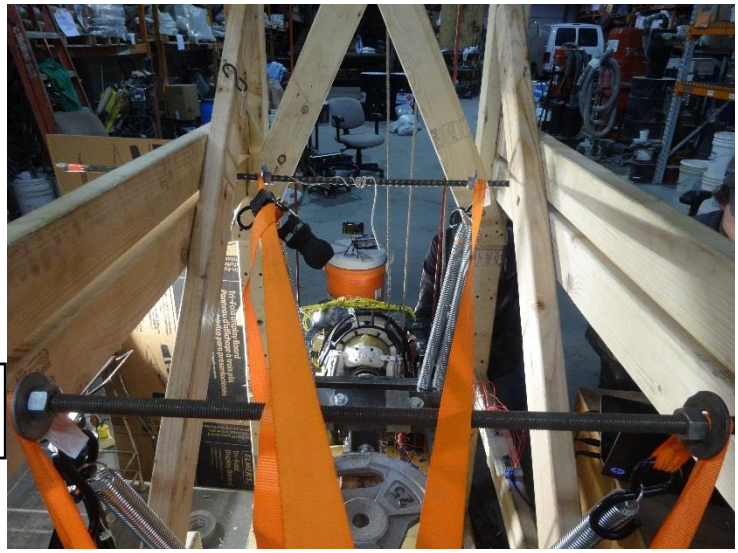

Figure 54: Torso Mounted to Test Rig

5.2 Experimental Design

To properly test the device, promising fluid and hole combinations first had to be determined. Preliminary testing was done first to eliminate certain fluid-hole combinations. This involved trial and error guessing of which fluid-hole combinations would perform the best, setting the device as such, and moving the device to feel the resistance from the fluid motion through the holes. Below is a complete list of fluids explored during initial device testing.

Fluids Explored

- Water
- Multipurpose Oil
- 5W Shock Fluid
- 15W Shock Fluid
- 50W Shock Fluid
- 50W Motor Oil
- Cornstarch and De-ionized water
    - 47.5% cornstarch by weight
    - 50% cornstarch by weight
    - 52.5% cornstarch by weight

Water and multipurpose oil were tested initially to determine the ideal hole sizes because they were the least viscous fluids, and would require the smallest holes to tune the shock properties. They enabled the team to gain an understanding of how much hole area is necessary to provide device feedback during

normal head movement (i.e. pressing on the device with our hands). Even though the water and multipurpose oil provided minimal resistance during slow device motion with various combinations of the ¼" holes, it was unknown how the fluid would react at impact speeds. Further initial testing was performed with the device attached to the test torso to collect preliminary data on device reaction during high speed impacts. Accelerometer data and video was recorded during this testing, but was minimally evaluated because its purpose was to help the team gain a broad understanding of how the device was reacting. Key information gathered was visual from both the head rotation from the high speed video and the shape of the acceleration graph from the tri-axial accelerometer. The testing began with six ¼" holes in the paddle, and was quickly narrowed down to just one ¼" hole. When even this gave minimal resistance during preliminary tests with water and multipurpose oil, new holes of six and eight millimeters were drilled in the paddle. Additional tests were performed with the smaller holes and a variety of fluids as listed above. This preliminary testing also enabled minor changes to be made to device placement and operation of the test rig before final testing was conducted.

By performing this set of preliminary tests, optimal fluid-hole combinations were narrowed down for testing. In Table 3 below are the ten fluid-hole combinations tested to gather data.

Table 3: Tested fluid and hole combinations for the device

	Number and Type of Holes					
Fluid	*None*	*One 6mm*	*One 8mm*	*Two 8mm*	*Six 1/4"*	*All Holes*
15W Shock Fluid	X	X	X			
50W Shock Fluid		X	X	X		
Cornstarch Mixture (50% wt)					X	X
Cornstarch Mixture (47.5% wt)					X	X

The shock fluids provided better resistance than water and multipurpose oil during preliminary testing of the device, as was expected due to their higher viscosities. The team wanted to explore cornstarch and water mixtures as well, as the reaction from non-Newtonian fluids in the device was theoretically an ideal situation. A non-Newtonian fluid would ideally provide low resistance during low paddle speeds, but high resistance during high paddle speeds. A study on cornstarch mixture reaction was used to narrow down the proper mixing ratios as described in the Problem Context section [24]. The critical range for shear thickening results in cornstarch and deionized water solutions was 45% to 52.5% cornstarch-to-water by weight. Only two ratios, 50% and 47.5%, were tested with two hole configurations which seemed most promising during initial sample mixing.

Testing Procedure

The test rig and procedure was designed after a study conducted by Pellman [11]. As described in the previous section, the test rig and apparatuses were built to create the most repeatable experiment. The procedure for one trial is described below.

1. Raise “striking” player by pulley system.
    a. Engage safety.
    b. Remove pulley and pulley-hook from “striking” player.
2. Adjust helmet on “struck” player for crown-crown impact.
3. Adjust device on “struck” player so it rests flat against back of helmet.
4. Stabilize “struck” player oscillations due to suspending springs.
5. Drop “striking” player.

In between trials certain components of the test rig were checked for continued functionality. The neck was routinely visually inspected for cracks and breaks due to impact. The cables guiding the “striking” player were checked for tautness and occasionally tensioned more. The accelerometer wiring to the breadboard was adjusted to ensure contact between wires.

The baseline testing, which was an impact on the torso without the device, was repeated multiple times until a desirable, repeatable acceleration curve was attained. Slight changes were made to the position of the torso and the distribution of the ninety pounds about the torso until the acceleration curve generated from the accelerometers placed in the head was reasonable. Adjustments were made until a curve similar to the one shown in Figure 55 below was generated [9]. Then five trials were conducted to conclude baseline testing. For each fluid-hole combination, four trials were conducted.

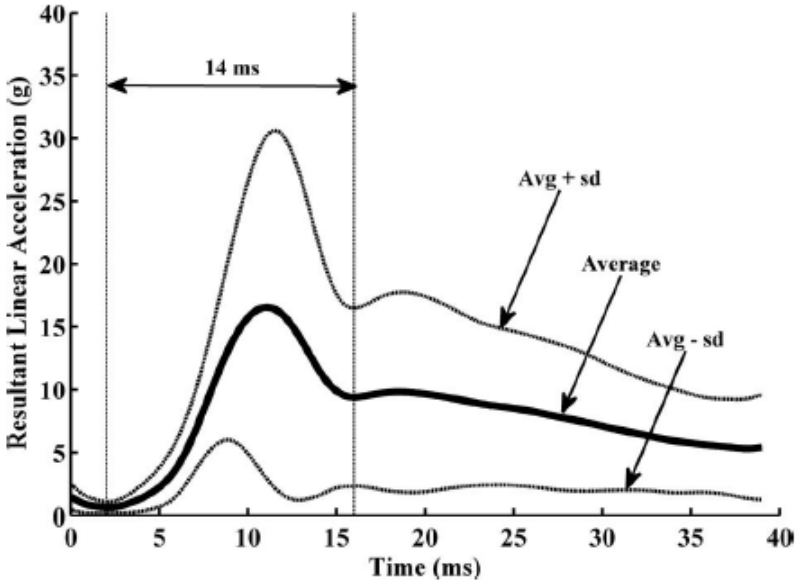

Figure 55: Graph of linear acceleration vs time of real time head acceleration data.

Device testing of ten fluid-hole combinations was conducted over the span of two days. To ensure the testing procedure was repeatable, baseline testing was conducted at the start of both days of testing. The first day of baseline testing was kept for evaluation, and the second day was conducted to verify the conditions had remained the same. The accelerometer data from the second day of baseline testing was very different than the first. After ruling out most contributors, it was determined that the neck had been tensioned while the head was supported which resulted in a higher tension on the cable than in the first tests. Once the neck cable was torqued to 5Nm, the data recorded was very similar to that of the original baseline testing. After baseline trials produced repeatable acceleration curves consistent with the first day of testing, the rest of the fluid-hole combination device testing was conducted.

6.0 Data Collection and Evaluation

Data was collected during each trial by two methods: high speed video and accelerometer readings. Video recordings (Casio EX-ZR100) were taken at 480 fps at two locations during testing to determine the final speed of the dropping head and the rotational displacement of the struck player's head. To record accelerations of the head and determine maximum velocities, the head was fit with a tri-axial accelerometer (ADXL377) at the center and six single-axis accelerometers (ADXL193) on the surface. The method of recording and converting accelerometer readings is described further in the section titled Data Gathering, while the analysis method of the accelerometer results is described below in the section titled Accelerometer Analysis.

6.1 Data Recording

All accelerometer readings were recorded with an Arduino Micro. Because of the remote location of testing, access to most university provided data acquisition loggers was unavailable. With the Arduino's open source software, relatively inexpensive cost, and high clock speed (16MHz), it was the best option for data recording. To maximize recording speeds, two Arduino Micros were used. Since the Arduino cannot sample all accelerometers are the same instant (it must cycle through the various inputs) the tri-axial and single-axis were separated to record on separate Arduinos. The tri-axial accelerometer, although rated at 1000 Hz, was able to record the three (X, Y, Z) accelerations over the period of one millisecond. The six single-axis accelerometers, rated at 400 Hz each, were able to record their accelerations over two milliseconds. When analyzed, the tri-axial acceleration results displays accelerations averaged over the duration of one millisecond, and the single-axis result is the acceleration averaged over two milliseconds.

The triple axial pins consisted of a power, ground and three outputs. These pins were soldered to wires and Table 4 displays how they were attached to the Arduino.

Table 4: Tri-axial accelerometer pin-out relations

Accelerometer Pin	Arduino Pin
V_{IN}	3V
GND	GND
X_{OUT}	A0
Y_{OUT}	A1
Z_{OUT}	A2

The six single axial accelerometers had a power, ground and three output pins. These were soldered to wires and attached as shown in Table 5.

Table 5: Single-axis accelerometer pin-out relations

Accelerometer Pin	Arduino Pin
V_{IN}	5V
GND	GND
A X_{OUT}	A0
B X_{OUT}	A1
C X_{OUT}	A2
D X_{OUT}	A3
E X_{OUT}	A4
F X_{OUT}	A5

An Arduino program for each was written for data collection. The program can be found in Appendix 10.1. The programs were sent to the circuit boards a few seconds before the test drop and were turned off a few seconds after the collision occurred. The data from each trial was then exported to excel to be converted to acceleration values.

Because the Arduinos are programmed to output sensor data in bytes, the data gathered was first converted from byte values to voltage then to accelerations. Since the triple axial was given a source voltage of 3V, 1.5V corresponds to the zero acceleration voltage. The equation below relates the bytes readings given by the Arduino to voltage.

$$voltage\ (V) = accelerometer\ reading\ (bytes) \cdot \frac{1.5\ (V)}{zero\ g\ reading\ (bytes)}$$

The accelerometer reading value corresponds to whatever value was displayed by the Arduino for that instant and the zero g reading value corresponds to a bytes value that represents zero acceleration. This was found by observing the data from the same trial before impact occurred. Since the struck dummy was not moving before impact, these values represent zero acceleration.

To determine how the voltage relates to acceleration, the data sheet of the accelerometer gives a mV to g rating and for the case of the ADXL 377 this value was 6.5 mV/g. Knowing this relation, it is used in the equation below to find acceleration.

$$acceleration\ (g) = \frac{\left(voltage\ (V) - 1.5\ (V)\right)}{.0065\ \left(\frac{V}{g}\right)}$$

Substituting the voltage equation into the above equation we obtain the bytes to acceleration equation shown below.

$$acceleration\ (g) = \frac{1.5\ (V) \cdot \left(\frac{accelerometer\ reading\ (bytes)}{zero\ g\ reading\ (bytes)} - 1\right)}{.0065\ \left(\frac{V}{g}\right)}$$

These acceleration values were then used to analyze the triple axial data.

The single axial accelerometer accelerations were extracted in a similar way. Since the ADXL 193's source voltage was 5V, 2.5V corresponds to the zero g voltage. The mV to g rating was also different being 8 mV/g instead of 6.5. These changes can be observed in the three equations below, ultimately relating byes to acceleration for the single axial accelerometers.

$$voltage\ (V) = accelerometer\ reading\ (bytes) \cdot \frac{2.5\ (V)}{zero\ g\ reading\ (bytes)}$$

$$acceleration\ (g) = \frac{\left(voltage\ (V) - 2.5\ (V)\right)}{.008\ \left(\frac{V}{g}\right)}$$

$$acceleration\ (g) = \frac{2.5\ (V) \cdot \left(\frac{accelerometer\ reading\ (bytes)}{zero\ g\ reading\ (bytes)} - 1\right)}{.008\ \left(\frac{V}{g}\right)}$$

6.2 Data Evaluation

The following sections outline the methodology in evaluating the high speed video footage, the tri-axial accelerometer results, and the six single-axis accelerometer results. Optimization techniques are described which were used in finding the resultant acceleration curves.

6.2.1 Video

The final speed of the dropping head can be determined from footage taken directly in front of the testing apparatus. A two-inch grid coupled with a bright index card on the dropping head allow for reference points during impact speed calculations, shown in Figure 56. The impact velocity of the striking player was determined by stepping through the 480 fps video and taking screen shots at each frame to track the player's position aside the yellow and black grid. The red line on each photo shows the progression of the striking player hitting the struck player.

Figure 56: High speed video frames of striking player

The maximum rotational displacement of the struck head relative to the torso is also determined through high speed footage taken during impact. Square markers were placed on the head and torso. Video recorded at 480 fps was stepped through frame-by-frame to select the initial head-torso position and the position with maximum head rotation. Both video screenshots were then imported into SolidWorks where the relative angle of rotation of the head relative to the torso could be measured. Sample video snapshots are shown below in Figure 57.

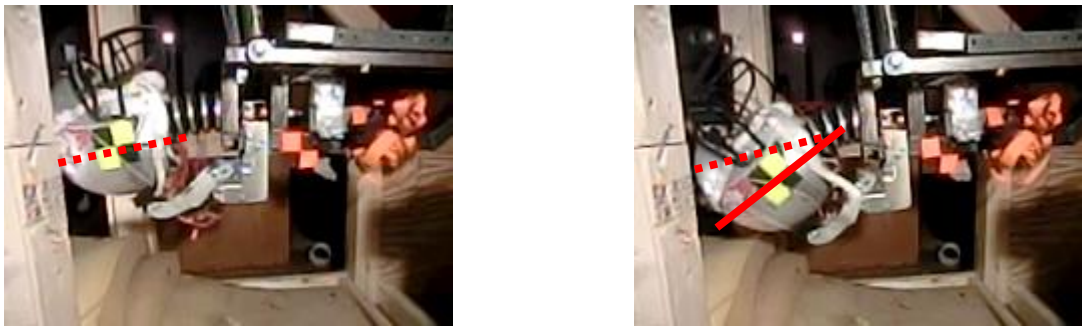

Figure 57: Side by side comparison of the rotation of the head relative to the torso at the beginning and middle of the impact

6.2.2 Accelerometers

Seven accelerometers were placed on the struck player head, recording nine different accelerations. Use of single-axis accelerometer arrays is common in sports impact analyses because a single accelerometer placed at the head center would not be feasible in real-life situations. One method of accelerometer placement is the 3-2-2-2 array in which nine, single-axis accelerometers are placed orthogonally around the head, or inside the helmet [27]. While this set up allows for a more accurate determination of the rotational acceleration achieved by the head, placing nine accelerometers in specific locations is difficult and expensive for this application. Alternatively, a study performed by Crisco found the optimum ratio of number of accelerometers to overall error of reported linear acceleration to be six, single-axis accelerometers placed in any convenient location around the head [28]. This technique is now used in commercial applications under the name Head Impact Telemetry System (HITS) for monitoring of real-time game situation head impacts. The benefit of using the six, single-axis accelerometer array is their pre-determined placement relative to each other about the head is not critical. The only criteria for placing these accelerometers is their recording axis must be orthogonal to the surface of the head, and for computation simplification, they must lie on the same spherical plane.

The tri-axial accelerometer readings were used for immediate results on the magnitude of head acceleration during testing. The six single-axis accelerometer readings were evaluated to give an overall head acceleration and direction. The collection of both sets of accelerometer readings helped with checking consistency of data and comparing trials. Since there was error in precisely placing all of the accelerometers, two sets of acceleration data per trial allowed for acceleration direction comparisons as well.

The tri-axial accelerometer readings were evaluated by taking the root of the sum of squares of each component.

$$H_{accel} = \sqrt{{a_x}^2 + {a_y}^2 + {a_z}^2}$$

The six single-axis accelerometers were evaluated to find the overall head acceleration and direction of acceleration. The equation below describes how each single-axis accelerometer can be written as a vector component of the overall head acceleration [28].

$$\|a_i\| = \|A(t)\| \cdot \cos(\beta_i)$$

Here A(t) is the overall head acceleration, a_i is the single-axis accelerometer reading, and β_i is the angle between the single-axis and overall head acceleration vectors. A visual representation of how this arranges on a spherical head is shown in Figure 58.

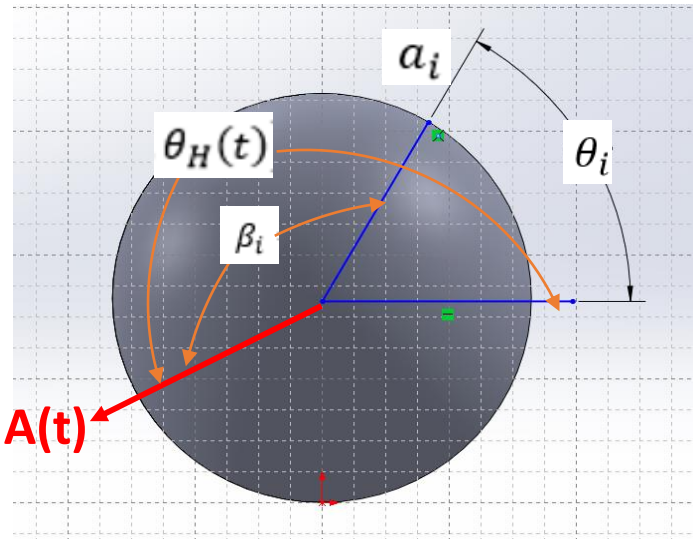

Figure 58: A spherical head with acceleration vectors

The cosine of the angle between both acceleration vectors is better represented in spherical coordinates where the angular position (θ_i, α_i) of the single-axis accelerometer is known. The direction of the head acceleration vector, A(t), is represented by (θ_H, α_H).

$$\|a_i\| = \|A(t)\| \cdot [\cos(\alpha_i) \cdot \cos(\alpha_H) \cdot \cos(\theta_i - \theta_H) + \sin(\alpha_i) \cdot \sin(\alpha_H)\,]$$

The above relationship holds true for each accelerometer placed on the spherical head-form. The magnitude and position of each accelerometer is known, but the magnitude and direction of the overall acceleration is not. With a six-accelerometer set up, this gives six equations with only three unknowns, or six constraints with three degrees of freedom. To satisfy this overdetermined system the method of least-square approximation was used. The least-square method is typically used for solving an overdetermined

system, one example being curve fitting of data points. The least-square error (i.e. the cost function) of our system can be written as. This yields

$$E(\|\boldsymbol{A}(\boldsymbol{t})\|, \alpha_H, \theta_H) = \sum_{i=1}^{6} [\,\|\boldsymbol{A}(\boldsymbol{t})\|(\cos\alpha_i \cos\alpha_H \cos(\theta_i - \theta_H) + \sin\alpha_i \sin\alpha_H) - \|\boldsymbol{a}_i\|]^2$$

There are various methods for minimizing the error of the above equation. Two methods were explored in this project: traditional nonlinear least squares minimization and simulated annealing optimization. The first method of nonlinear least square approximation takes the Jacobian of the function and aims to simultaneously minimize it for the three variables in question. Alternatively, simulated annealing explores the entire state space with decreasing "temperature" values. Both methods were applied to initial data to determine the best one moving forward. While the nonlinear least square approximation method was often significantly faster than simulated annealing optimization, it did not always converge in its solutions finding possible local minima. Simulated annealing is known for its ability to often find the global minima of an optimization problem, no matter the proximity of the initial guess. Therefore, simulated annealing optimization, described in further detail in the following section, was chosen to evaluate all of the single-axis accelerometer data for this project.

Simulated Annealing Optimization

The method of simulated annealing is part of the stochastic optimization family, meaning it relies on the generation of random sampling to converge to a solution [29]. Example applications include the traveling salesman example or for protein folding [30]. It gets its name by mimicking the annealing process applied to metals by which the temperature is increased and decreased to change the physical properties. Simulated annealing uses "temperature" selection and a Metropolis Monte Carlo optimization technique of random sampling in the state space to find the global minimum.

The "temperature" parameter allows the algorithm to thoroughly explore the energy function to find the global minimum. The function being optimized is known as the energy function which is in contact with a thermal system at temperature "T". A summarized outline of the simulated annealing process is included below.

1. *High initial temperature selected.*
2. *Random point in the state space is chosen to start.*
3. *Second random point in the state space is chosen to compare.*
4. *Move to second point if…*
    a. *Second point has lower "energy" (function value) than original.*
    b. *Second point has higher "energy" (function value) than original and probability function is satisfied.*
        i. $Probability = e^{\frac{-\Delta E}{k_B T}}$

ii. $k = Boltzmann's\ constant$
$\Delta E = difference\ in\ energy\ values\ of\ two\ points$
$T = current\ temperature$

5. *Steps 3 and 4 are repeated while decreasing the temperature.*
6. *Stopping criteria achieved; possibilities below.*
    a. *Minimum temperature value reached.*
    b. *Number of iterations passed without accepting new solution.*
    c. *Maximum number of iterations exceeded.*

The reason the simulated annealing process is effective at finding global minima, and not getting caught in local minima, is the temperature and probability function. At high temperatures, the probability function allows the algorithm to accept worse points as the new starting condition. This lets the process search the entire state space before narrowing in on a possible minima. The temperature schedule, not discussed in the above process, play a role in how extensively and quickly the algorithm converges to a solution. Depending on size of the optimization and preference, the number of iterations (steps 3 and 4) can be constant at each temperature step throughout the process, or change as the process progresses. It is desirable to increase iterations at lower temperatures to narrow in on the solution. The degree in which temperature steps are taken, known as the cooling schedule, also affects convergence speed and effectiveness. Temperature can decrease linearly, geometrically, or dynamically as the optimization continues.

Matlab Adaptive Simulated Annealing

In our analysis we used the Matlab built in function simulated annealing to evaluate the results from the six, single axis accelerometers. There are a few distinct differences between the Matlab method and the traditional simulated annealing as described above. Matlab implements a variation of simulated annealing known as “adaptive”; meaning key parameters such as temperature and step selection are automatically updated after each iteration depending on proximity to converging to a solution. The benefits of using this adaptive method instead of writing a basic simulated annealing code is the iterative process can change its method as the solution converges, allowing for a quicker process. The Matlab code used to run simulated annealing is in the Appendix.

Since this was a small, only three degrees of freedom to solve for, straight forward optimization, most of the Matlab defaults for simulated annealing were kept. The default temperature step was 100, and the default maximum number of iterations is 3000 times the degrees of freedom (or 9000). While the temperature step starts at 100, the way in which it steps is also adjusted as the iterative process continues. The new temperature is dependent on the initial temperature and the current iteration number, k.

$$T = T_0 \cdot 0.95^k$$

Below in Figure 59 is the graphical output that Matlab gives during optimization. The Cost Function decreases as the optimization finds values with lower energies.

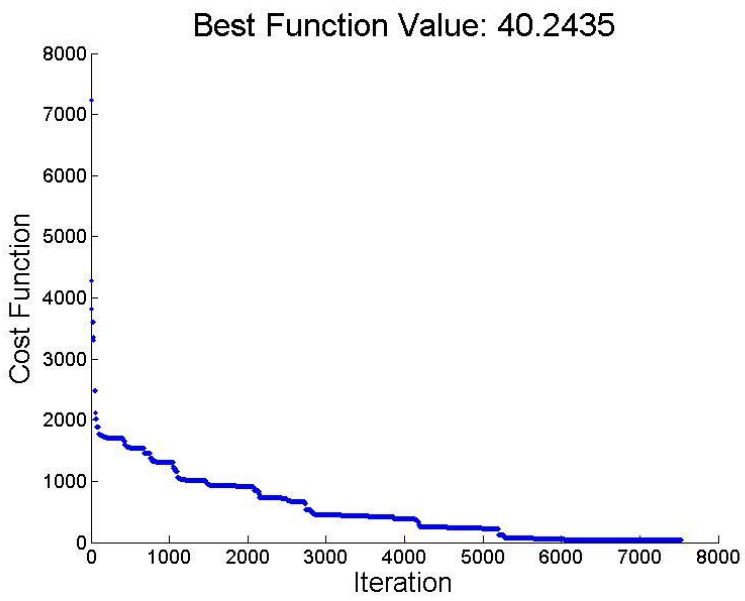

Figure 59: Cost function values as the simulated annealing steps through iterations looking for the lowest value in the phase space

The acceptance criteria Matlab uses is shown below. It is a little different than the standard acceptance criteria in that it does not use Boltzmann's constant.

$$Acceptance = \frac{1}{1 - e^{\frac{\Delta}{MaxT}}}$$

Where Δ is the difference in objective function value between the two points in question, and MaxT is the current temperature step.

Choosing a Better Initial Guess

The speed of convergence during optimization problems depends on the proximity the initial guess (starting point) of the function is to the global minima. A poor initial guess can lead to the iterative process getting caught in local minima, although the use of simulated annealing aids in preventing this.

Varying the initial guess for the magnitude of overall acceleration did not significantly affect the speed of convergence or the value to which the process converged to. Because of the nature of the motion of the test head and torso, guesses for the acceleration angle in the theta direction is fairly straight forward. The head/torso can only rotate about one axis, so the theta angle of acceleration will typically be pi or zero. The angle α_H of head acceleration was the driving initial guess that would enable much quicker convergences, or enabling selection of local instead of global minima.

To help in choosing an appropriate initial guess for the angle of head acceleration alpha, a 3-D contour map of the cost function was created in Matlab by setting the magnitude of acceleration equal to a constant and plotting the cost function over the theta and alpha angle range [-pi, pi] radians. Below is an example of this contour plot of the cost function. The low red areas indicate local minima, with one being the global minima. The plot, shown below in Figure 60, only needs to span a range of 2pi of each angle because of the sinusoidal nature of the cost function.

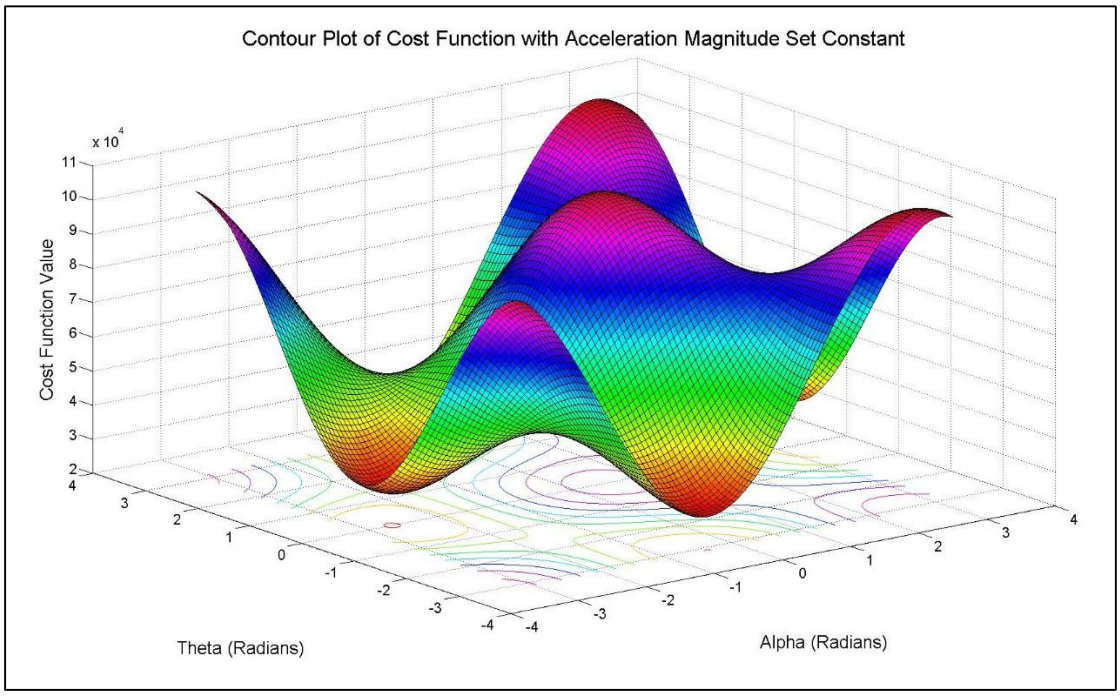

Figure 60: Contour plot of the cost function with constant acceleration magnitude to assist in choosing better angle initial guesses

This process of contour plotting to get a better initial guess was only performed when certain sets of accelerometer data would not converge or would converge with a large final value for the cost function.

Optimizing for Accelerometer Placement

The positioning of the six, single-axis accelerometers in the head ended up being extremely critical to the accuracy of results obtained. The accelerometers could only be positioned by hand with an accuracy of about four degrees. This was not sufficient in analyzing the accelerometer data. To measure the accelerometer positions to an accuracy of one degree, simulated annealing was used to optimize the results for accelerometer placement. A large optimization was conducted where the accelerometer positions, theta and alpha for all six accelerometers, and the resulting head acceleration and direction, A(t) theta and alpha, were solved for at once. Using a set of thirty points this resulted in optimizing for 102 degrees of freedom. While this method was most ideal, due to various constraints it did not work out well. Instead two optimization were conducted in parallel to find the accelerometer positions.

Taking a set of data over 60 milliseconds, 30 sets of single-axis accelerometer data, the overall head acceleration and direction (A(t), α_H, θ_H) were optimized for using simulated annealing. The average value of the cost function was found for this initial optimization to create a starting point. It is this average value that the rest of the process will aim to minimize. Using the values for overall head acceleration, a different simulated annealing program was used to optimize for accelerometer position. This was a twelve degree of freedom optimization. The accelerometer position angles returned from this optimization were then used in the first optimization as the accelerometer positions and the process was repeated. Using this "brute-force" way of optimizing with simulated annealing, the process only needed four iterations before the angle values and average cost function value did not change.

Below in Table 6 and Table 7 are the comparisons of accelerometer position before (the best approximation of locating the accelerometers by hand) and after optimization. The bounds on the optimization was +/- 5 degrees. While the theta angles seemed to converge to a value, the alpha degrees reached the bounds and could not continue changing to help the optimization. The new optimized positions were tested on a few trials and the results were compared to results determined from the original positions to ensure this optimization was true for all trials. After confirmation, the optimization positions were used to evaluate all of the single-axis accelerometer results.

Table 6: Original accelerometer positions in angles theta and alpha

Original (Degrees)	
Theta	*Alpha*
0	20
0	60
180	60
180	20
270	30
90	30

Table 7: Optimized accelerometer positions in angles theta and alpha

Optimized (Degrees)	
Theta	*Alpha*
-5	25
1	55
182	60
185	25
267	25
93	25

7.0 Results and Discussion

The design team conducted device tests with various fluids, paddle designs, and accelerometer configurations. Processing the information to accurately determine whether the device was working as intended, and in order to quantify how well it was working, required multiple iterations of data evaluation starting with video analysis. Only the best paddle configuration of each fluid is shown graphically in the following sections.

7.1 Deflection

The results from the high-speed footage captured displayed two major things: the overall angular deflection of the neck with respect to the torso and the deflection of the torso with respect to its initial position. Additionally, the video footage was used to identify the speed of the striking player prior to impact to estimate the amount of potential energy put into the impact. As previously mentioned, SolidWorks was utilized to measure the angular deflections of the frames captured by the high-speed camera. The results of max head and max torso deflection for a variety of fluids and hole patterns can be seen in Table 8 below; additionally a bar chart comparing the various fluids, which have been fitted with standard error, to the baseline data can be seen in Figure 61.

*All Holes means two 6mm holes, two 8mm holes, and six ¼" holes.

Table 8: Video Analysis - Torso and Head/Neck Deflection

Fluid-Hole Combination	Max Head Deflection (Degrees)	Max Angle Torso (Degrees)
Baseline (No Device)	59.6	23.2
15W No Holes	43.8	23.8
15W One 6mm Hole	47.7	24.1
15W One 8mm Hole	49.9	25.1
50W One 6mm Hole	43.6	28.5
50W One 8mm Hole	43.6	27.5
50W Two 8mm Holes	48.3	24.4
Cornstarch 47.5% Six 1/4" Holes	61.6	24.3
*Cornstarch 47.5% All Holes**	61.9	23.9
Cornstarch 50% Six 1/4" Holes	56.3	25.6
*Cornstarch 50% All Holes**	58.1	22.6

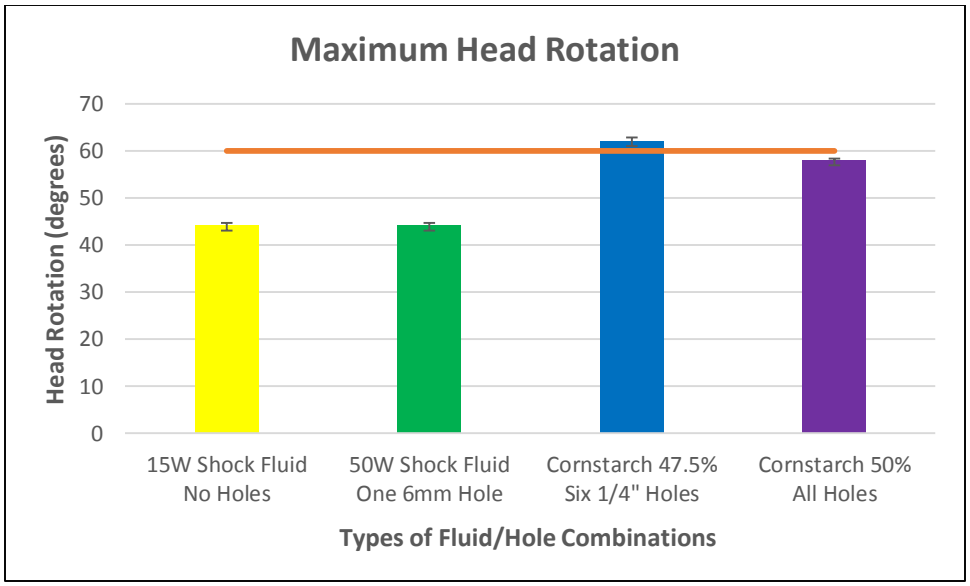

Figure 61: Bar Chart - Maximum Head Rotation for Various Fluids

The video analysis also determined the speed of impact was consistently 7.5 m/s. The rotational displacement data shown in the table above shows the relationship that exists between no device and a device loaded with either 15W, 50W, or corn starch mixture. As expected the device reduces the angular displacement of the head with respect to the torso, and consequently increases the total angular deflection of the torso with respect to its initial position. This is consistent with the device expectations, as it shows it is effectively transferring energy from the impact to the torso. The best fluid and hole combination, 50W fluid with a paddle design of one #6 tapped hole, showed an improvement in the neck displacement of roughly 27 percent while increasing the torso deflection by 23 percent.

7.2 Speed and Acceleration

The incorporation of two sets of accelerometers into the struck player enabled the group to optimize calculations determining the direction and magnitude of the angular acceleration affecting the player. While the tri-axial accelerometers gave quick feedback regarding the magnitude of the head acceleration during the impact, the set of six single-axis accelerometers were used to evaluate the overall acceleration magnitude and direction. By employing both sets of data the team was able to reduce the total amount of error and check for consistencies in the measuring techniques.

To most confidently determine the repeatability and reproducibility of the data the team performed multiple trials for the various fluids and hole patterns. Baseline testing without the device attached was completed first in order to develop a model to which experimental data could be compared. Baseline testing was completed with 5 trials while each individual fluid and hole pattern was tested with a total of 4 trials. The results were amalgamated into one excel spreadsheet for analysis; first separating the single from the tri-axial accelerometer data. Figure 62 and Figure 63 below show bar graphs of the maximum head velocity (the area under the curve prior to deceleration) and maximum acceleration in g's for each

of the fluids tested with their optimal hole pattern obtained from the tri-axial accelerometer; notice that the data for each fluid, which has been adjusted to shown standard error, is compared to data from baseline testing (the orange bar).

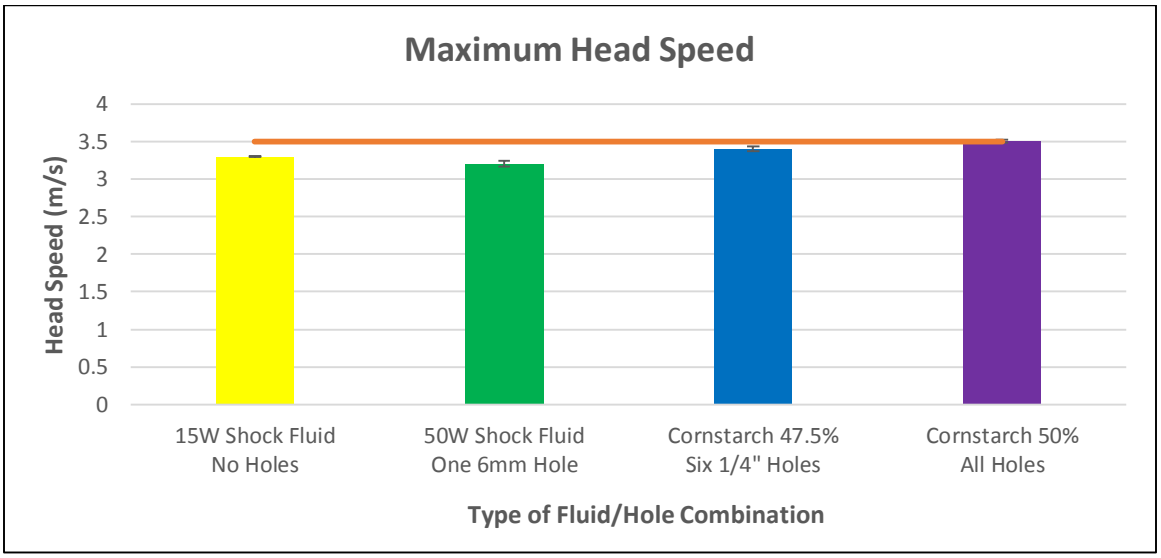

Figure 62: Bar Chart - Maximum Head Speed for Various Fluids

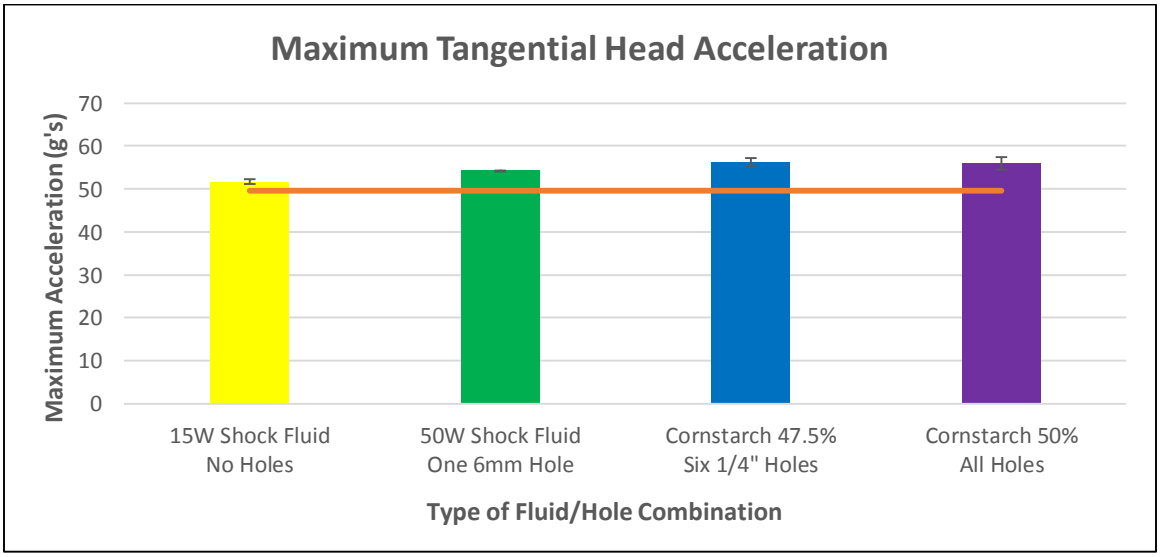

Figure 63: Bar Chart - Maximum Tangential Head Acceleration for Various Fluids

With the data obtained from the tri-axial accelerometers it became apparent that the team's best fluid and paddle combination was the 50 weight shock fluid coupled with one 6mm hole. The results using this fluid showed improvements when compared to baseline testing and resulting in a decrease of head velocity of roughly 8% and a decrease in the time required to start decelerating of 35%. The graph below shows the acceleration curve for all four trials of the 50W shock fluid with one #6 hole as compared to the average baseline curve. The repeatability of the data is shown very clearly.

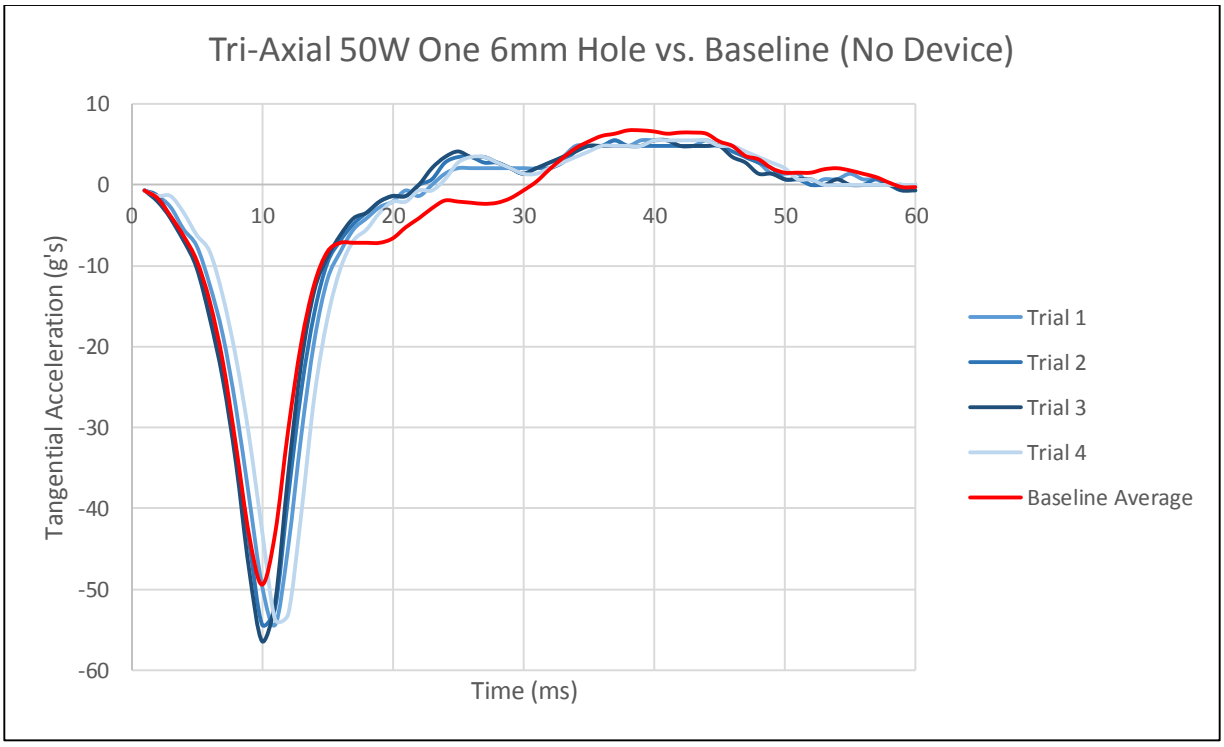

Figure 64: Acceleration of 50W Shock Fluid with One #6 Hole vs. Baseline (No Device) Data

In Figure 64 shows the general trendline for all experimental data. The various shades of blue curves plot the data from the 50W one #6 shock fluid trials. As can be seen, the time to reach deceleration is much sooner than that of the baseline testing. It can also be noted that the peak acceleration actually increases, signifying the simulation of a rigid neck. The area under the curve, quantified as the tangential velocity of the head, is the largest telling factor of the severity of the impact and therefore, is the value that the team sought most to reduce.

Having compiled the data from the tri-axial accelerometer, the team next proceeded to compile the data from the six individual single-axis accelerometers using the previously mentioned optimization process in MATLAB. The acceleration curve of the same set of trials derived from the tri-axial and the six single-axis accelerometers were consistent, as shown below in Figure 65. Not only were the trials reproducible, but the two methods of data collection and evaluation were consistent. Since the six single-axis accelerometer results do not offer new information regarding the magnitude of acceleration, their results will be used exclusively for direction of acceleration information.

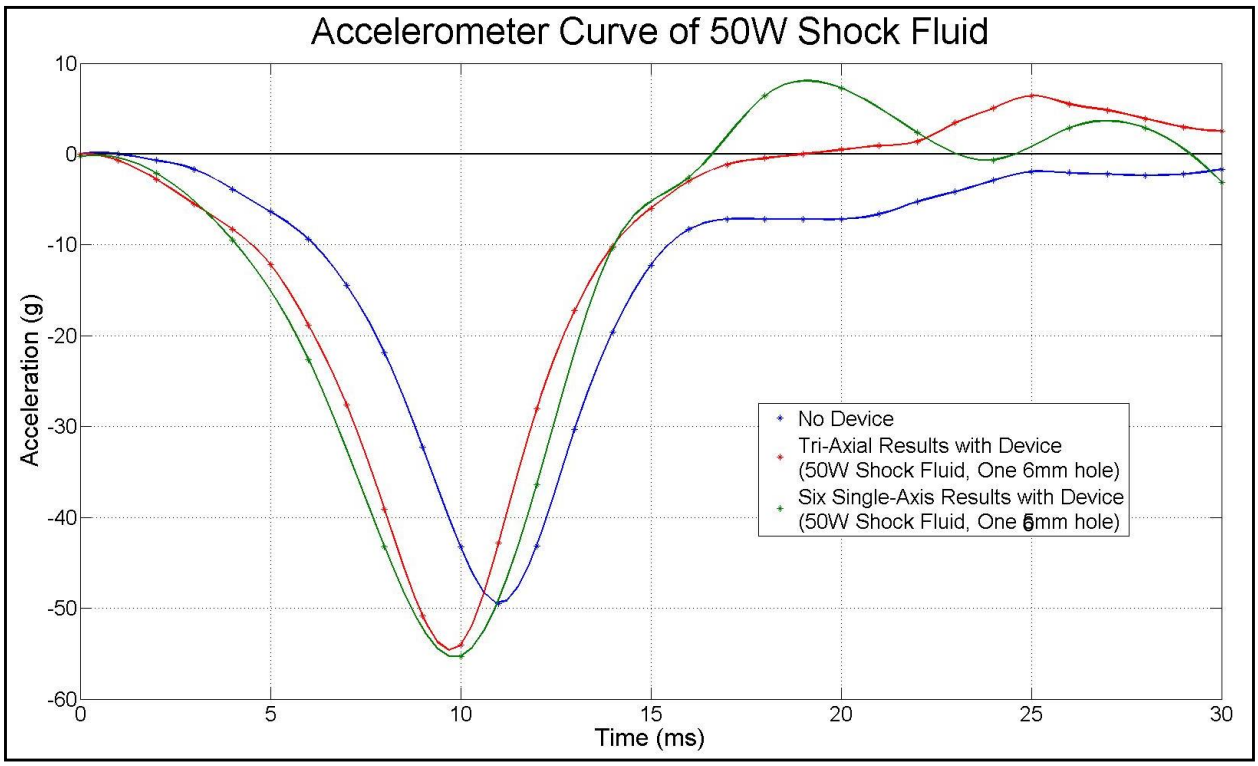

Figure 65: 50W One #6 Hole - Single-Axis, Tri-Axial, and Baseline Acceleration Curves

7.3 Direction of Acceleration

While the tri-axial accelerometer results were evaluated just for the tangential acceleration of the head, the six single-axis accelerometer results gave an insight to the direction of the overall head acceleration. The single-axis accelerometers gave three results: magnitude of the head acceleration, angle theta and angle alpha of direction of acceleration. The magnitude was used in the previous section to verify the tri-axial results. The angles theta and alpha are the spherical coordinates of the acceleration vector at the center of the head. If the head were the Earth with the North Pole at the top of the head and the South Pole near the chin, the theta measure would be in longitude and the alpha measure would be in latitude.

As expected, the theta angle of acceleration direction was almost always close to zero or close to +/-180. While the torso is not fully constrained about any axis, the impact does only encourage rotation about one axis. The difference between the theta as zero and as +/-180 is minimal as it can be corrected for in the magnitude of corresponding acceleration. Figure 66 below shows the plot of the angle theta direction of head acceleration. Less than 30% of the data collected determined a theta angle other than 0 or +/-180, indicating the theta direction of acceleration of the head is almost always tangential to the motion. In the graph below, angles that are outside the zero or 180 range lie around the 20 millisecond mark. This is after the impact and it is possible the torso or head rotated slightly about another axis to cause this difference.

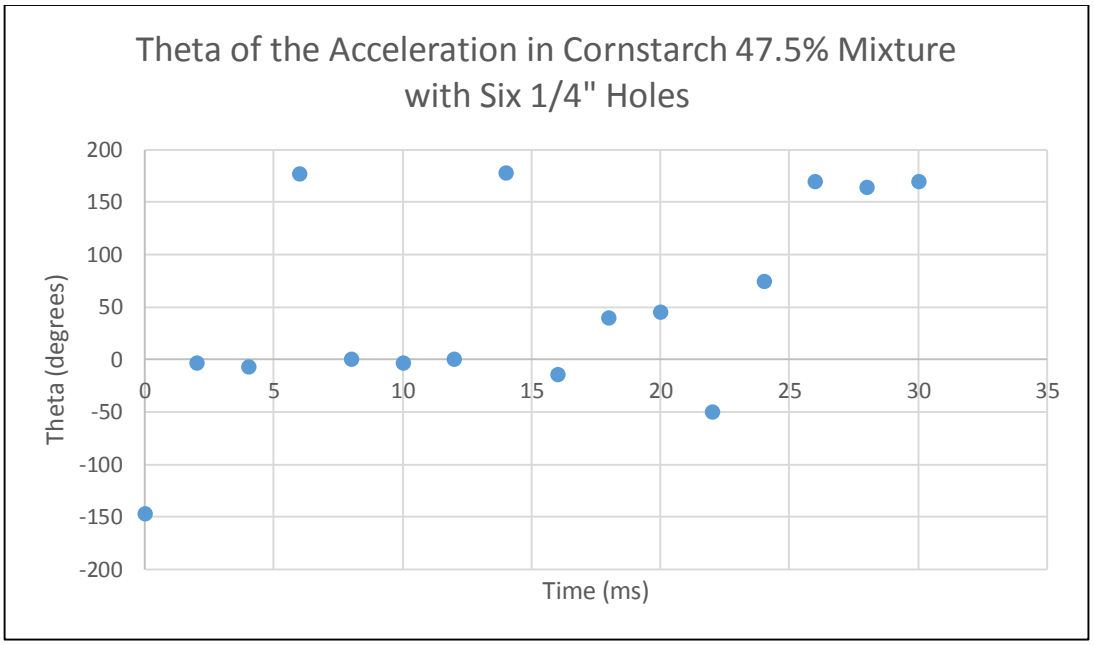

Figure 66: Plot of the theta direction of head acceleration during one of the 47.5% cornstarch mixture with six ¼" hole trials

While the theta angle of head acceleration was predictable, the alpha angle was a bit more unknown. But on analysis, it showed a similar trend as the theta angle of acceleration direction. Most of the alpha angles were about zero or +/-180. Figure 67 below shows this relationship. The initial impact lasts around 15 milliseconds, so it isn't until after that that the alpha angle changes. For the alpha angle, an angle other than zero or +/-180 indicates the acceleration is pointed toward (or away from) the axis of the neck indicating neck compression. This seems to occur after the initial impact, which might be a result of the flexion of the rubber neck upon release.

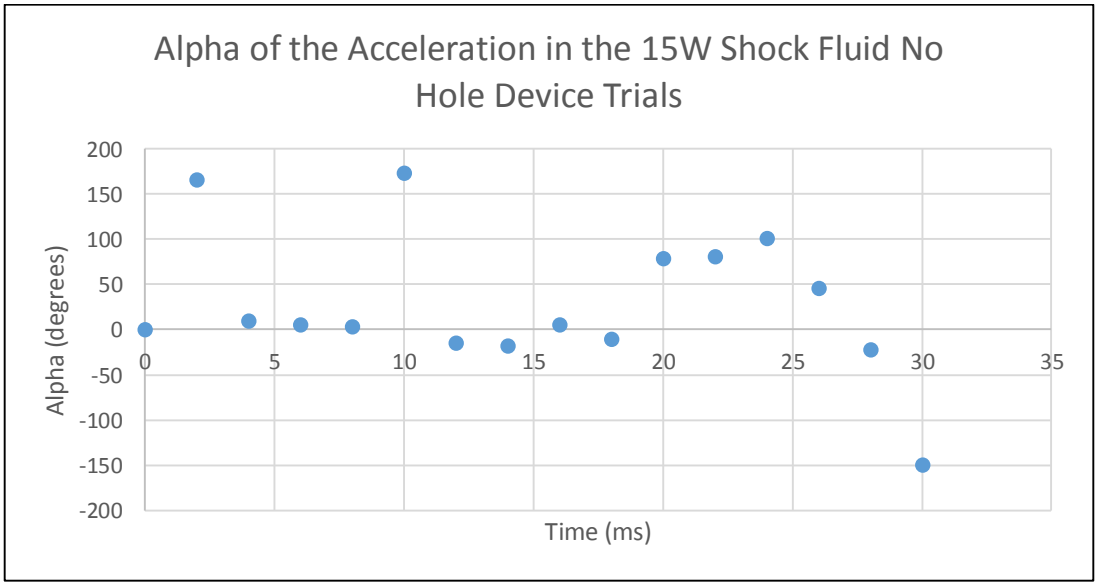

Figure 67: Plot of the alpha direction of head acceleration during one of the 15W-No Holes device trials

Analysis of the direction of head acceleration further shows using the tangential tri-axial acceleration result for analysis is adequate as most acceleration is tangential to the head.

7.4 Head Injury Criterion (HIC)

A typical equation employed by sports scientists, automotive safety personnel, and neurologists alike is the HIC (Head Injury Criterion). Defined by the acceleration and time stamps marking the beginning and end of the steepest peak/trough, the equation fundamentally solves for the area under the curve to determine the tangential head velocity achieved. Studies have found that large percentages of conditions occur not from the direct impact to the skull, but instead, by the relative stillness of the brain with respect to the rotationally accelerated head. To most effectively reduce the severity of the impact, and therefore to reduce the probability of sustaining a concussion, the team aimed at lowering the HIC value by means of decreasing the time to achieve deceleration and to reduce the area under the curve (representative of the velocity of the head).

As previously mentioned, the HIC equation shown below depends on the acceleration as a function of time as well as the duration of the peak/trough. The resulting *Head Injury Criterion* values for four different fluid combinations, with calculated standard error, can be seen below in Figure 68.

$$HIC \equiv \left\{\left[\frac{1}{t_2 - t_1}\int_{t_1}^{t_2} a(t)dt\right]^{2.5}(t_2 - t_1)\right\}_{max}$$

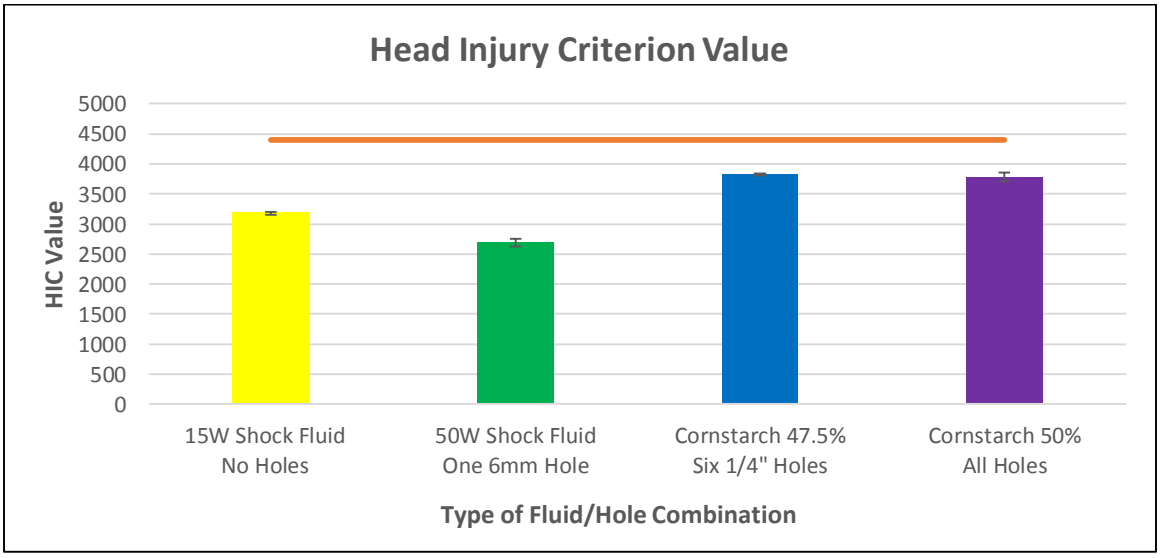

Figure 68: Bar Chart - Maximum Tangential Head Acceleration for Various Fluids

With all of the data evaluated, the team was able to identify the best fluid and hole pattern combination for reducing the likelihood of sustaining a concussion from a large impact hit. Across the board the 50W one #6 fluid and hole pattern design performed the best. The maximum head rotation was decreased by

26%, the maximum velocity was reduced by 8%, the velocity after 30ms was reduced by 17%, the point of deceleration was decreased by 35%, and the HIC value was reduced by an impressive 39%. Table 9 summarizes the data obtained for various fluids and hole patterns.

Table 9: Device Results from Various Fluids as Compared to Baseline Testing

Fluid-Hole Combination	Max. Head Rotation (degrees)	Max. Velocity (m/s)	Time of Deceleration (ms)	Max. Acceleration (g)	Head Injury Criterion
Baseline (No Device)	60	-3.5	30.3	-49.5	4402
15W Shock Fluid No Holes	44	-3.3	22.8	-51.7	3178
15W Shock Fluid One 6mm Hole	48	-3.4	23.3	-52.9	3456
15W Shock Fluid One 8mm Hole	50	-3.4	24.5	-57.7	3540
50W Shock Fluid One 6mm Hole	44	-3.2	19.5	-54.2	2686
50W Shock Fluid One 8mm Hole	44	-3.3	22.5	-53.3	3106
50W Shock Fluid Two 8mm Hole	48	-3.5	23.5	-54.8	3779
Cornstarch 47.5% Six 1/4" Holes	62	-3.4	25.0	-56.3	3822
Cornstarch 47.5% All Holes	62	-3.4	24.8	-54.6	3837
Cornstarch 50% Six 1/4" Holes	56	-3.4	24.3	-55.7	3788
Cornstarch 50% All Holes	58	-3.5	23.3	-56.0	3780

7.5 Sources of Error

The data obtained through testing operations was unavoidably toleranced by a series of errors. Tolerance stack-up, a term generally used to describe tolerances which combine to form worst-case scenarios for manufacturing or testing, contribute error to the system which skews the credibility slightly.

Considering the impact itself, one may realize the amount of energy lost through the system by means of vibrations, friction between the cables and the dropping player, sound, and deformation. These variables, while marginal when considering the total amount of energy in the system, play a role in determining the difference between the gravitational potential energy of the player atop the rig and the actual kinetic energy delivered to the receiving player.

Another source for error within the testing procedure was within data acquisition. The single-axis accelerometers utilized by the team were given an accuracy of +/- 4% while the tri-axial accelerometer was given an accuracy of +/- 7%. Additionally, the Arduinos used to interpret the signals from the accelerometers were given a tolerance of +/- .5% from the manufacturer. Other sources of error such as the frame rate used to determine the angular deflection and speed of the impacting player also contribute to small calculation errors within the testing procedure.

8.0 Conclusions and Recommendations for Future Work

Developing a device to help prevent the severity, and therefore the likelihood, of concussions in football required a design with quick reaction times, comfort, and minimized motion restriction. The final rotational shock absorber design fulfilled all of the design criteria and allowed the team to validate the proof of concept.

Results from testing various fluid and hole combinations suggested that device reaction times were fast enough to change the acceleration versus time experienced by the head of the struck player. Optimization of fluid densities, viscosities, and the correct hole patterns was one of the more difficult processes involved in the design and testing of the device. The team retrieved data which displayed reductions in the *Head Injury Criterion* (HIC) values of the struck player's head acceleration when the device was in place. Of the ten fluid-hole combinations tested, the 50 weight shock fluid with one 6mm hole was the most successful in reducing key parameters associated with concussions. Compared to results of testing without the device, 50 weight shock fluid with one 6mm hole reduced the rotation of the head relative to the torso by 26%, the maximum velocity of the head by 8%, the velocity of the head at 30 milliseconds by 17%, the point of head deceleration by 35%, and HIC value by 39%.

8.1 Future Work

While the results from this experiment show the concept design is effective at reducing parameters related to concussions, a significant amount of future work would be necessary for further testing of the device and eventual commercialization. Testing would include improvement of impact methods and data evaluation, as well as exploration into different fluid and paddle combinations. To move forward with the device as a wearable, usable product, changes would need to be made to material, size, and placement of the device on the torso.

To compare HIC results from use of the rotational shock absorber to real football game data, the testing procedure used in this project would need to be adjusted to more closely replicate actual game-like concussive hits. The HIC values returned from the existing testing were as much as four times higher than game-recorded HIC values. Until testing is developed that reproduces more relevant HIC values, results will only serve to show a relationship between device usage and HIC reduction, not injury-risk reduction. Ways to more accurately recreate game-like concussive impacts would include replacing the steel-frame torso and epoxy head with a Hybrid III male dummy torso and head to generate more human-like responses, using a Hybrid III neck on the striking player, and adjusting the manner in which the struck player is suspended from the test rig.

More accurate data collection and evaluation would be another step forward in pursuing the development of the rotational shock absorber. Accelerometers that have higher recording rates are desirable so a more accurate acceleration vs. time curve can be developed, as this will help in evaluation of the HIC values. Along with better accelerometers, further optimization to locate the position of the single axis

accelerometers is necessary. Using simulated annealing it is possible to locate the accelerometers on the head, but more time must go into defining the phase space so the angles converge to reasonable solutions. Due to time constraints this was not possible for this project, but moving forward it would be necessary. Alternatively, having a machine position the accelerometers in the head would eliminate the need for optimizing for accelerometer position because the accuracy of the machine placement would be close to $1/10^{th}$ of a degree.

Once a better testing and data evaluation method are determined, the device could be tested for a multitude of fluid and hole combinations. With the results of this project serving as a basis for which types of fluids work best, further finite element analysis with ANSYS Fluent could be performed to optimize the paddle design for those fluids. While most Newtonian fluid research and optimization could be performed through ANSYS, the licenses available to our team do not include fluids with non-Newtonian behavior. Since the cornstarch and water mixture behaved so poorly in this project, research into other non-Newtonian fluids would be beneficial. A variety of shear-thickening fluids such as PEG and suspended silica nanoparticles, could be combined with different paddle designs to modify apparent shear rates and flow rates within the paddle compartment. Redesign of the actual size and shape of the paddle could force fluid through a larger surface area encompassing both the holes in the paddle as well as the distance between the edge of the paddle and the case walls. The use of electrorheological or magnetorheological fluids might also be explored, allowing results similar to those obtained with shear-thickening fluids but eliminating the need for shear rates to “activate” the fluid to become more viscous.

It may be beneficial to validate the use of dynamic, pressure-dependent paddle designs to allow for a more significant change in feedback forces between normal motion and impact motion of the head and paddle. This paddle might have a variable hole area dependent on the pressure within the compartment so that a sudden spike in internal pressure would block certain holes and restrict flow across the paddle, amplifying the paddle restriction during an high impact collision while lowering resistance during normal head movement. One way to implement this is through the use of spring/ball combination within holes so that an increase in pressure compresses the spring and causes the hole to be blocked by the ball. Technology currently being developed for automobile dampers could very well be explored for this application.

In addition to improvements in varying fluids and paddles, future work would also include the optimization of a variety of device parameters to make the rotational shock more applicable in a real game manner. The size of the paddle compartment could be decreased to make the device more user-friendly and size effective. The materials used for each component could also be optimized to reduce the overall weight and cost of the device. While aluminum was the main material used for the prototype device, it is expected that future designs could utilize a vast amount of plastics to limit bulk mass. Material selection would decrease the device in size and weight and make a majority of the components easier to manufacture. A

variety of plastics can be injection molded to create mass quantities of parts, which are not only accurate, but also very cost efficient and durable. Reduced size might allow a pair of devices to be mounted just above the shoulder blades of the player, enabling for protection in both the front-back and side-side directions as well as everything in between.

Future work could include the design and manufacturing of a wearable device and include the full development of a comfortable interface to mount the device to existing equipment utilized by the player. It is believed that the device could be strapped to the shoulder pads of the player and manipulated into a neck roll or shoulder pad stack design. Jerseys worn by the player could be worn over the device interface, blending it further with existing equipment. Testing of this wearable product would also be conducted to ensure a comfortable, effective use of the product. It is suggested that additional prototypes be tested until a final, marketable product is developed.

9.0 References

1. "AANS." - *Sports-related Head Injury*. N.p., n.d. Web. 21 Sept. 2013.
2. Broglio, Steven P. “High school collegiate football athlete concussions: a biomechanical review.” Annals of Biomedical Engineering. 40.1: January 2012. pp. 37-46.
3. “Standard Performance Specification for Newly Manufactured Football Helmets.” NOCSAE DOC (ND) 002-11m12. National Operating Committee on Standards for Athletic Equipment. Modified May 2012.
4. Meehan III, William, and Richard Bachur. "Sport-Related Concussion." *Pediatrics*. 123.1 (2009): 114-123. Web. 18 Oct. 2013.
5. Hovda, David. "The Neurometabolic Cascade of Concussion."*Journal of Athletic Training*. 36.3 (2001): 228-235. Web. 18 Oct. 2013.
6. X. Sha, K. Yu, et. al. “Shear thickening behavior of nanoparticle suspensions with carbon nanofillers.” Springer Science. June 2013.
7. Shaw, Nigel. "The neurophysiology of concussion." *Progress in Neurobiology*. 67. (2002): 281-344. Web. 18 Oct. 2013.
8. Stern, Robert A., et al. “Long-term consequences of repetitive brain trauma: chronic traumatic encephalopathy.” American Academy of Physical Medicine and Rehabilitation. 3: S460-S467, 2011.
9. Funk, J. R. “Biomechanical risk estimates for mild traumatic brain injury.” Association for the Advancement of Automotive Medicine. 51st Annual Proceedings. 342-361.
10. Rowson, Steven, et. al. “Rotational Head Kinematics in Football Impacts: An Injury Risk Function for Concussion.”
11. Pellman, Elliot J., and David C. Viano. "Concussion in Professional Football." *Neurosurgical FOCUS* 21.4 (2006): 313-328. Print.
12. Yoganandan, Narayan. Frontiers in Head and Neck Trauma: Clinical and Biomedical. IOS Press, Jan 1, 1998.
13. "NFL Communications - Definition of a Defenseless Player «." *NFL Communications - Definition of a Defenseless Player «*. Section (a) Lines 1-8. Web. 19 Sept. 2013.
14. Irvine, Martha. "NFL Reaches $765 Million Deal in Concussion Suits with 4,500 Ex-players, including Cowboys Stars." The Dallas Morning News. Sports Day DFW, n.d. Web. 14 Jan. 2014.
15. Levy, Michael L. “Birth an evolution of the football helmet.” Neurosurgery 2004 (0148-396X), 55 (3), p. 656.
16. Doherty, John. "Chemistry commands concussion comeback." *Preps*. 02 Oct 2010: n. page. Web. 18 Oct. 2013
17. ASTM Standard F717-10. Standard Specification for Football Helmets.
18. "The Guardian Cap | Guardian." *Guardian*. Web. 09 Sept. 2013.
19. "Riddell 360 Helmet - Flex Facemask." Riddell. Web. 09 Sept. 2013.
20. "6D-ATR1 Helmets.” 6D Advanced Impact Defense. 6D Helmets. Web. 10 Sept. 2013.
21. "Xenith Epic – Helmet Technology.” Xenith Technology Web. 10 Sept. 2013.
22. Borden, Sam. "Glory Has Faded for the Neck Roll; Memories Have Not." Glory Has Faded for the Neck Roll; Memories Have Not. New York Times, 20 Oct. 2011. Web. 10 Sept. 2013.
23. *Viano DC, Casson IR, Pellman EJ. “Concussion in professional football: biomechanics of the struck player—part 14.” Neurosurgery.2007.*
24. Crawford, Nathan C., et al. “Shear thickening of corn starch suspensions: Does concentration matter?” Journal of Colloid and Interface Science: 396 (2013) 83-89.
25. "O-Ring Design Dimensions." O-Ring Design and Materials Guide. R. L. Hudson and Company. Web. 21 Jan. 2014.

26. "eFunda: O-Ring Design Guidelines." eFunda: O-Ring Design Guidelines. EFunda. Web. 21 Jan. 2014.
27. Padgaonkar, AJ., Kreiger, KW., King, AI. “Measurement of angular accelerations of a rigid body using linear accelerometers.” Journal of Applied Mechanics, 42: 552-556, 1975.
28. Crisco, J. J., J. J. Chu, and R. M. Greenwald. An algorithm for estimating acceleration magnitude and impact location using multiple nonorthogonal single-axis accelerometers. J. Biomech. Eng. 126:849–854, 2004.
29. Giordano, Nicholas J. and Nakanishi, Hisao. Computational Physics, Second Edition. Pearson Education, NJ. 2006.
30. *Sureja, N., and B. Chawda. "Random Travelling Salesman Problem using SA." International Journal of Emerging Technology and Advanced Engineering 2.4 (2012).*
31. “Facts about sports concussion from the American Headache Society.” American Headache Society. 10 November 2011.
32. Ashrafiuon, H., Colbert, R. “Modeling of a deformable manikin neck for multibody dynamic simulation.” Mathl. Comput. Modeling. 24-2: 45-56, 1996..
33. Moser, Whet. “A brief history of football head injuries and a look towards the future.” Chicago Mag. May 2012. http://www.chicagomag.com/Chicago-Magazine/The-312/May-2012/A-Brief-History-of-Football-Head-Injuries-and-a-Look-Towards-the-Future/
34. Pratt, David. “NFL Week 2 Injuries: Concussion epidemic continues.” Bleacher Report. September 2013. http://bleacherreport.com/articles/1776323-nfl-week-2-injuries-concussion-epidemic-continues
35. Florio, Mike. “Failure to use HIT system exposes league to future concussion liability.” NBC Sports. 24 June 2012. http://profootballtalk.nbcsports.com/2012/06/24/failure-to-use-hit-system-exposes-league-to-future-concussion-liability/
36. Jager, Marinus Karel Johannes de. Mathematical head-neck models for acceleration impacts. University of Technology Thesis. 2000.
37. Patent US3609764, March 20, 1969. Morgan, Gerard E.

10.0 Appendix

10.1 Arduino Code

10.1.1 Tri-Axial Accelerometer Code

```
const int xpin = A0;                  // x-axis
const int ypin = A1;                  // y-axis
const int zpin = A2;                  // z-axis

void setup()
{
  Serial.begin(115200);
}

void loop()
{
  Serial.print(analogRead(xpin));
  Serial.print("\t");
  Serial.print(analogRead(ypin));
  Serial.print("\t");
  Serial.print(analogRead(zpin));
  Serial.println();
}
```

10.1.2 Single-Axis Accelerometer Code

```
const int apin = A0;
const int bpin = A1;
const int cpin = A2;
const int dpin = A3;
const int epin = A4;
const int fpin = A5;
void setup()
{
  Serial.begin(115200);
}
void loop()
{
  Serial.print(analogRead(apin));
  Serial.print("\t");
  Serial.print(analogRead(bpin));
  Serial.print("\t");
  Serial.print(analogRead(cpin));
  Serial.print("\t");
  Serial.print(analogRead(dpin));
  Serial.print("\t");
  Serial.print(analogRead(epin));
```

```
  Serial.print("\t");
  Serial.print(analogRead(fpin));
  Serial.println();
}
```

10.2 MatLab Code

```
%% Simulated Annealing Program

clc; clear; close all;

lb = [-200 -2*pi -2*pi];
ub = [200 2*pi 2*pi];

options = saoptimset('PlotFcns', @saplotbestf);

%% Read the Excel Data sheet and assign to vectors.
filename = 'Corn_50AllHoles.xlsx';

rows = 'BC720:BH735';

a1 = xlsread(filename, 'BC720:BC735');
a2 = xlsread(filename, 'BD720:BD735');
a3 = xlsread(filename, 'BE720:BE735');
a4 = xlsread(filename, 'BF720:BF735');
a5 = xlsread(filename, 'BG720:BG735');
a6 = xlsread(filename, 'BH720:BH735');


%% Define position vectors of the accelerometers.
HMAS = [-5 25; 1 55; 182 60; 185 25; 267 25; 93 25]*pi/180;
alpha = HMAS(:,2)';
theta = HMAS(:,1)';

%% Create storage variable
y = size(a1);
z = y(1);

HeadAcc = ones(z,3);
error = ones(z,1);
flag = ones(z,1);

%% Evaluation
for i = 1:size(a1);
    a = [a1(i) a2(i) a3(i) a4(i) a5(i) a6(i)];

    ObjectiveFunction = @(H)smafun(H, a, theta, alpha);
    H0 = [24 pi pi/4];
    [H, fval, exitflag, output] = simulannealbnd(ObjectiveFunction, H0, lb,
ub, options);

    for j = 1:3;
        HeadAcc (i,j) = H(1,j);
    end

    error(i) = fval;

    flag(i) = exitflag;
end
```

```
%% Write results to Excel file.

header = {'Magnitude', 'Theta', 'Alpha', 'Error', 'Exitflag'};

results = [HeadAcc error flag];
filename2 = 'CS50_AllResults.xlsx';
sheetname = 'Sheet4';


--------------------------------------------------------------------------------

function  F = smafun(H, a, theta, alpha)

T = ones(1,6);

for k=1:6;
    T(k) = (H(1)*(cos(alpha(k))*cos(H(3)).*cos(theta(k)-
H(2))+sin(alpha(k))*sin(H(3)))-a(k))^2;

end

F = T(1)+T(2)+T(3)+T(4)+T(5)+T(6);
```

10.3 Results of the Tri-Axial Accelerometers

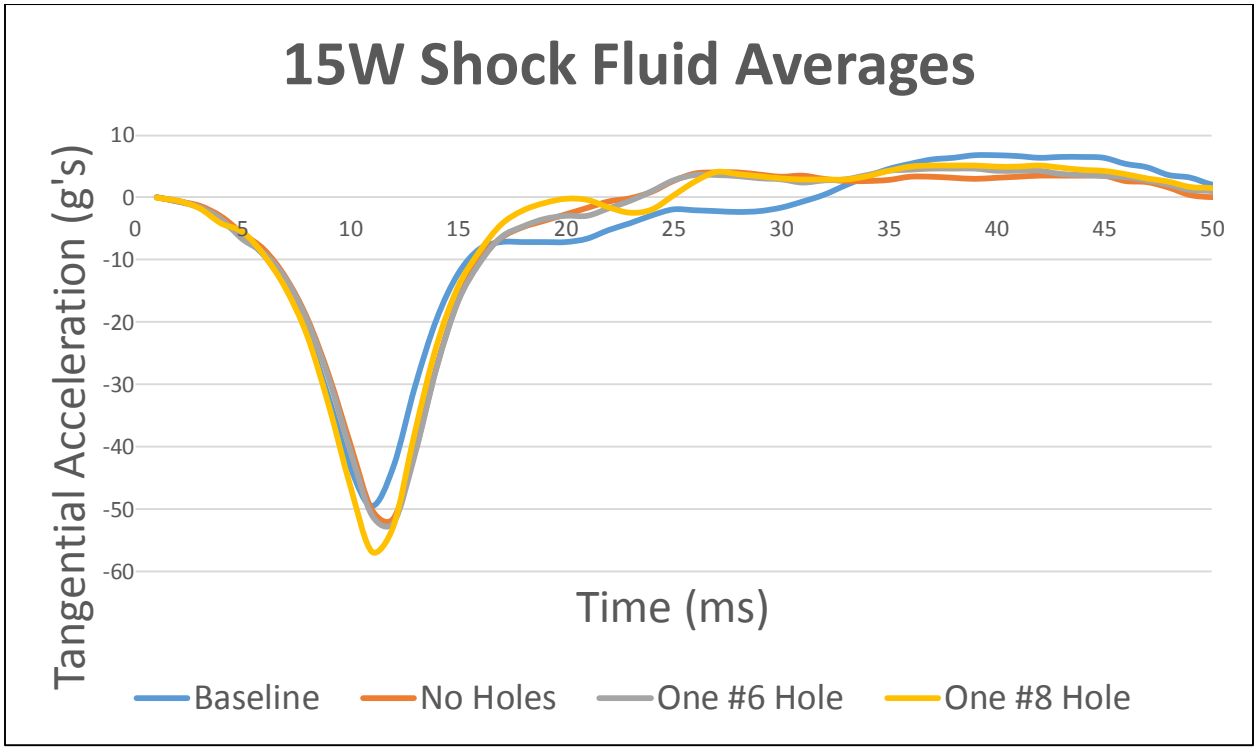

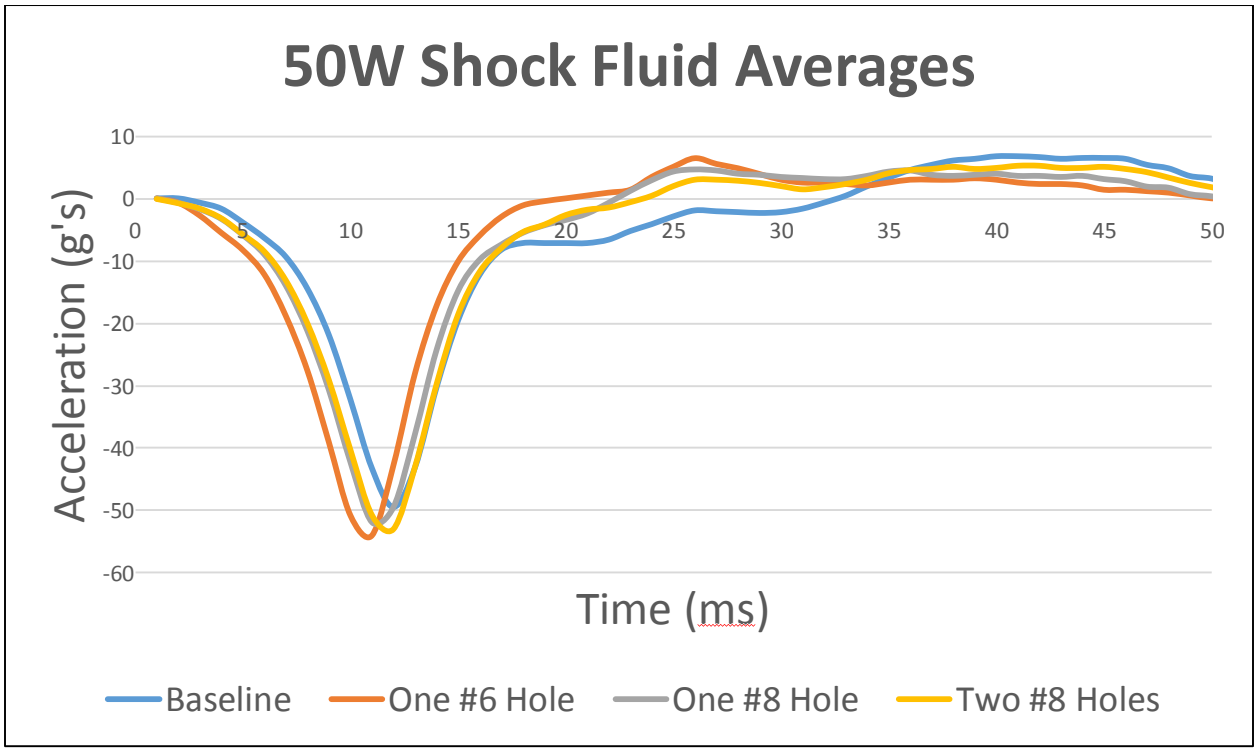

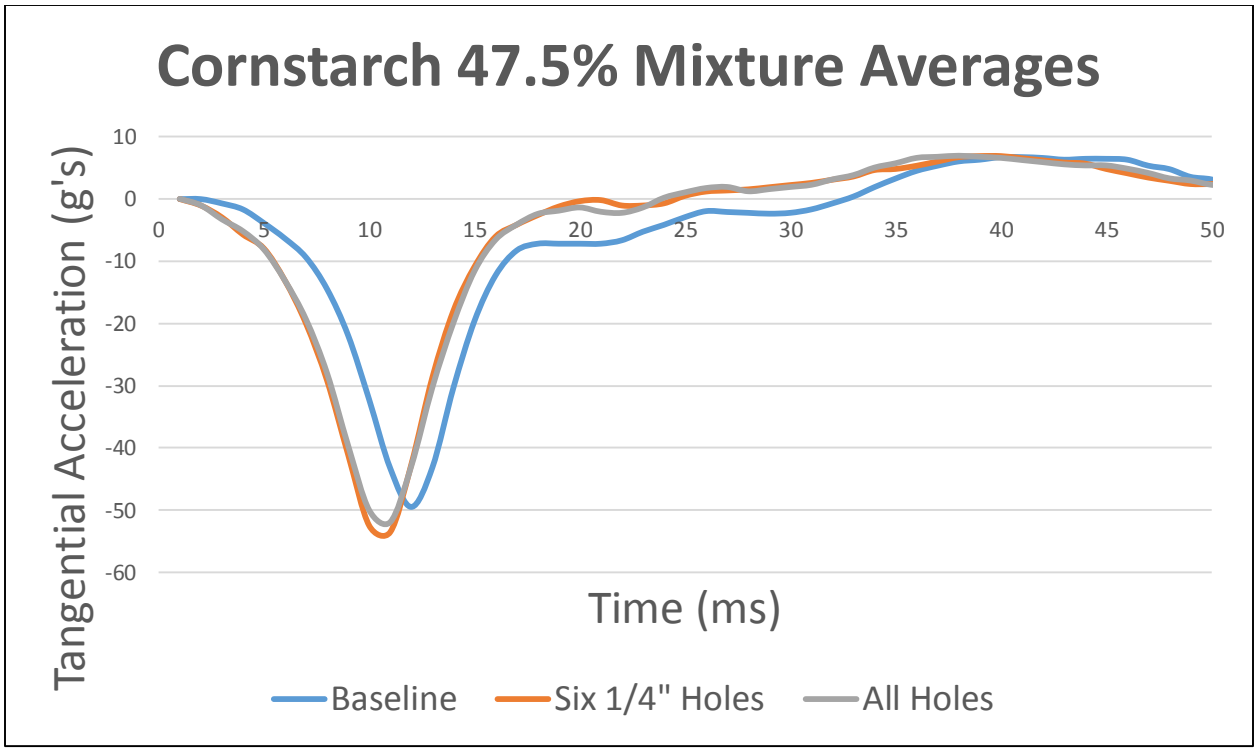
Cornstarch 47.5% Mixture Averages
Tangential Acceleration (g's)
10
0
-10
-20
-30
-40
-50
-60
0
5
10
15
20
25
30
35
40
45
50
Time (ms)
Baseline
Six 1/4" Holes
All Holes

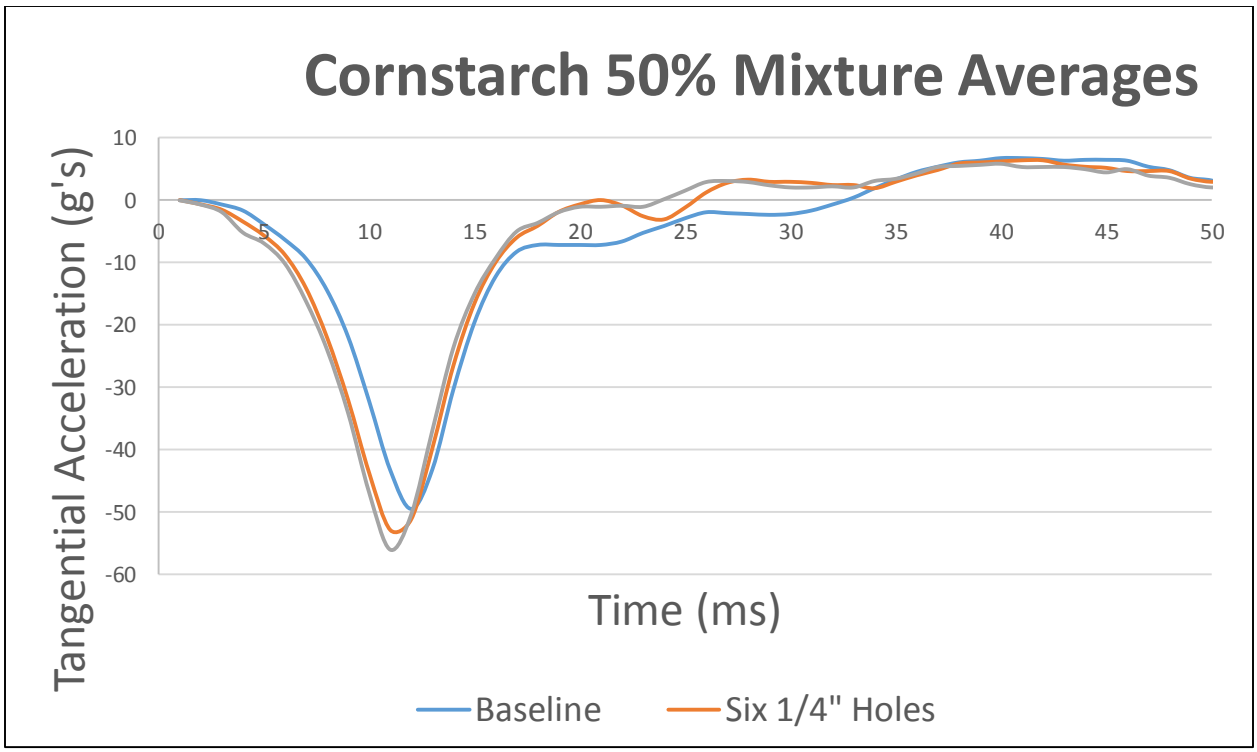
Cornstarch 50% Mixture Averages
Tangential Acceleration (g's)
10
0
-10
-20
-30
-40
-50
-60
0
5
10
15
20
25
30
35
40
45
50
Time (ms)
Baseline
Six 1/4" Holes

10.4 Results of the Six, Single-Axis Accelerometers

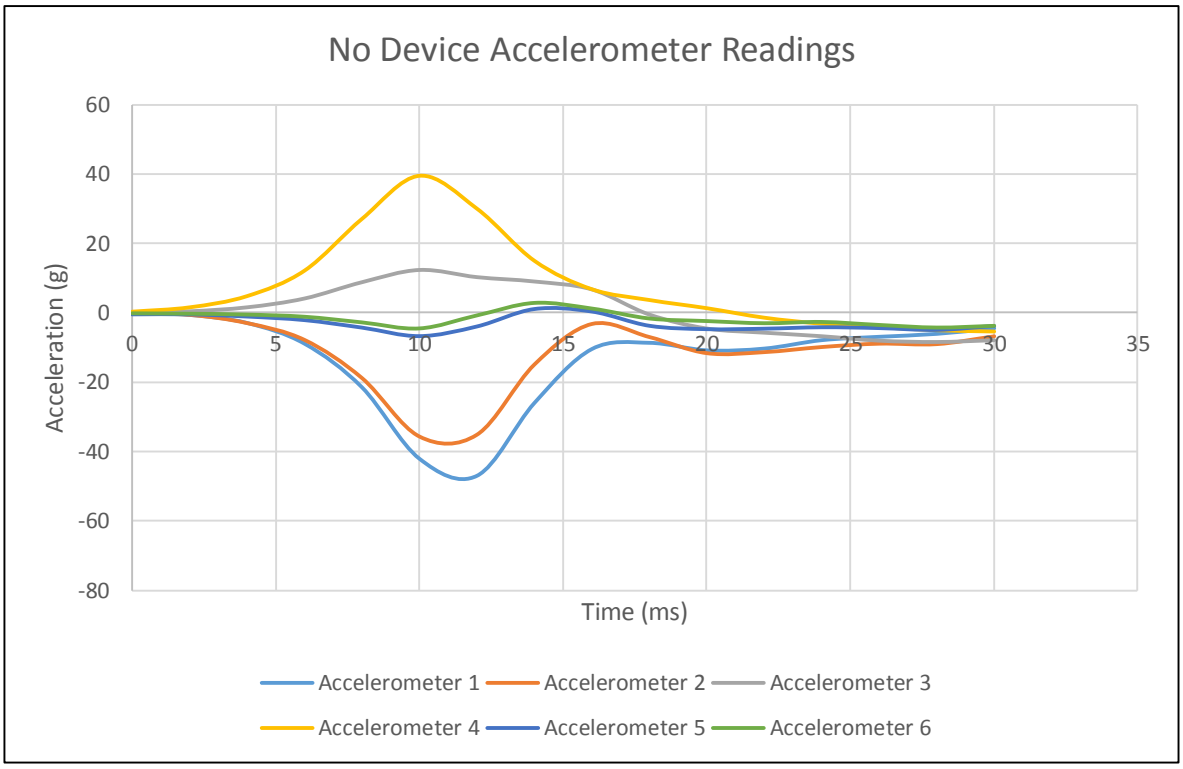

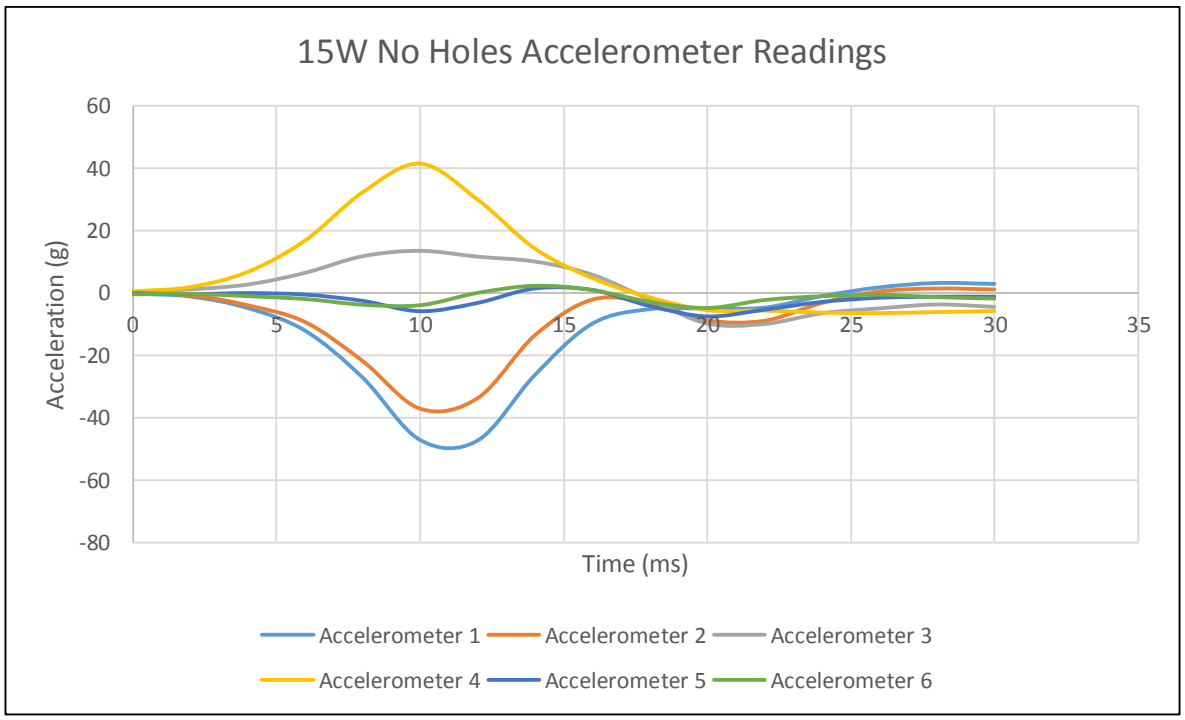

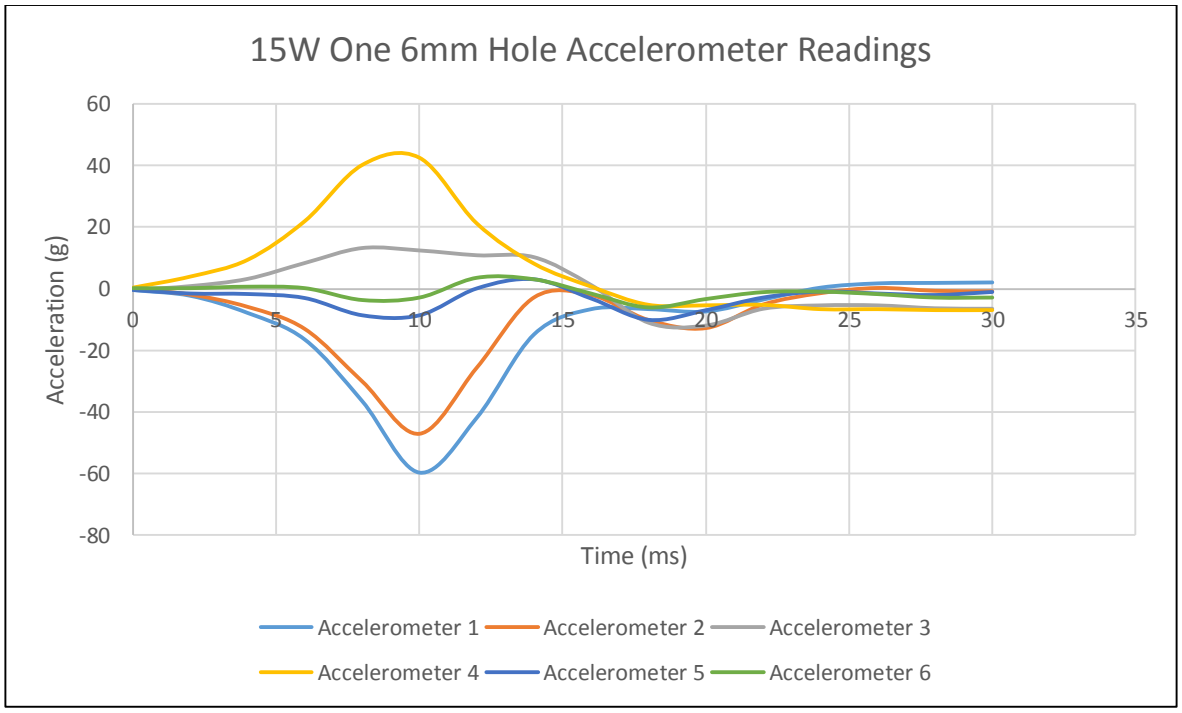
15W One 6mm Hole Accelerometer Readings
Acceleration (g)
60
40
20
0
-20
-40
-60
-80
0
5
10
15
20
25
30
35
Time (ms)
Accelerometer 1
Accelerometer 2
Accelerometer 3
Accelerometer 4
Accelerometer 5
Accelerometer 6

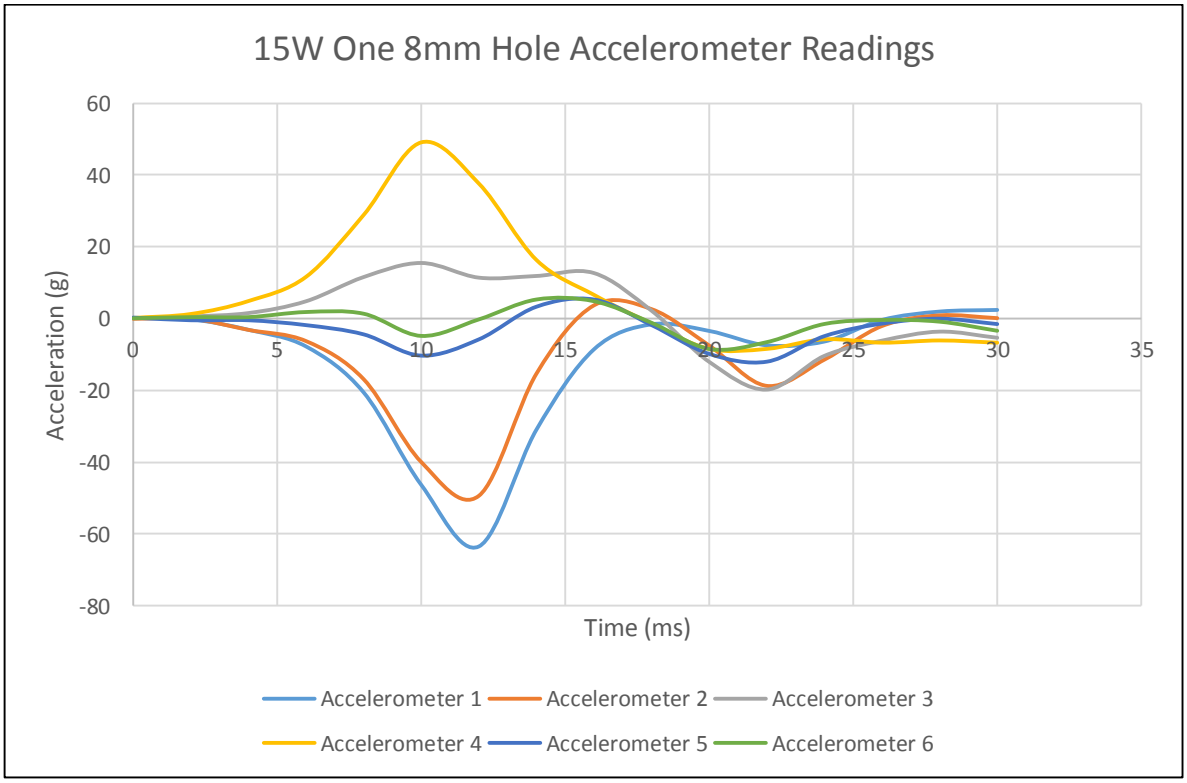
15W One 8mm Hole Accelerometer Readings
Acceleration (g)
60
40
20
0
-20
-40
-60
-80
0
5
10
15
20
25
30
35
Time (ms)
Accelerometer 1
Accelerometer 2
Accelerometer 3
Accelerometer 4
Accelerometer 5
Accelerometer 6

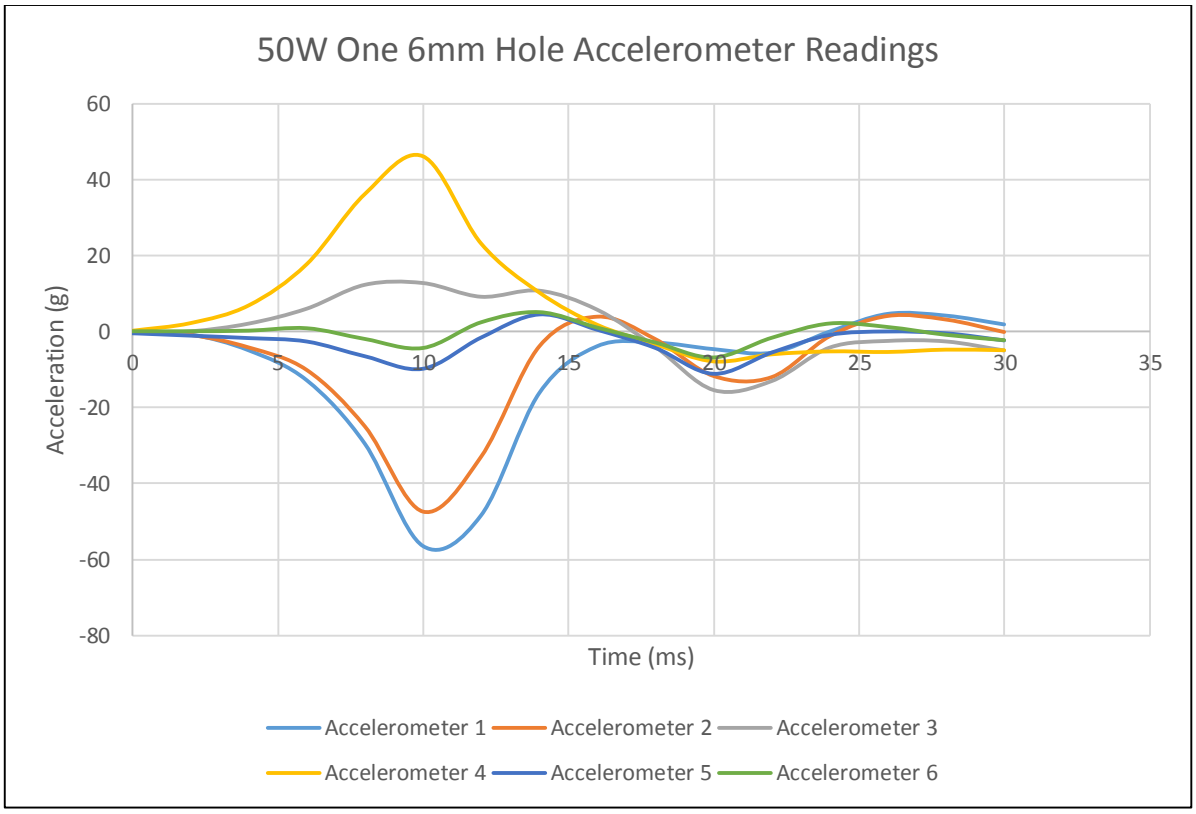
50W One 6mm Hole Accelerometer Readings
Acceleration (g)
60
40
20
0
-20
-40
-60
-80
0
5
10
15
20
25
30
35
Time (ms)
Accelerometer 1
Accelerometer 2
Accelerometer 3
Accelerometer 4
Accelerometer 5
Accelerometer 6

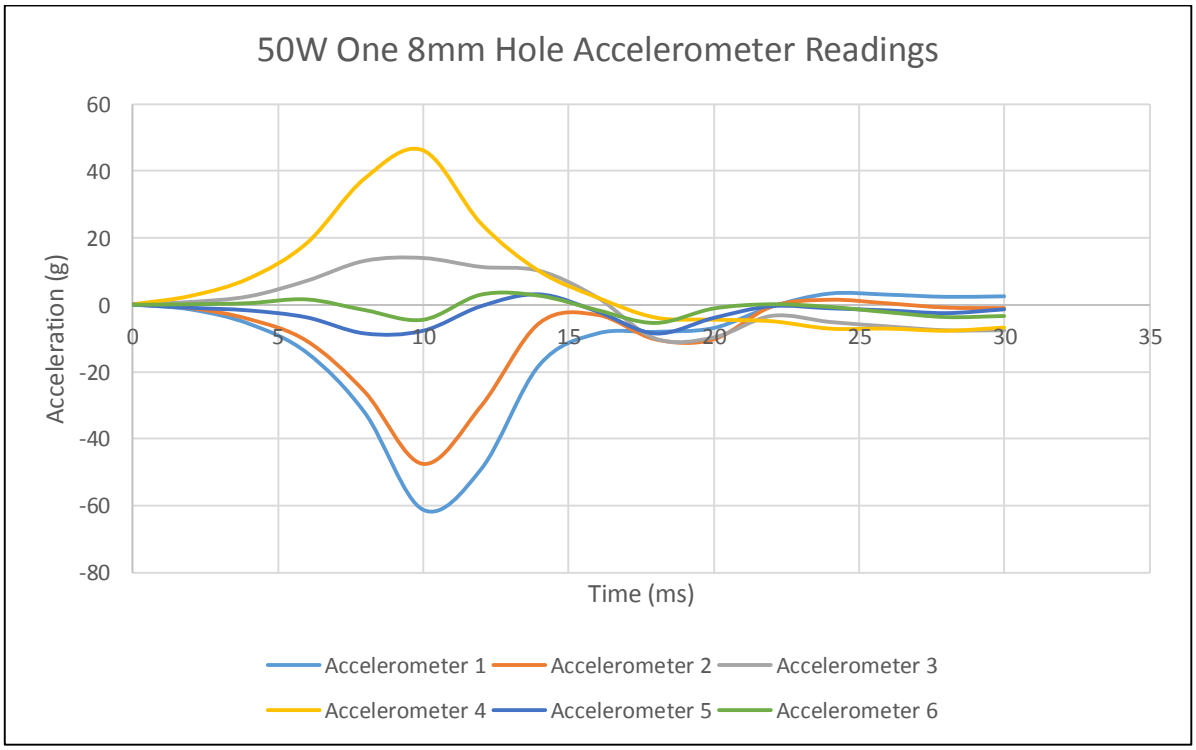
50W One 8mm Hole Accelerometer Readings
Acceleration (g)
60
40
20
0
-20
-40
-60
-80
0
5
10
15
20
25
30
35
Time (ms)
Accelerometer 1
Accelerometer 2
Accelerometer 3
Accelerometer 4
Accelerometer 5
Accelerometer 6

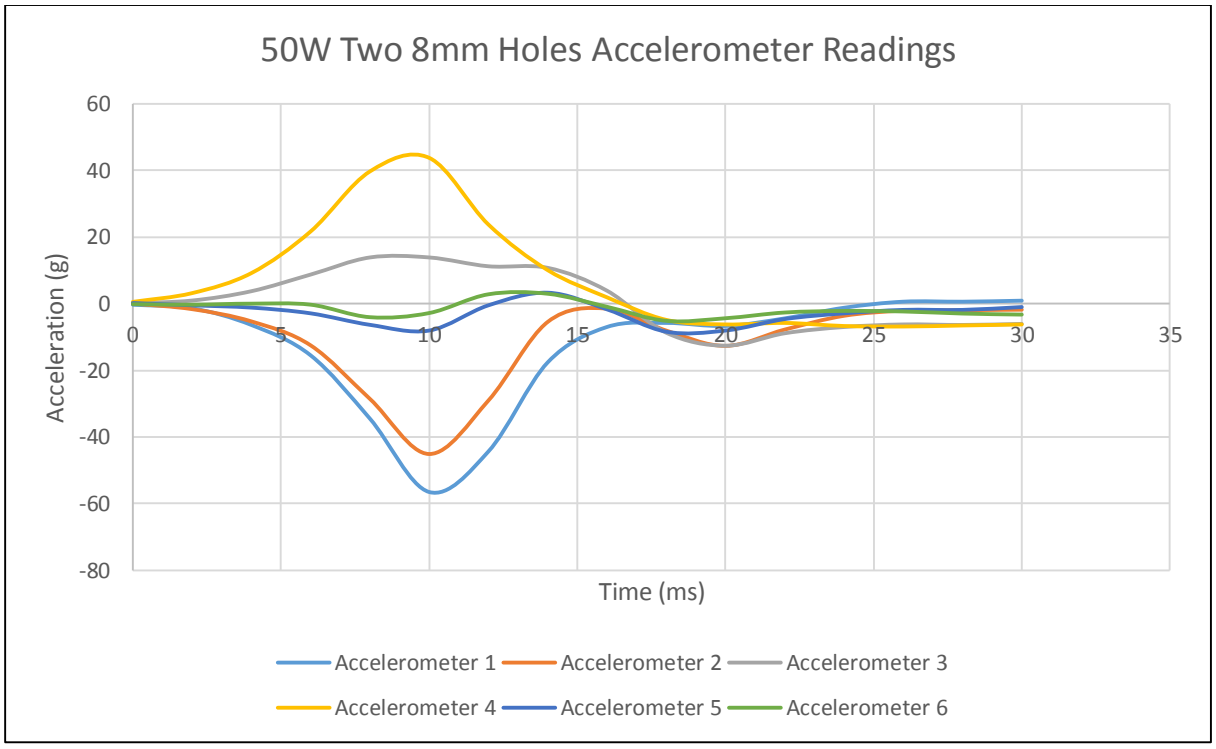
50W Two 8mm Holes Accelerometer Readings
60
40
20
0
-20
-40
-60
-80
Acceleration (g)
0
5
10
15
20
25
30
35
Time (ms)
Accelerometer 1
Accelerometer 2
Accelerometer 3
Accelerometer 4
Accelerometer 5
Accelerometer 6

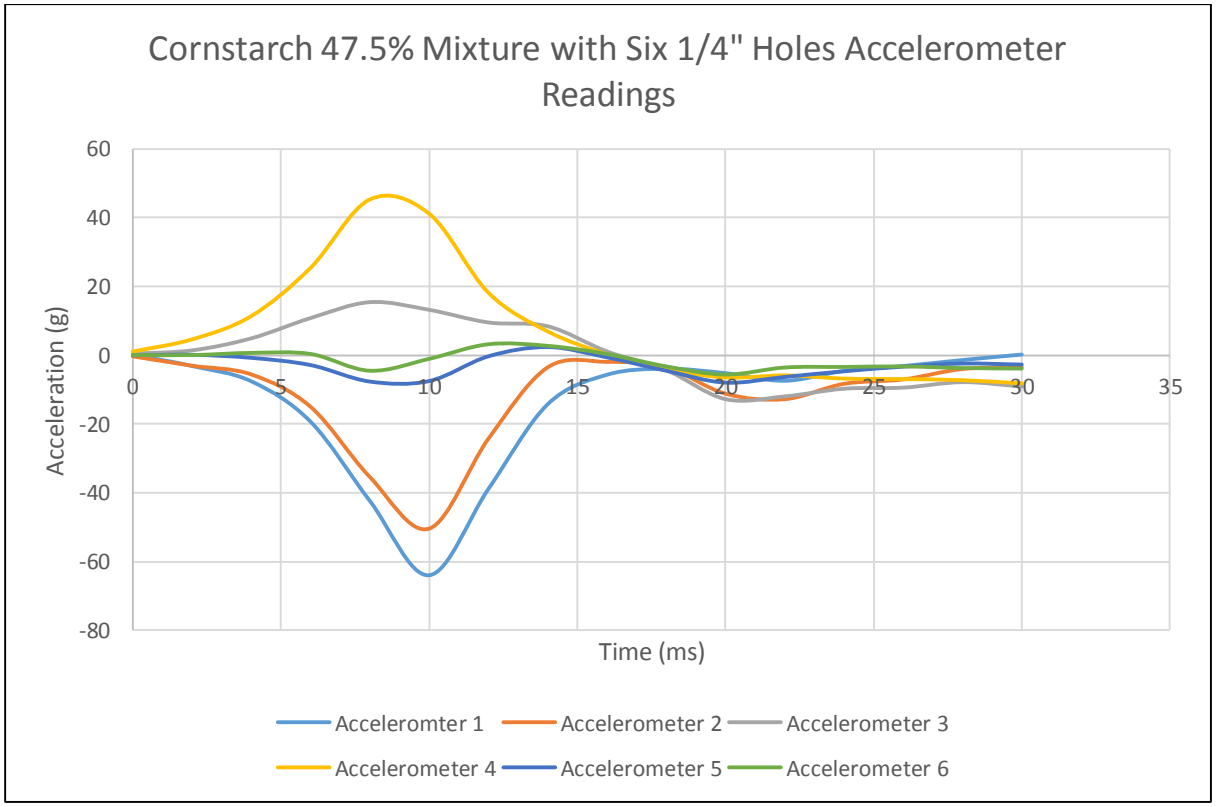
Cornstarch 47.5% Mixture with Six 1/4" Holes Accelerometer Readings
60
40
20
0
-20
-40
-60
-80
Acceleration (g)
0
5
10
15
20
25
30
35
Time (ms)
Acceleromter 1
Accelerometer 2
Accelerometer 3
Accelerometer 4
Accelerometer 5
Accelerometer 6

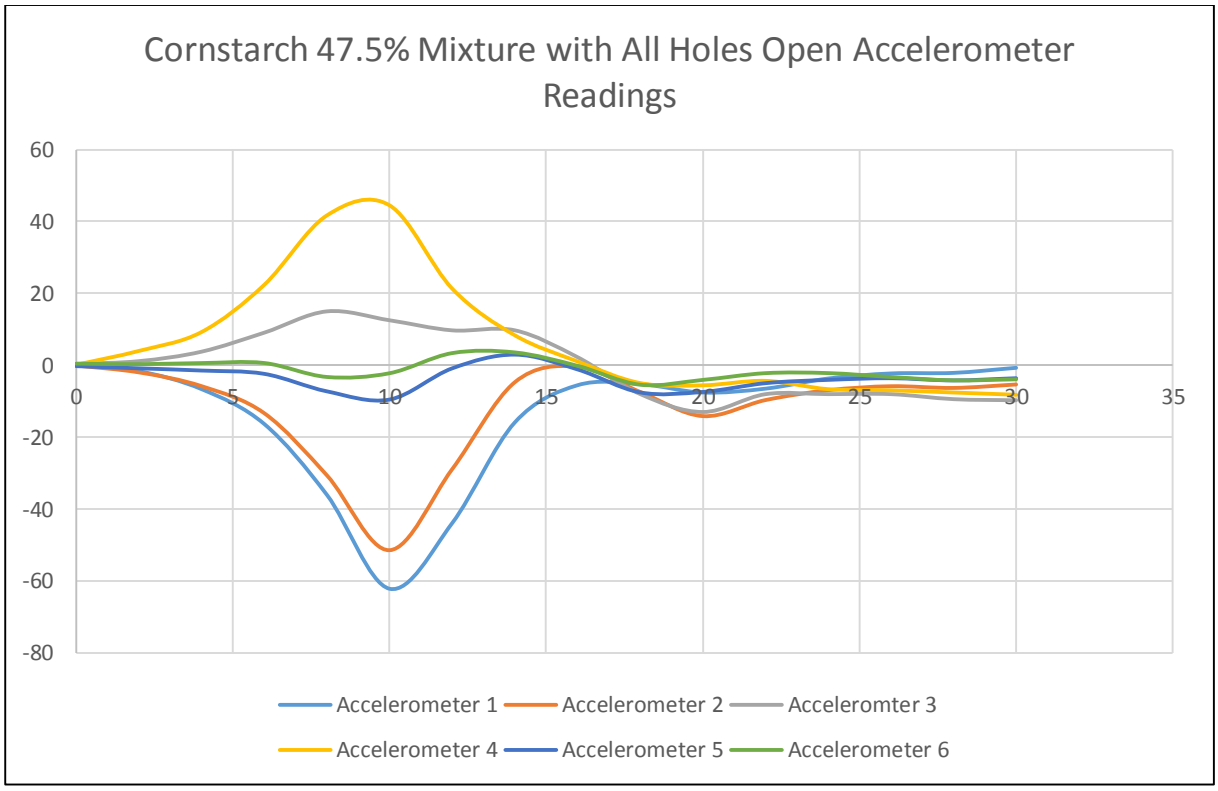
Cornstarch 47.5% Mixture with All Holes Open Accelerometer Readings
60
40
20
0
-20
-40
-60
-80
0
5
10
15
20
25
30
35
Accelerometer 1
Accelerometer 2
Acceleromter 3
Accelerometer 4
Accelerometer 5
Accelerometer 6

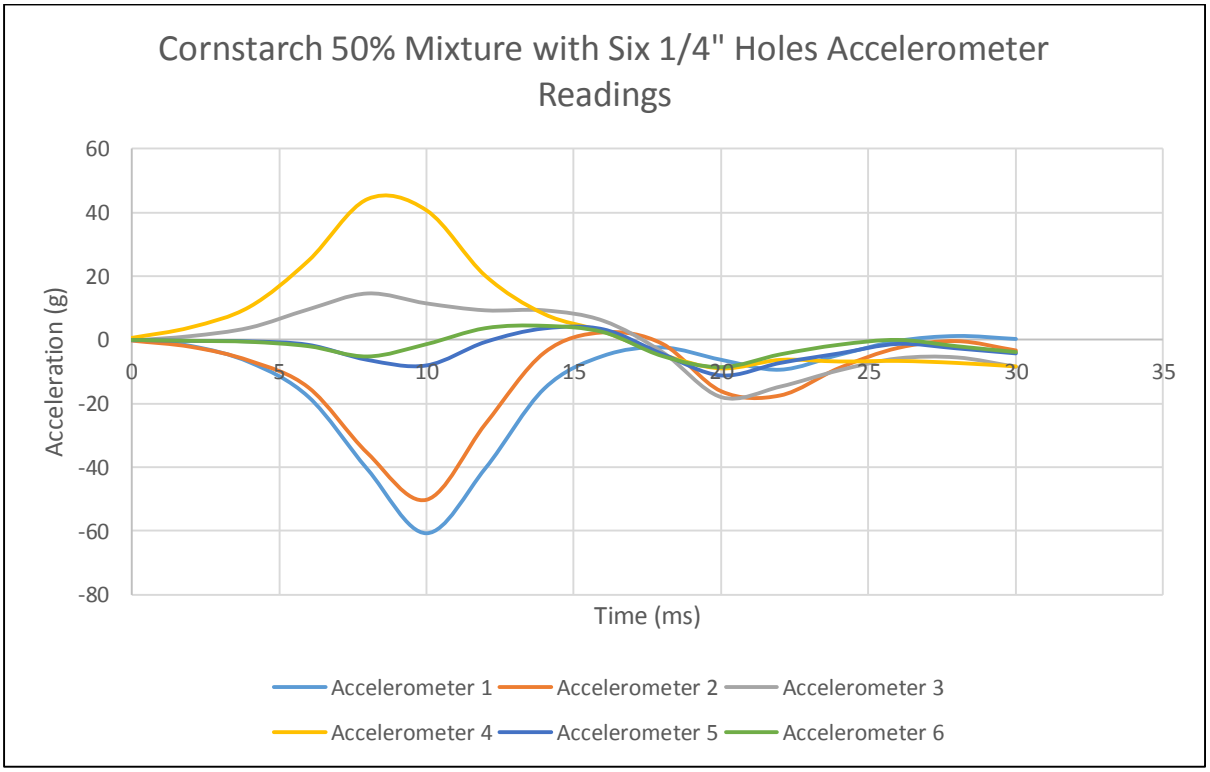
Cornstarch 50% Mixture with Six 1/4" Holes Accelerometer Readings
Acceleration (g)
60
40
20
0
-20
-40
-60
-80
0
5
10
15
20
25
30
35
Time (ms)
Accelerometer 1
Accelerometer 2
Accelerometer 3
Accelerometer 4
Accelerometer 5
Accelerometer 6

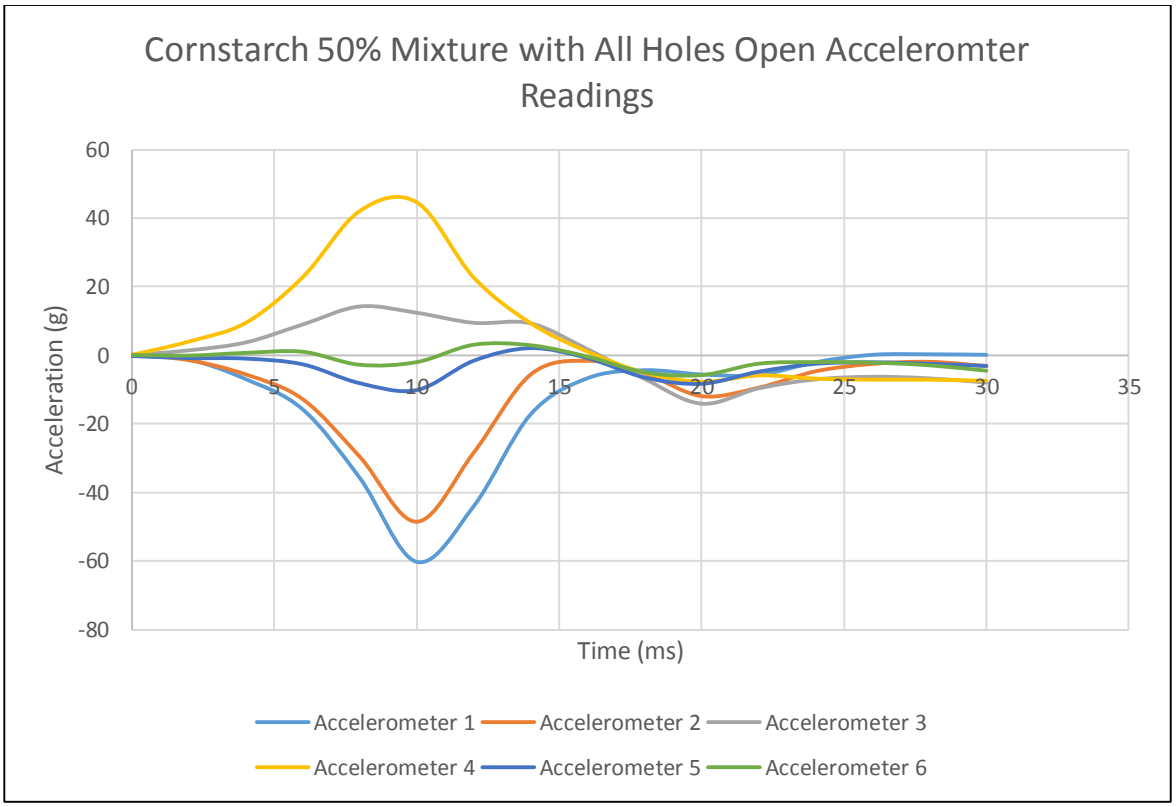
Cornstarch 50% Mixture with All Holes Open Acceleromter Readings
60
40
20
0
-20
-40
-60
-80
Acceleration (g)
0
5
10
15
20
25
30
35
Time (ms)
Accelerometer 1
Accelerometer 2
Accelerometer 3
Accelerometer 4
Accelerometer 5
Accelerometer 6